IDENTIFICATION OF GENES FROM *TRICHODERMA VIRENS* INVOLVED IN THE COLONIZATION OF MAIZE ROOTS AND INDUCED SYSTEMIC RESISTANCE

A Dissertation

by

JAMES TALMAGE TAYLOR, JR

Submitted to the Office of Graduate and Professional Studies of
Texas A&M University
in partial fulfillment of the requirements for the degree of

DOCTOR OF PHILOSOPHY

Chair of Committee,	Charles Kenerley
Co-Chair of Committee,	Michael Kolomiets
Committee Members,	Herman Scholthof
	Ping He
Head of Department,	Leland S. Pierson, III

August 2020

Major Subject: Plant Pathology

ABSTRACT

The filamentous fungus, *Trichoderma virens*, is a well-known mycoparasitic plant symbiont, valued for its biocontrol capabilities. *T. virens* initiates a symbiotic relationship with a plant host through the colonization of its roots. To achieve colonization, the fungus must communicate with the host and evade its innate defenses. In this study, I explored genes involved with the colonization process through transcriptomic profiling and reverse genetic characterization of genes of interest. Transcriptome profiles of the *T. virens* colonization of maize roots over time revealed that 24 hours post inoculation appeared to be a key time for plant-microbe communication, with many key gene categories peaking in differential expression. The transcriptomic profiles of *Sm1* and *Sir1* deletion mutants in the presence of plants demonstrated that *Sir1*, rather than Sm1, appears to be the key regulator of the fungal response to maize. Additionally, we developed a novel algorithm to select potential colonization related gene targets for characterization. About 40% of the genes identified by the algorithm would have been missed using previous methods for selecting genes. The class I hydrophobin, *HFB9a*, from *T. virens* plays a potential role in root colonization as the deletion mutants colonized less than the wild-type strain. The mutants were also unable to induce systemic resistance against *Colletotrichum graminicola*, and showed decreased cell wall degrading enzyme activity, which could be complemented by the purified HFB9a protein. HFB9a protein also induced phosphorylation of Arabidopsis MAP kinases, suggesting it might function as a microbe-associated molecular pattern to trigger immune responses. The mutants of a *T. virens* non-

ribosomal peptide synthetase, *Tex7*, resulted in the production of a large amount of the antibiotics heptelidic acid and viridin. Heptelidic acid is not typically produced by the wild-type *T. virens* strain and is used as a characteristic for classification of *T. virens* strains. In addition to heptelidic acid production by the mutant, a small amount of the compound was detected in the wild-type strain, suggesting that this compound should not be used for strain classification. Finally, plants treated with *Tex7* deletion mutants were significantly smaller than control and wild-type *T. virens* treated plants.

DEDICATION

This work is dedicated to my loving and supportive wife, Julie, and son, Wyatt.

ACKNOWLEDGEMENTS

I would like to thank my committee co-chairs, Dr. Charles Kenerley and Dr. Mike Kolomiets, and my committee members, Dr. Ping He, and Dr. Herman Scholthof, for their guidance and support throughout the course of this research.

Thanks also go to my friends and colleagues and the department faculty and staff for making my time at Texas A&M University a great experience. Thanks to Dr. Inna Krieger for her expertise in protein purification.

Finally, thanks to my mother and father for their encouragement and support, to Nola Schmidt for instilling in me a sense of curiosity and interest in biology, and to my wife, Julie, for her patience, love, and support.

CONTRIBUTORS AND FUNDING SOURCES

This work was supervised by a dissertation committee consisting of Professors Charles Kenerley and Michael Kolomiets, who acted as co-advisors, and Professor Herman Scholthof of the Department of Plant Pathology and Microbiology, and Professor Ping He of the Department of Biochemistry and Biophysics.

HPLC analysis was performed by Dr. Lorraine Puckhaber of the USDA-ARS Southern Plains Agricultural Research Station. NMR analysis was conducted by Dr. Karuna Dixit and Dr. Tatyana Igumenova of the Department of Biochemistry and Biophysics at Texas A&M University. Transcript sequencing was performed by the Genomics Core of Technion Institute of Technology in Haifa, Israel. Untargeted LC-MS/MS analysis was conducted by the Protein Chemistry Laboratory at Texas A&M University. All other work for the dissertation was completed independently by the student.

This work was made possible in part by Binational Science Foundation grant #2013202. Graduate study was also supported by a fellowship from Texas A&M University.

TABLE OF CONTENTS

Page

LIST OF FIGURES

Page

LIST OF TABLES

Page

CHAPTER I

INTRODUCTION

The genus *Trichoderma* consists of ascomycete fungi of the order Hypocreales that are distributed throughout most environments (Samuels, 2006). As the anamorphic or asexual stage, members reproduce by conidiation and production of chlamydospores (a survival spore). The teleomorph of sexually reproducing species is *Hypocrea*, though sexual reproduction is rare (Chaverri *et al.*, 2001; Steyaert *et al.*, 2010). These fungi are well known mycoparasites that also live saprophytically (Kubicek *et al.*, 2011). They can directly antagonize and parasitize other fungi through secretion of cell wall degrading enzymes, production of antibiotic secondary metabolites, and physically coiling around hyphae of the target host (Baek *et al.*, 1999; Kubicek *et al.*, 2011; Vargas *et al.*, 2014). When living saprophytically, these fungi secrete a variety of enzymes to degrade organic matter and recover nutrients (Adav and Sze, 2014; Lamdan *et al.*, 2015a). Because of their propensity to produce enzymes, they are often used for industrial production of cellulases and chitinases (Kovács *et al.*, 2009; Delabona *et al.*, 2012; Ellilä *et al.*, 2017). In addition to a free-living lifestyle, *Trichoderma* spp. form close symbiotic associations with plant roots, wherein the fungus receives carbon in the form of secreted sugars, and as discussed in detail below, the plant receives a range of benefits from the fungus (Vargas *et al.*, 2009; Contreras-Cornejo *et al.*, 2014; Mendoza-Mendoza *et al.*, 2018). This association is initiated by the colonization of plant roots by the symbiont, which is a complex process involving signaling molecules of both host and fungal origins, and recognition events.

Trichoderma spp. are attracted to plant root exudates (Mendoza-Mendoza *et al.*, 2018), and as the fungus grows within the rhizosphere and on the root epidermis, secretion of effectors and cell wall degrading enzymes facilitates internal colonization of the roots (Brotman *et al.*, 2013). These fungi have not been reported to colonize individual plant cells or form typical mycorrhizal arbuscules. However, a haustorium-like structure has been visualized and hypothesized to be involved in the mechanical separation of root cells at common borders to permit the intercellular growth of these root symbionts (Nogueira-Lopez *et al.*, 2018). Once the fungus has colonized the first several layers of root cortical cells, colonization ceases, and the fungus lives symbiotically within the plant roots (Vargas *et al.*, 2009). During this interaction, the fungus provides protection against both root and foliar pathogens through mycoparasitism and induced systemic resistance (ISR), respectively (Nawrocka and Małolepsza, 2013; Monfil and Casas-Flores, 2014; Saldajeno *et al.*, 2014). Additionally, these symbionts can enhance plant growth through enhancement of nutrient scavenging and uptake (Altomare *et al.*, 1999; Hermosa *et al.*, 2013; Mukherjee *et al.*, 2018). Secreted proteins from *Trichoderma spp.* have also been demonstrated to improve root structure and architecture which can enrich nutrient accessibility and promote a healthier plant host (Contreras-Cornejo *et al.*, 2009; Saravanakumar *et al.*, 2016; Mendoza-Mendoza *et al.*, 2018). To explore the interactions between plants and *Trichoderma spp.*, we selected *T. virens* (Teleomorph *Hypocrea virens*, Chaverri, Samuels, and Stewart 2001) as a model for our studies.

Trichoderma derived plant benefits

Mycoparasitism and secondary metabolite production

Trichoderma virens is known to parasitize other fungi through secretion of cell wall degrading enzymes and active peptides, such as peptaibols, and hyphal coiling (Baek *et al.*, 1999; Djonović *et al.*, 2006b). Such attributes have led to the use of *T. virens* as a biocontrol agent with many commercial seed coatings preparations applied to prevent damping off of seedlings by pathogens such as *Rhizoctonia solani* and *Pythium ultimum* (Junaid *et al.*, 2013; Degenkolb *et al.*, 2015). *T. virens* also produces secondary metabolites that benefit the host by protection of roots through antibiotic activity (Lumsden *et al.*, 1992; Howell *et al.*, 1993; Zeilinger *et al.*, 2016). Many of these secondary metabolites are produced by gene clusters containing a nonribosomal peptide synthetase (NRPS) or polyketide synthase (PKS). The NRPS or PKS assembles a short polypeptide that is acted upon by downstream members of the cluster, often consisting of cytochrome p450s and transporters. Several of these clusters are significantly upregulated in the presence of plant roots, indicating an important role for the metabolites in the plant-fungus interactions (Mukherjee *et al.*, 2012a; Malinich *et al.*, 2019). For instance, *T. virens* produces a suite of antibiotic compounds including, gliotoxin, viridin, gliovirin, and heptelidic acid (Howell *et al.*, 1993). *T. virens* species has been subdivided into two strain groupings, “P” and “Q”, based on which major antibiotics the strains produce (Howell *et al.*, 1993). P strains were characterized as producing gliovirin and heptelidic acid and are incapable of producing gliotoxin or dimethyl gliotoxin. The Q strains produce gliotoxin and dimethyl gliotoxin but are not reported to produce gliovirin or heptelidic acid.

Gliotoxin is a potent antibiotic with high activity against bacterial, insect, and fungal species (Howell, 2003; Vargas *et al.*, 2014). Deletion of the GliP gene, encoding an NRPS, renders the fungus unable to control the damping off disease caused by *P. ultimum*, reduces degradation of *Sclerotinia sclerotiorum* sclerotia, and hinders the ability to kill wax moth larvae (Vargas *et al.*, 2014).

Induced systemic resistance

Induced systemic resistance (ISR) is one of the most beneficial effects resulting from the colonization of plant roots by *Trichoderma spp*. ISR is thought to be mediated by ethylene and jasmonic acid (JA) signaling (Shoresh et al. 2005; Choudhary et al. 2007). JA is synthesized from fatty acids in a well understood pathway and serves as a signal molecule for multiple functions (Creelman and Mullet, 1997). Lipoxygenases play a crucial role in plant defense regulation and production of JA and a large number of other oxylipins. The maize lipoxygenase ZmLOX2 positively regulates biosynthesis of JA, while ZmLOX3 appears to negatively regulate the expression of ZmLOX2 and other maize lipoxygenases necessary for JA synthesis (Constantino *et al.*, 2013; Yan *et al.*, 2013; Huang, 2017). In *Zmlox3* mutants, several other lipoxygenases involved in JA biosynthesis are highly upregulated. Additionally, the mutants display a constitutive ISR phenotype when no fungus is present on their roots, suggesting that ZmLOX3 is a negative regulator of ISR (Constantino *et al.*, 2013). Despite the current dogma of JA serving as the major hormone involved in ISR, a recent study determined that a different oxylipin, an α-ketol of octadecadienoic acid (KODA), is the plant signal required for *T. virens* mediated ISR in maize and that JA is actually dispensable in this interaction (Wang *et al.*,

2020b). ZmLOX10 is another maize lipoxygenase involved in the production of green leafy volatiles and other volatile compounds typically associated with herbivory defense. Interestingly, *Zmlox10* mutants displayed a heightened defense against foliar pathogens, similar to *Zmlox3* mutants (Christensen *et al.*, 2013; Gorman *et al.*, 2020).. However, when treated with *T. virens*, *Zmlox10* mutants exhibit induced systemic susceptibility (ISS), where foliar lesions are larger compared to the plants that were not treated with *T. virens* (Wang *et al.*, 2020b).

Growth

There are many examples where the root application of *Trichoderma spp.* enhances plant growth through the activities of increased nutrient scavenging, production of plant growth hormones, and secretion of enzymes and proteins. For instance, *T. virens* produces several siderophores that chelate iron and allow its uptake by the plant and the fungus (Wilhite *et al.*, 2001). One of these siderophores, ferricrocin, has been shown to be involved in the ability of the fungus to properly colonize and induce systemic resistance in maize plants (Mukherjee *et al.*, 2018). In addition to increasing availability of iron, *T. virens* can also improve phosphate and micronutrient solubility through acidification of the rhizosphere (Altomare *et al.*, 1999). *T. virens* directly produces growth promoting phytohormones (auxins) which, in addition to enlarging cell size, alter the root structure of host plants, that in turn can lead to better nutrient uptake and increased growth (Contreras-Cornejo *et al.*, 2009). Secretion of enzymes and small proteins that alter the transcriptional activity of the plant have also been demonstrated for *Trichoderma spp*. (Lamdan *et al.*, 2015a; Shaw *et al.*, 2016; Malinich *et al.*, 2019). These compounds when

secreted into plant roots can lead to changes in the levels of hormone production by the plant and shift the allocation of resources to allow for increased growth (Hermosa *et al.*, 2013; Contreras-Cornejo *et al.*, 2014; Kazan and Lyons, 2014).

Colonization by *Trichoderma*

Trichoderma spp. utilize several strategies for colonization of plant roots (Viterbo and Chet, 2006; Kubicek *et al.*, 2008; Brotman *et al.*, 2008; Taylor *et al.*, 2017). A large number of glycoside hydrolases are secreted in the presence of maize roots (Lamdan *et al.*, 2015a), suggesting that colonization is mainly an enzymatic process. However, other non-catalytic proteins have also been shown to be necessary for efficient root colonization by *T. virens* (Crutcher *et al.*, 2015; Taylor *et al.*, 2017). Some of these proteins are involved in communication with the plant host by acting as elicitors (Brotman *et al.*, 2008; Crutcher *et al.*, 2015). Other proteins can influence the colonization process by regulation of metabolism and nutrient uptake. For example, TvInv and TvSuc are involved in sucrose metabolism and transport, respectively. These proteins are required for colonization of maize roots, and the deletion of TvInv causes the fungus to colonize roots significantly more than a wild-type strain (Gv29-8), suggesting that the uptake and metabolism of sucrose is a vital switch in the colonization process (Vargas *et al.*, 2009; Vargas *et al.*, 2011). My research has focused on hydrophobin protein signals involved in the over-all colonization process, and transcriptomic analysis of *T. virens* during the early stages of colonization.

Effectors and MAMPs

Plants have developed complex microbe detection and defense mechanisms to battle the onslaught of microbes attempting to gain an infectious advantage (Heil and Bostock, 2002). Plants recognize motifs and patterns exhibited by microbes termed microbe or pathogen associated molecular patterns (MAMPs and PAMPs, respectively). Through pattern recognition receptors (PRRs) that target these motifs, the plant can detect microbes and enact defenses and transcriptional reprogramming tailored specifically to the recognized pattern (Boller and He, 2009; Yu *et al.*, 2017). Additionally, microbes can utilize these receptors to initiate effects of their own through secretion of proteins targeting PRRs (Boller and He, 2009). Pathogens will use these mechanisms for their own benefit, but beneficial microorganisms can use PRRs to induce transcriptional changes in the plant that enable symbiosis to occur (Trdá *et al.*, 2015). An example of this in relation to colonization is the protein Swollenin produced by *T. asperellum*, which exhibits cellulolytic enzymatic activity and contains a cellulose binding domain that is recognized as a MAMP by the host plant. The MAMP recognition of the protein greatly enhances colonization compared to the protein's enzymatic activity, suggesting that the plant can recognize this MAMP as being associated with a beneficial microbe (Brotman *et al.*, 2008). The secretion of elicitors by *T. virens* has also been shown to influence the delivery of benefits to the plant (Howell *et al.*, 2000; Djonović *et al.*, 2006a; Djonović *et al.*, 2007; Viterbo *et al.*, 2007). One such elicitor, SM1, has been shown to be required for ISR in maize (Djonović *et al.*, 2007), though the mechanism by which SM1 acts has yet to be fully determined. SM2 is a paralog of SM1 and has also been demonstrated to function

as an elicitor in host colonization and induction of systemic resistance against the foliar pathogen *Cochliobolus heterostrophus* (Crutcher *et al.*, 2015; Gaderer *et al.*, 2015). Additionally, in the presence of plant roots, many other putative elicitors from *T. virens* are upregulated, highlighting their importance in this process (Morán-Diez *et al.*, 2015; Malinich *et al.*, 2019). Lamdan et al. identified putative effectors by proteomic profiling whose presence appeared to decrease systemic defense initiated by the fungus (Lamdan *et al.*, 2015a). Malinich et al. sought to better understand the transcriptomic changes that occur during colonization of maize roots by *T. virens* when interacting in a hydroponic system (Malinich *et al.*, 2019). This analysis established several target genes with putative roles in colonization and ISR based on differential expression.

In this dissertation, I describe a transcriptomic analysis pipeline to identify high-impact genes in the colonization process, and my research on a hydrophobin protein with a role in colonization and as a microbe-associated molecular pattern, an NRPS whose deletion induces production of heptelidic acid.

CHAPTER II

TRANSCRIPTOMIC ANALYSIS OF MAIZE ROOT COLONIZATION BY *TRICHODERMA VIRENS*

Introduction

The rhizospheric fungus *Trichoderma virens* is well known for its role as a plant symbiont that protects its host from pathogenic attack directly through mycoparasitism and indirectly through the induction of plant systemic defenses (Howell, 1987; Djonović *et al.*, 2006a; Djonović *et al.*, 2006b; Djonović *et al.*, 2007; Kubicek *et al.*, 2011; Nawrocka and Małolepsza, 2013; Guzmán-Guzmán *et al.*, 2017). This symbiotic relationship is perceived to be the result of fungal root colonization and communication with the host. There have been several studies that have described elements of the interaction between *T. virens* or other *Trichoderma* species and host plants (Brotman *et al.*, 2008; Salas-Marina *et al.*, 2011; Dubey *et al.*, 2014; Crutcher *et al.*, 2015; Morán-Diez *et al.*, 2015; Lamdan *et al.*, 2015b; Nogueira-Lopez *et al.*, 2018; Malinich *et al.*, 2019). *T. virens* has been microscopically visualized extensively colonizing the external surface of maize roots, and internally colonizing a few cell layers deep before ceasing ingress (Nogueira-Lopez *et al.*, 2018). Much of the initial penetration of the fungus is mediated by physical interactions, and secretion of elicitor proteins and hydrophobins (Viterbo and Chet, 2006; Brotman *et al.*, 2008; Brotman *et al.*, 2013; Crutcher *et al.*, 2015; Gaderer *et al.*, 2015). The expansin-like protein, Swollenin, was shown to have roles in both mechanical separation of plant cells to increase intercellular spaces and the plant recognition of a carbohydrate binding domain as a potential MAMP (Brotman *et al.*,

2008). *TasHyd1* is a hydrophobin that was demonstrated to be involved in the attachment of *T. asperellum* to cucumber roots, and when the gene was deleted, fungal colonization was significantly reduced compared to the wild-type strain (Viterbo and Chet, 2006). Additionally, a cerato-platanin family protein paralog of the elicitor protein SM1, designated SM2, was shown to be necessary for induced systemic resistance against *Cochliobolus heterostrophus* and in colonization of maize roots (Crutcher *et al.*, 2015; Gaderer *et al.*, 2015). Internal colonization appears to be influenced by plant derived sucrose (Vargas *et al.*, 2009; Vargas *et al.*, 2011). Vargas *et al.* found that mutant strains of *T. virens* lacking a key sucrose invertase colonized the roots at significantly greater levels than the wild type strain (Vargas *et al.*, 2009).

Other transcriptomic studies have been performed to provide a greater understanding of the colonization process by *T. virens* (Morán-Diez *et al.*, 2015; Malinich *et al.*, 2019). These studies were conducted in hydroponic systems, but with significantly different timescales. Malinich *et al.* selected 6 and 30 hours post inoculation (hpi) for an RNA-seq based transcriptomic study, while Moran-Diez *et al.* sampled at a single time point of 72 hpi for a microarray based transcriptomic study. There were significant findings from each of these studies. Moran-Diez *et al.* explored the differences in *T. virens* gene expression in the presence of monocot and dicot hosts and Malinich *et al.* gave an in-depth analysis of the changes in *T. virens* gene transcription after the fungus recognizes a plant host and during colonization (6 and 30 hpi; Morán-Diez *et al.*, 2015; Malinich *et al.*, 2019). Despite the insights gleaned from these studies, the transcriptomic events of the very early stages of *T. virens* colonization (i.e. between 6 and 30 hpi) are not well

known. Additionally, the approach often used to select target genes for characterization and identification of potential roles in plant-microbe interactions following analysis of transcriptomic data sets largely uses a “rack-and-stack” gene prioritization. This approach yields large lists of genes potentially involved in the colonization process that requires high throughput systems to identify those that are involved in plant-microbe interactions (Lamdan *et al.*, 2015a; Morán-Diez *et al.*, 2015; Nogueira-Lopez *et al.*, 2018). To further define the host-mediated response of maize to *T. virens* colonization, Wang *et al.* identified new oxylipin signals responsible for *T. virens* mediated induced systemic resistance by comparing the plant response to colonization by the wild-type strain, *Sm1* deletion mutant, or *Sir1* deletion mutant (Wang *et al.*, 2020b). SM1 is an elicitor required for the induced systemic resistance response mediated by *T. virens* (Djonović *et al.*, 2006a; Djonović *et al.*, 2007). SIR1 is a small, secreted cysteine rich protein whose deletion increases the ISR response of colonized maize plants (Lamdan *et al.*, 2015a). However, comparatively little is known about the fungal response to the interaction with maize when these key genes are deleted. Therefore, in this study we initiated an RNA-seq based transcriptomic study to explore the early events of colonization between 6 and 36 hpi. We developed a novel target enrichment pipeline that uses gene co-expression networks to select gene targets with higher likelihood of functional relevance to the interaction between fungus and plant and analyzed a previously sequenced transcriptomic dataset of the *T. virens* mutants *ΔSm1* and *ΔSir1* to compare to the wild-type strain.

Materials and Methods

Strains and hydroponic system

T. virens strain Gv29-8 (WT) was maintained on potato dextrose agar (PDA, BD Biosciences) at 27 ºC. *Zea mays* (Silver queen hybrid, Burpee) was grown in a hydroponic system (Lamdan *et al.*, 2015b) as the host for the transcriptomic study with *T. virens*. The hydroponic system consisted of mason jars (500ml, wide mouth) with a four-pronged shaker clamp placed inside. The jar was filled to the top of the clamp (~220ml) with 0.5x Murashige-Skoog basal medium containing Gamborg's vitamins and supplemented with 0.5% sucrose. The unit was covered with a glass petri dish bottom and autoclaved. Plastic mesh (7 holes/linear inch) previously cut into discs to fit within the jars was autoclaved separately. After sterilization, the mesh discs were placed on top of the clamps, and pregerminated seeds with roots approximately 2 cm long were threaded through the mesh to contact the growth medium. The glass petri dish bottoms were replaced with sterile plastic petri dish bottoms to ensure a tighter fit.

Colonization assay

Following three days of incubation under lamps (Sun Blaze T5) with 6500K and 3000K lights at room temperature under a 14:10 light:dark regime with shaking at 50 rpm (New Brunswick Orbital Shaker), the roots of the seedlings were dipped in a suspension of 24-hour old *T. virens* tissue (4g in 200 ml MS medium) for 30 seconds with gentle shaking. The inoculated roots were placed back into their original jars and returned to shaking under the light bank. Seedlings were harvested every three hours for 12 hours starting at 6 hpi. The harvested seedlings were gently rinsed in tap water and surfaced

sterilized for one minute in 1% sodium hypochlorite, followed by a rinse for one minute in sterile distilled water. Roots were detached from the seedlings and sliced into approximately 1 cm sections. The sections were plated on GVSM (Park *et al.*, 1992, gliotoxin excluded) and incubated at 27C for 24 hours. The plates were observed for growth of the fungus originating from inside the root.

Transcriptomic study

Hydroponic systems were established and roots inoculated as described previously. One gram of fungal tissue was used to inoculate hydroponic systems without plants to serve as controls. Colonized plant roots or fungal tissue cultured alone were harvested at 6, 12, 15, 24, and 36 hours post inoculation, immediately flash frozen in liquid nitrogen, and stored for extraction. There were three biological replicates (5 plants pooled per biorep) per time point, giving a total of 30 samples.

RNA extraction and preservation

The frozen roots were thoroughly ground in a mortar and pestle with liquid nitrogen. Approximately 500 mg of frozen powder was placed into a microfuge tube and 500 ul of TRI-reagent added. The mixture was allowed to fully thaw and vortexed to ensure homogenization of the sample. 500 ul of chloroform was added to the sample and vortexed to mix. The sample was then centrifuged for 10 minutes at 4C and 14,000 rpm. The upper aqueous layer was collected in a new tube and one volume of ice-cold isopropanol added to precipitate the nucleic acids. The precipitant was spun in a microcentrifuge for 10 minutes at 4C and maximum speed. The pellet was washed with 70% ethanol and allowed to dry before resuspending in 200 ul of nuclease free water. The

sample was treated with DNAse I (Invitrogen, USA) as per manufacturer instructions. The sample was then electrophoresed on an agarose gel treated with 1% bleach to determine quality of the RNA and ensure that any DNA was degraded. The samples were then shipped on dry ice to Technion Institute of Technology in Haifa, Israel for sequencing at a collaborating laboratory.

Analysis of reads from RNA-seq

Resulting raw reads for each sample were analyzed for read quality with fastQC software. All reads were then aligned with HISAT2 software and quantitated with StringTie. Differential expression analysis was performed in EdgeR. Differentially expressed genes (DEGs) were filtered to only those that had a SignalP score of 0.5 or higher. All scripts are available in the following github repository: (https://github.com/jamestaylorjr/Trichoderma_Transcriptome_Metabolome).

In addition to the differential expression analysis, the reads were normalized by the TMM method and exported as a separate file for clustering analysis. A co-expression network was generated using raw read counts from StringTie with the NetMiner software, with modifications to allow the use of StringTie formatted reads. The resulting co-expression network was used for further target gene selection.

Target enrichment pipeline

The Scikit-learn (sklearn) python library was used to perform principal component analysis on the TMM normalized read counts produced in previous steps of the analysis. The top three principal components were used as input to the sklearn DBSCAN algorithm for clustering. The generated co-expression network was queried for the centrality of each

gene in each cluster using the betweenness centrality function in the Networkx python library. The most central gene in each cluster was selected as a putative target. Each unique gene in the list of putative targets was examined for putative function, domains, expression in other datasets, and putative subcellular localization.

Transcriptomic analysis of ΔSir1/ΔSm1 mutants

Reads from an RNA-seq transcriptomic experiment were obtained as in Malinich *et al.* (Malinich *et al.*, 2019). Briefly, hydroponic systems were constructed with and without B73 plants and inoculated with one of three strains: *ΔSm1* mutant, *ΔSir1* mutant, or WT. At each time point there were four biological replicates of each mutant strain with and without seedlings, ten biological replicates of the wild-type strain with seedlings, and four biological replicates of the wild-type strain without seedlings, for a total of 44 samples. Samples were collected at 6 and 30 hpi, RNA extracted, and sequenced. The reads were analyzed for differentially expressed genes as previously described, without filtering for the presence of a signal peptide.

Results

Selection of timepoints for transcriptomic experiment

The colonization time course experiment was performed to determine when the fungus had begun its ingress of the roots. These data revealed that the fungus internally colonized as early as 12 hours post inoculation. Replicate studies indicated that the fungus colonized approximately 50% of samples at 12 hpi and consistently colonized the internal portion of all roots sampled at 15 hpi. Thus, we concluded that 12 hpi was a transitionary

period in the colonization process, and 15 hpi represented the time of full ingress of the root in our system. To ensure immediate and consistent attachment of fungal inoculum to roots, our experimental set up employed a root dip method of inoculation. Five time points were selected (6, 12, 15, 24, and 36 hpi) for tissue harvest that were considered to span the colonization process, including fungal-host communication.

Analysis of time-course transcriptomic data

A quality check of sequenced reads was performed using fastqc, which demonstrated that the reads for all samples were of extremely high quality (>30 score). Alignment, quantification, and differential expression analysis were performed as described in the methods. As a previous study examined the general transcriptomic activity of *T. virens* in the presence of maize roots in great detail (Malinich *et al.*, 2019), this study only focuses on proteins that were predicted to be secreted.. Filtering of DEGS to only those with a SignalP score >0.5 reduced the number of DEGs from 2290 to 248. These genes were then grouped by the KOGG category to which they belong for comparison of up or downregulated genes across time. Only 8 KOGG categories were selected for further study due to having a high likelihood of involvement in plant-microbe interactions.

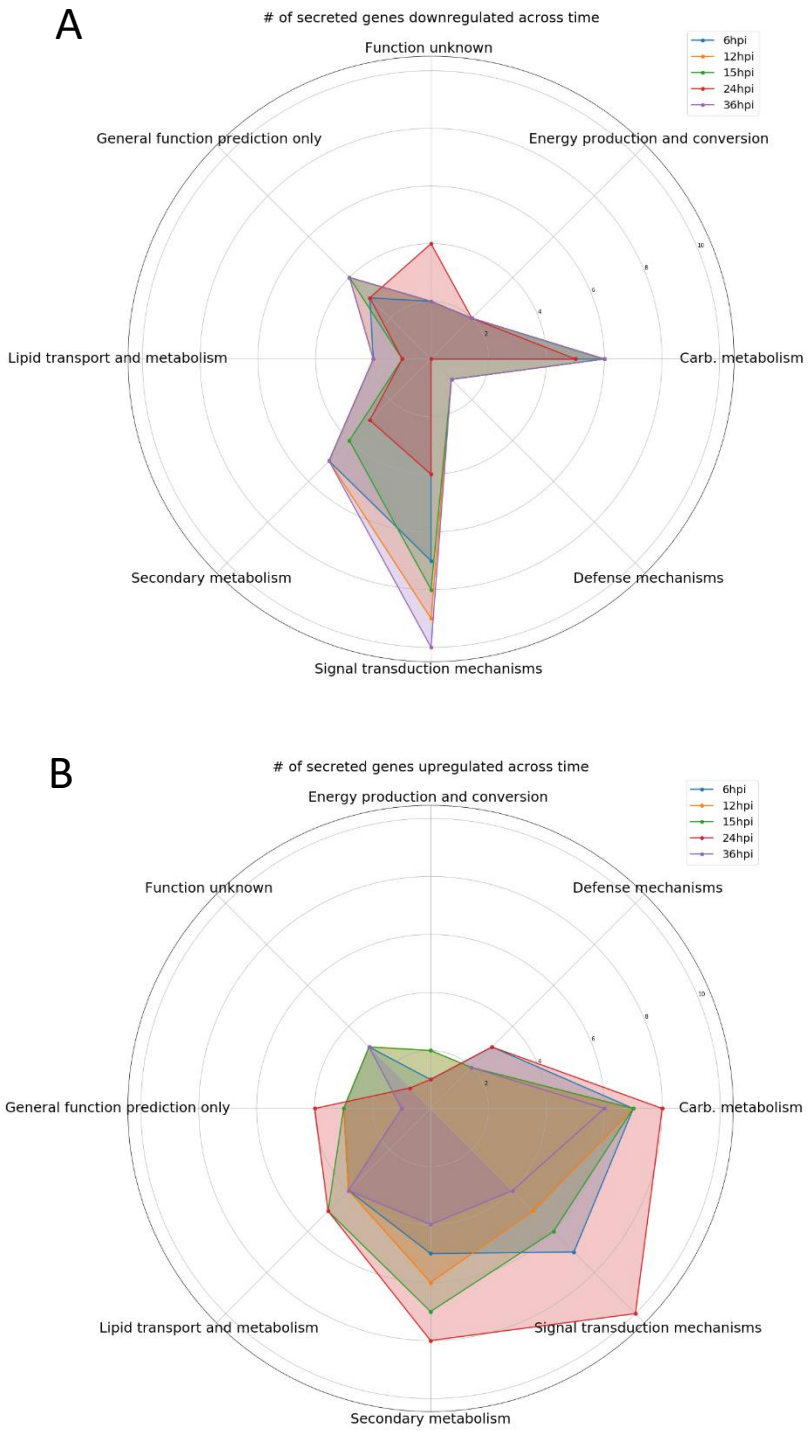

Figure 1. Comparison of the number of differentially expressed secreted genes over time. Gene categories were selected based on perceived likelihood of involvement in signaling between the fungus and plant.

Signal transduction mechanisms

Interestingly, there was an increase in the number of downregulated DEGs involved in signal transduction between 6 and 12 hpi (Figure 1a). However, the number of upregulated DEGs increased from 12 to 24 hpi before dropping off significantly at 36 hpi (Figure 1b). Gene 111479, encoding a putative chitosanase, was upregulated throughout the time course, except at 24 hpi where it was significantly downregulated (Figure 2). Notably, there was a peak in expression of a ceramidase (34323) between 15 and 24 hpi, whereas a second ceramidase (179276) was upregulated throughout the interaction with the plant. Gene 10277, which contains the GLEYA motif associated with fungal adhesin proteins, was upregulated at 6 and 24 hpi. A putative CFEM domain gene (81869) was upregulated solely at 24 hpi. There were several serine/threonine protein kinases identified (192926, 77550, 216090, 216568, and 229760). Interestingly, one of these kinases (77550) also has a putative function as an alpha-1,3-glucan invertase based on interpro annotation.

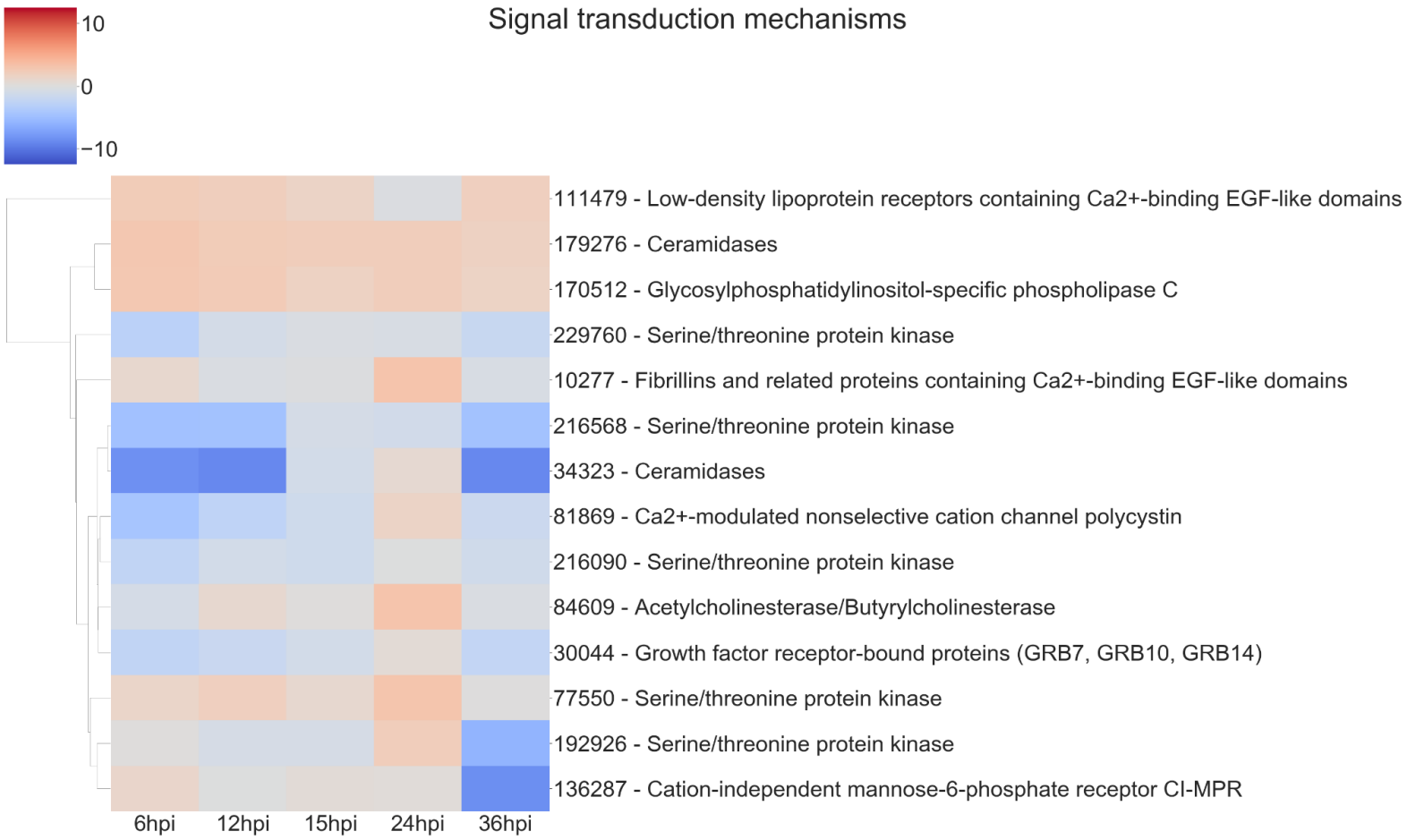

Figure 2. Expression heatmap of genes involved in signal transduction mechanisms.

Carbohydrate transport and metabolism

At 6 hpi, there was significant downregulation of DEGs involved in carbohydrate transport and metabolism by the fungus (Figure 1a). The number of up and downregulated carbohydrate transport and metabolism genes remained largely unchanged until 24 hpi, when there was a spike in the number of upregulated genes, followed by a dip and corresponding spike in downregulated genes at 36 hpi (Figure 1a and 1b). There were five chitinases identified (111866, 77608, 52335, 53606, and 66683; Figure 3). A LysM domain was present in 66683, which was largely downregulated during the interaction, but was induced at 24 hpi. Three of the five chitinases identified (52335, 111866, and 53606) belonged to the glycosyl hydrolase 18 family. Interestingly, these three chitinases showed quite different patterns of expression from one another. 111866 was mostly upregulated throughout the sampled times, whereas 52335 and 53606 were mostly downregulated. 43166, a putative sucrose transporter, showed upregulation at every timepoint except 24 hpi, where it was downregulated.

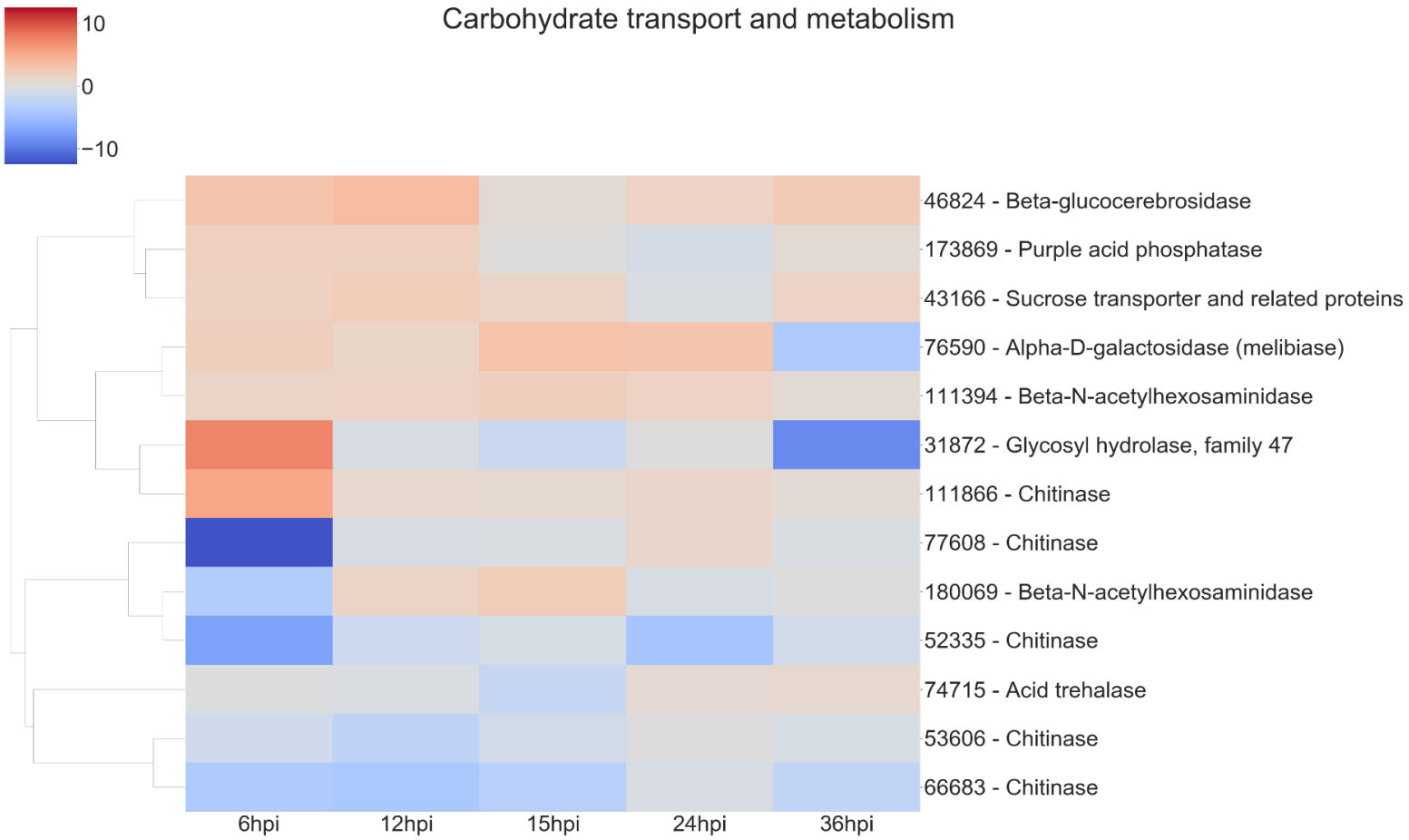

Figure 3. Expression heatmap of genes involved in carbohydrate transport and metabolism.

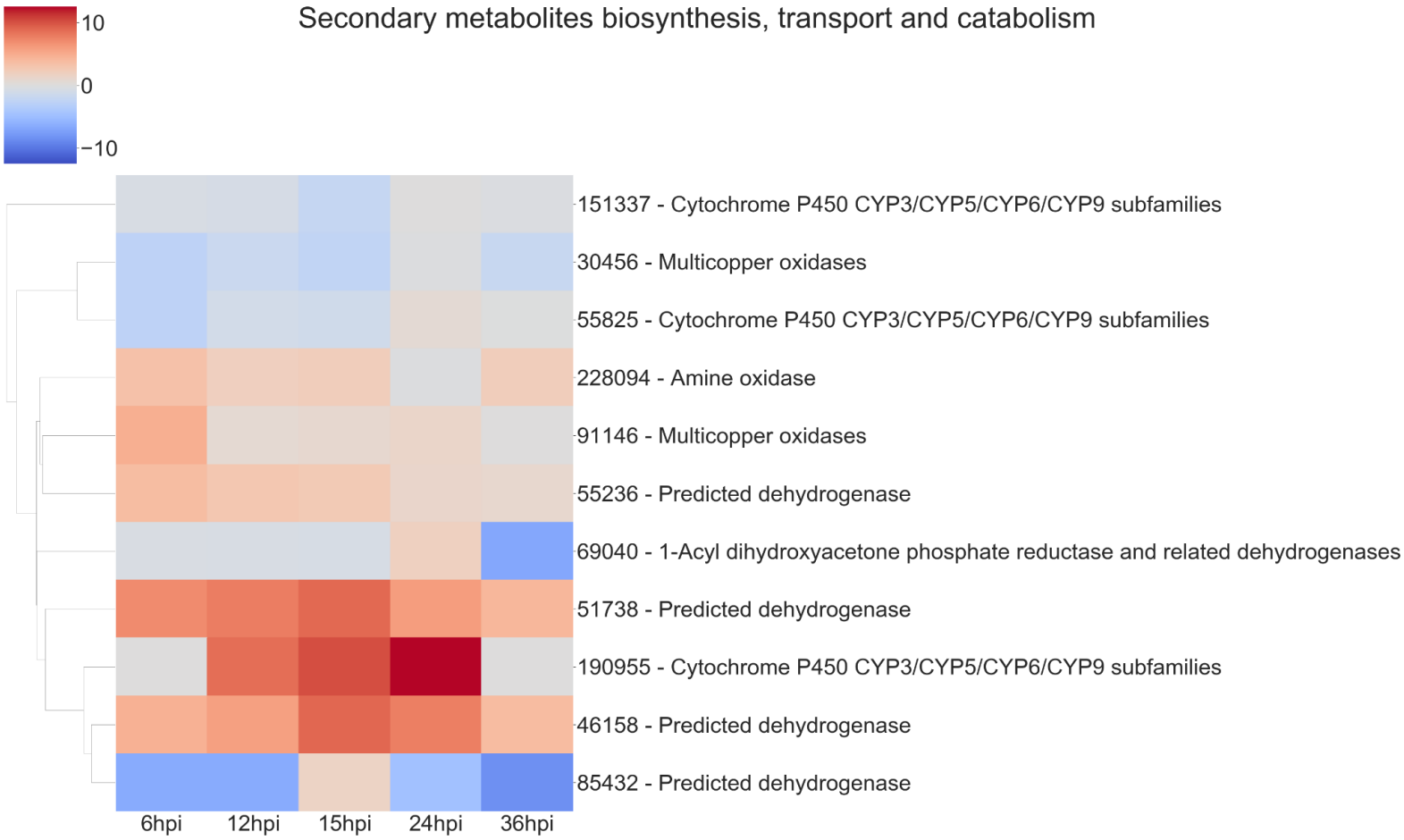

Figure 4. Expression heatmap of genes involved in secondary metabolism.

Secondary metabolism

Intriguingly, the expression pattern of secondary metabolism related genes was similar to that of signal transduction mechanism genes, where the number of upregulated genes gradually increased between 6 and 24 hpi, followed by a sharp decrease (Figure 1b). DEGs in this category were largely dehydrogenases (46158, 51738, 85432, and 55236) and cytochrome P450s (151337, 55825, and 190955). There were also multicopper oxidases (91146 and 30456) and an amine oxidase (228094) that could be associated with nutrient scavenging (Figure 4).

Defense mechanisms

DEGs associated with defense mechanisms remained largely upregulated throughout the time course (Figure 1a and 1b). The three DEGs in this category were two von Willebrand factor/coagulation proteins (207931 and 204989) and a putative myrosinase precursor (113721, Figure 5).

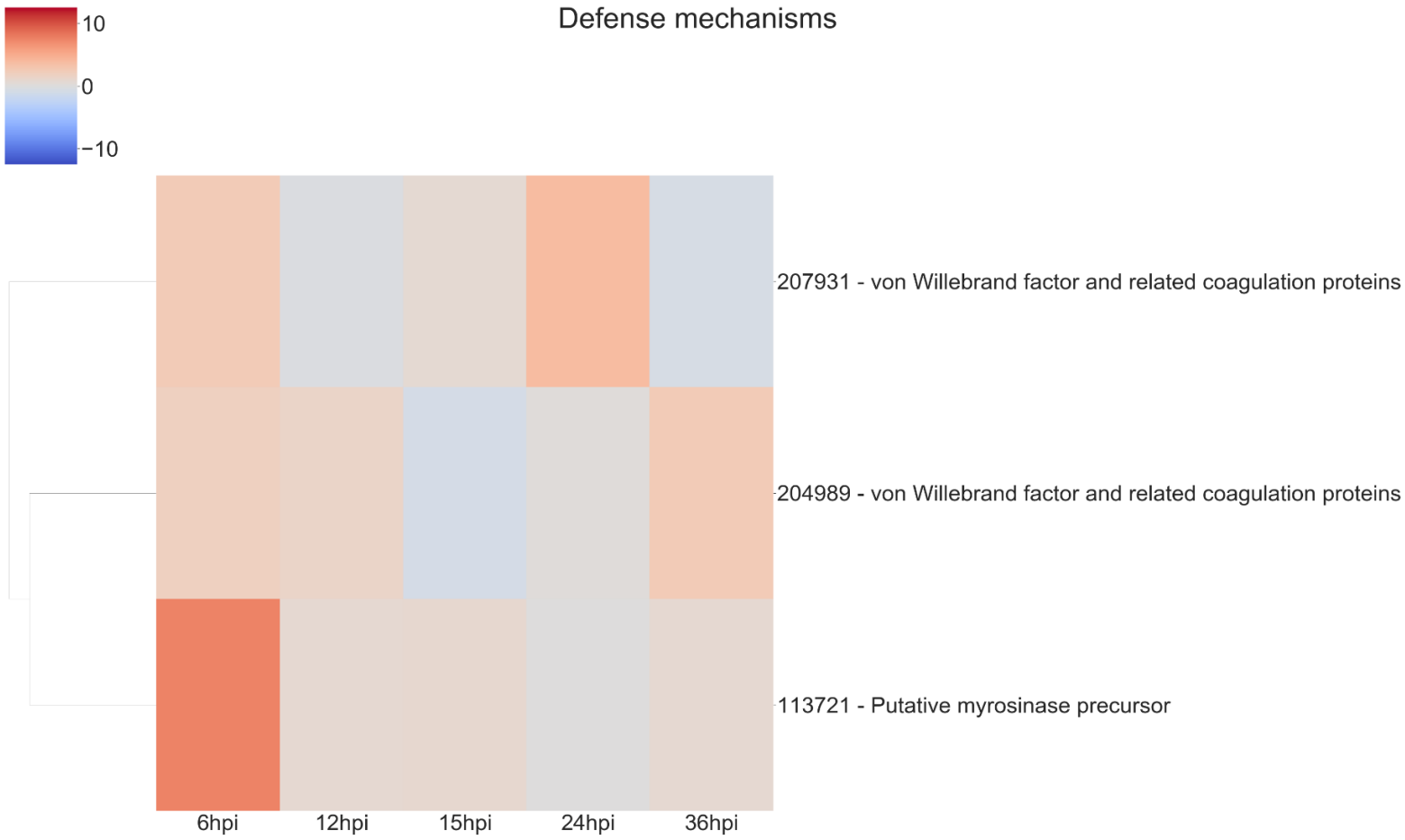

Figure 5. Expression heatmap of genes involved in defense mechanisms.

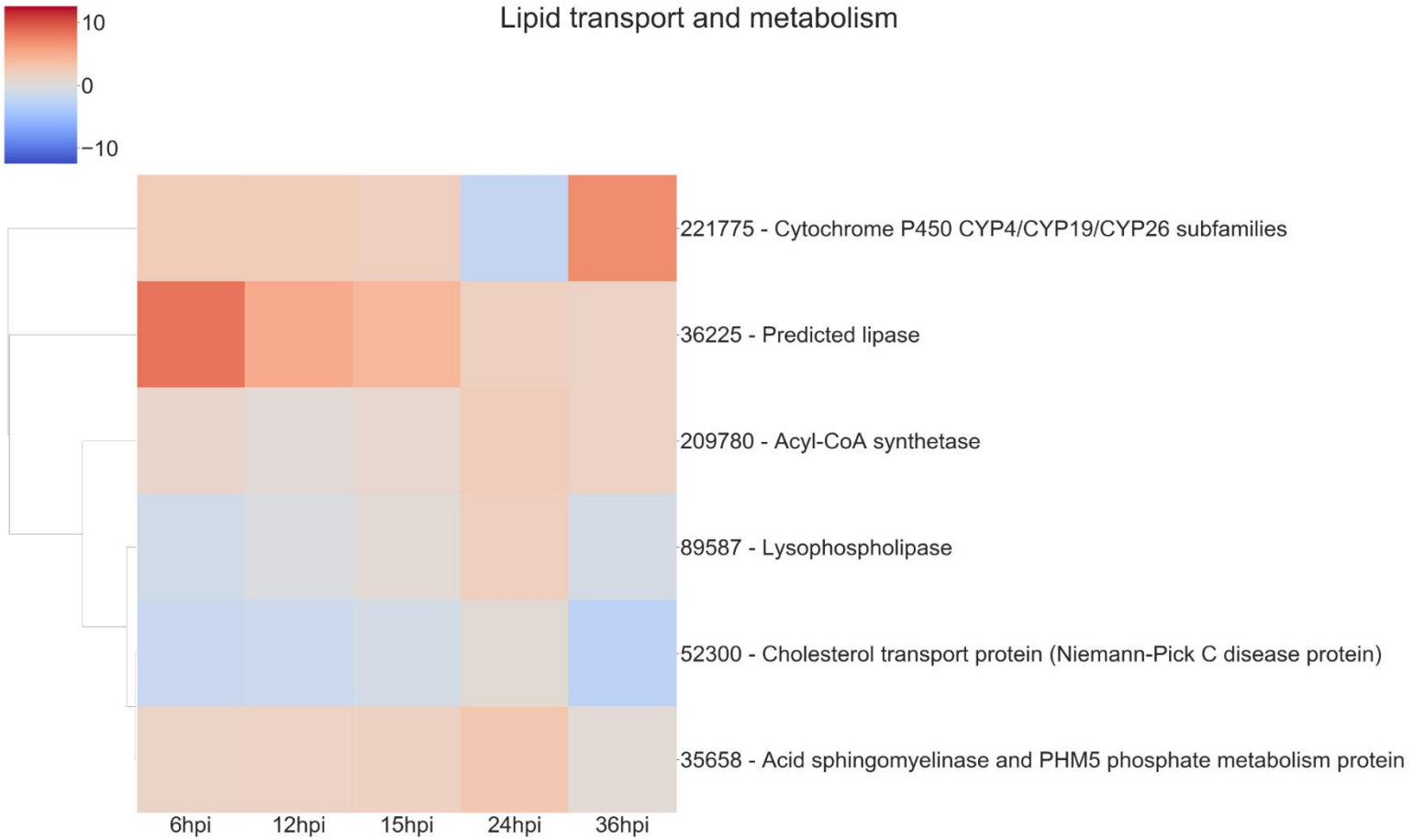

Figure 6. Expression heatmap of genes involved in lipid transport and metabolism.

Lipid transport and metabolism

Lipid transport and metabolism related genes followed a similar pattern as defense mechanism related genes, with four upregulated DEGs at 6, 12, and 36 hpi, and five upregulated genes at 15 and 24 hpi (Figure 1a and 1b). Interestingly, one of the DEGs was a cytochrome P450 (221775), while the rest were lipases (36225 and 89587), cholesterol transport (52300), and other cell membrane associated enzymes (35658 and 209780; Figure 6). The cytochrome P450, 221775, was moderately upregulated throughout the interaction, until 24 hpi, where it was moderately downregulated followed by strong induction at 36 hpi. 36225, a predicted lipase, was highly upregulated at 6 hpi, and remained upregulated throughout the time course, but with a lower magnitude as time passed.

Energy production and conversion

Genes associated with energy production and conversion were largely downregulated across the time course (Figure 1a and 1b). At 6 and 12 hpi, a protein containing the FAD binding domain (227182) was highly upregulated, but expression returned roughly to that of the WT fungus alone from 15 to 36 hpi (Figure 7). Another protein with a FAD binding domain (126766) showed a remarkably different expression pattern of downregulation throughout the interaction with a spike in expression at 24 hpi. 85732, a glycerol-3-phosphate dehydrogenase, showed a similar pattern of expression to 126766.

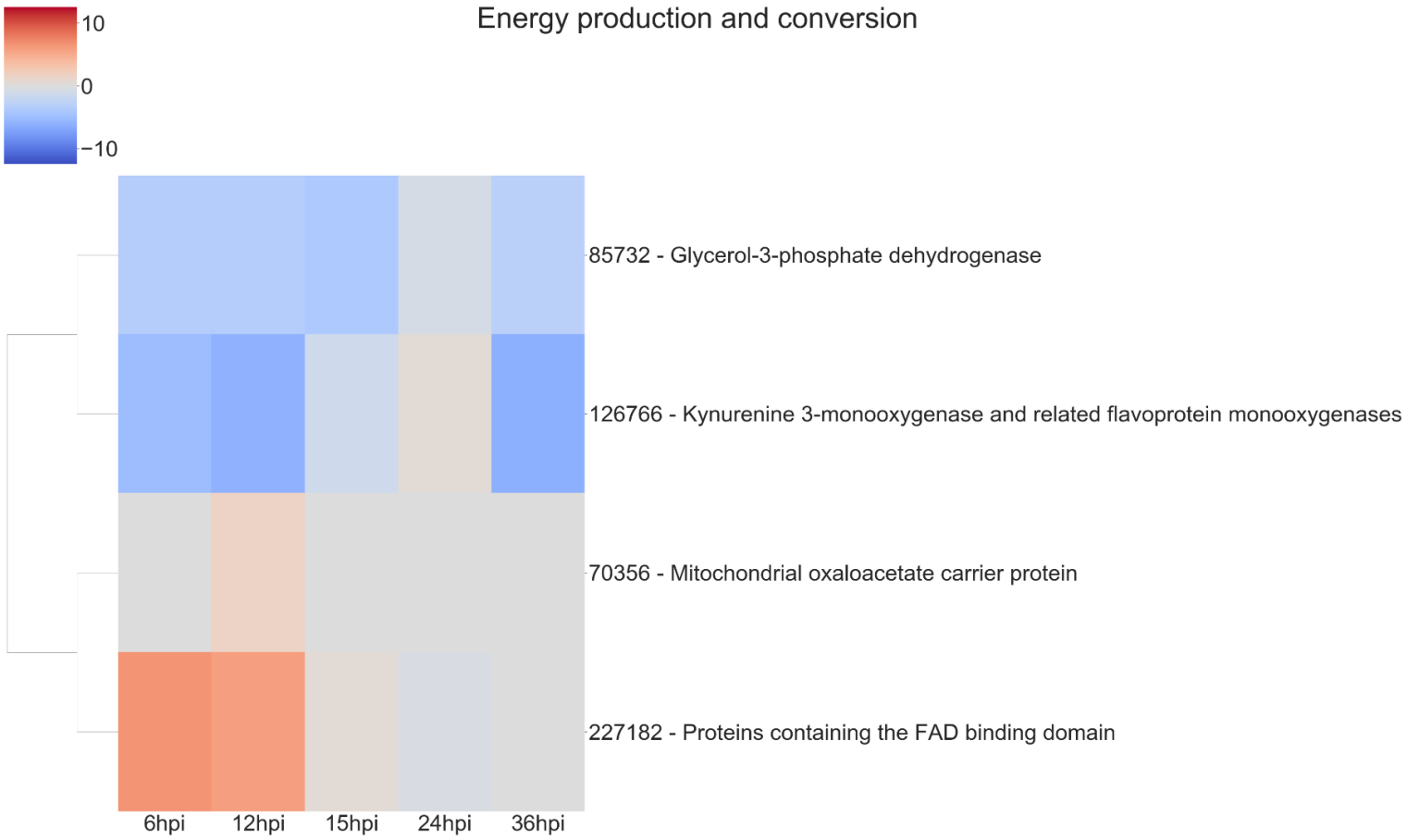

Figure 7. Expression heatmap of genes involved in energy production and conversion.

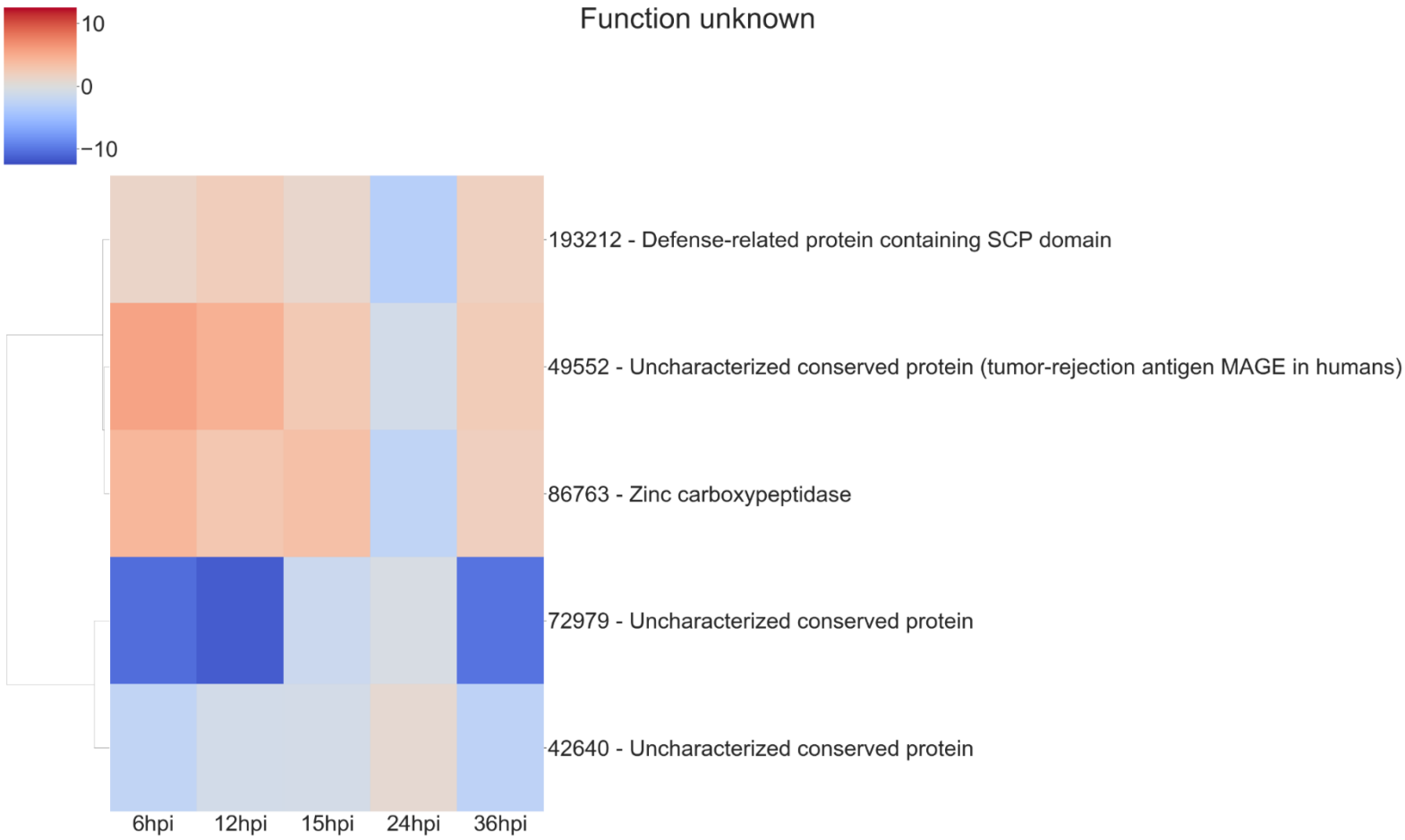

Figure 8. Expression heatmap of genes with unknown functions.

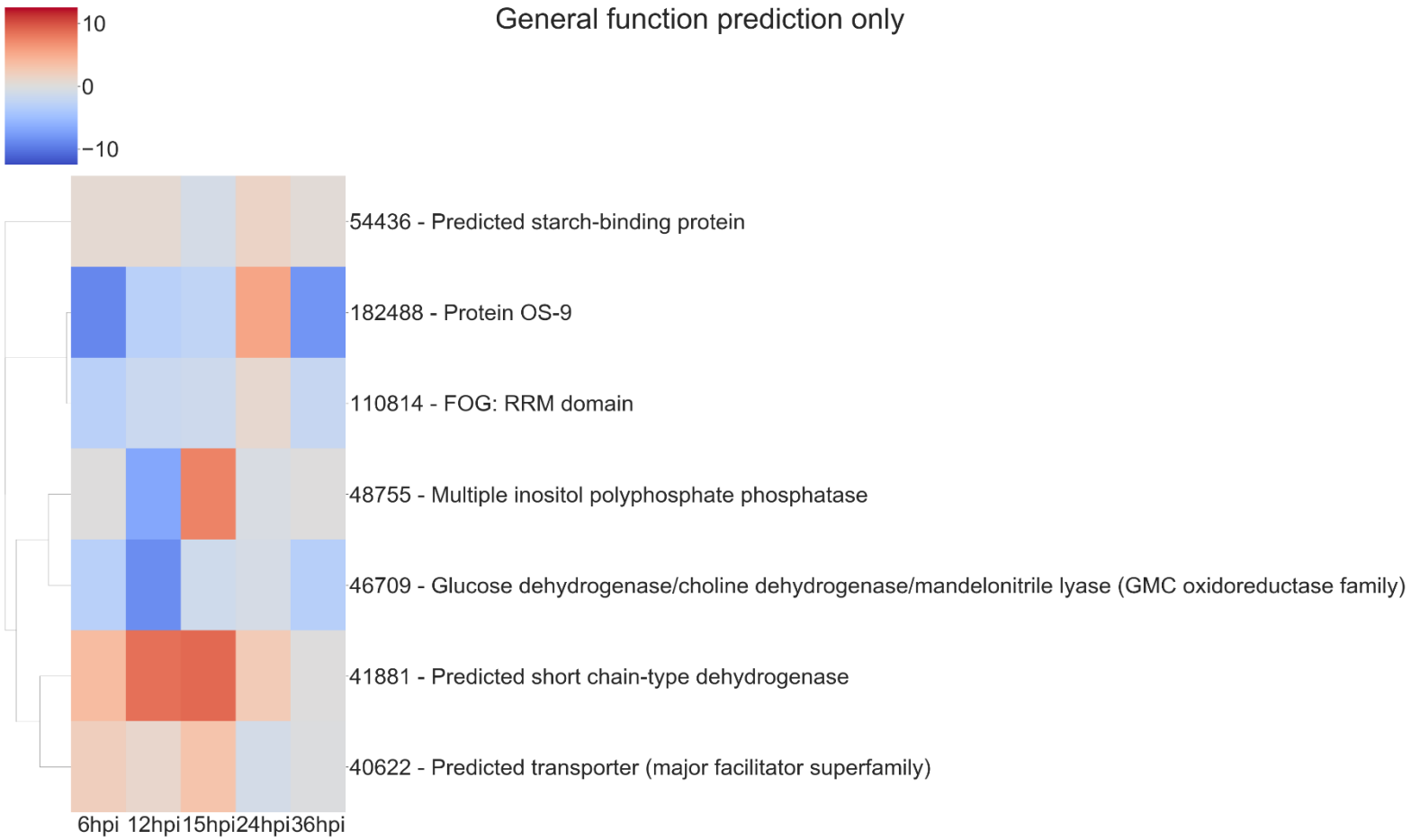

Figure 9. Expression heatmap of genes with only general function predictions.

General function prediction and function unknown

The genes in these categories have no known function or a very broad general function prediction. Their expression does not follow a consistent pattern (Figure 1a and 1b). However, these classes still contain interesting DEGs (Figure 8 and 9). A notable DEG was a defense related protein containing the SCP domain (193212) that was upregulated at all time points except for 24 hpi, where it was significantly downregulated (Figure 8). 72979 was highly downregulated at 6, 12, and 36 hpi, with a peak in expression at 24 hpi. This gene was annotated as a putative stress response protein. A predicted short chain dehydrogenase (41881) showed significant upregulation of approximately 10 log2fold change at 12 and 15 hpi, which breaks from the pattern generally observed of a peak in differential expression at 24 hpi.

Gene network analysis and target enrichment

A gene co-expression network was developed from the normalized read counts of the time course dataset to potentially identify "hub" genes with increased likelihood of a phenotypic effect in plant-microbe interactions. On its own, the co-expression network provides little insight due to its sheer size (Figure 10). Therefore, a method of clustering secreted genes for correlation with the network was utilized. This method used a 3-dimensional principal component analysis matrix to cluster genes (Figure 11). The generated co-expression network was queried for the centrality of each gene in each of the 18 clusters. The most central gene in each cluster was selected as a putative target for study of plant-fungus interactions.

Target selection from clustering

Each unique gene in the list of putative targets was examined for putative function, domains, expression in other datasets, and putative subcellular localization (Table 1). One of the identified targets was the characterized elicitor SM2 (111830). This protein has been demonstrated to have roles in both ISR and root colonization. Additionally, there are other putative targets that have a high likelihood of a large phenotypic impact due to predicted characteristics (i.e. secretion signals, gene ontology, kogg categories, etc.) and previously reported experimental data. Six out of the 18 enriched targets were small, secreted cysteine-rich proteins (70780, 111642, 93159, 111830, 110875, and 58093), a trait commonly found in effector proteins. 50666 was previously isolated from the apoplast of maize plants treated with *T. virens*, though its function is unknown (Nogueira-Lopez *et al.*, 2018). 214993 was found to contain a family 9 carbohydrate binding domain associated with cellulase activity. In addition to the method described, the network was queried for the gene with the highest degree, or largest number of connections. This revealed the previously identified, but uncharacterized gene *MRSP1*.

Table 1. List of enriched targets as determined by PCA, clustering, and centrality analysis. Gene annotations were included as available.

Gene	Domain
TRIVIDRAFT_220864	NA
TRIVIDRAFT_70780	SSCP
TRIVIDRAFT_32983	Histidine phosphatase
TRIVIDRAFT_50666	predicted bicupin
TRIVIDRAFT_60427	Ribonuclease
TRIVIDRAFT_111642	SSCP
TRIVIDRAFT_83765	NA
TRIVIDRAFT_93159	SSCP
TRIVIDRAFT_59198	RLP-like
TRIVIDRAFT_41881	Predicted short chain-type dehydrogenase
TRIVIDRAFT_111830	**SM2 (known defense elicitor)**
TRIVIDRAFT_110875	SSCP
TRIVIDRAFT_78354	Phospholipase A2
TRIVIDRAFT_70901	Polysaccharide lyase
TRIVIDRAFT_203083	NA
TRIVIDRAFT_58093	SSCP (Killer Toxin KP4)
TRIVIDRAFT_177054	S8 protease inhibitor
TRIVIDRAFT_214993	Contains carbohydrate binding domain

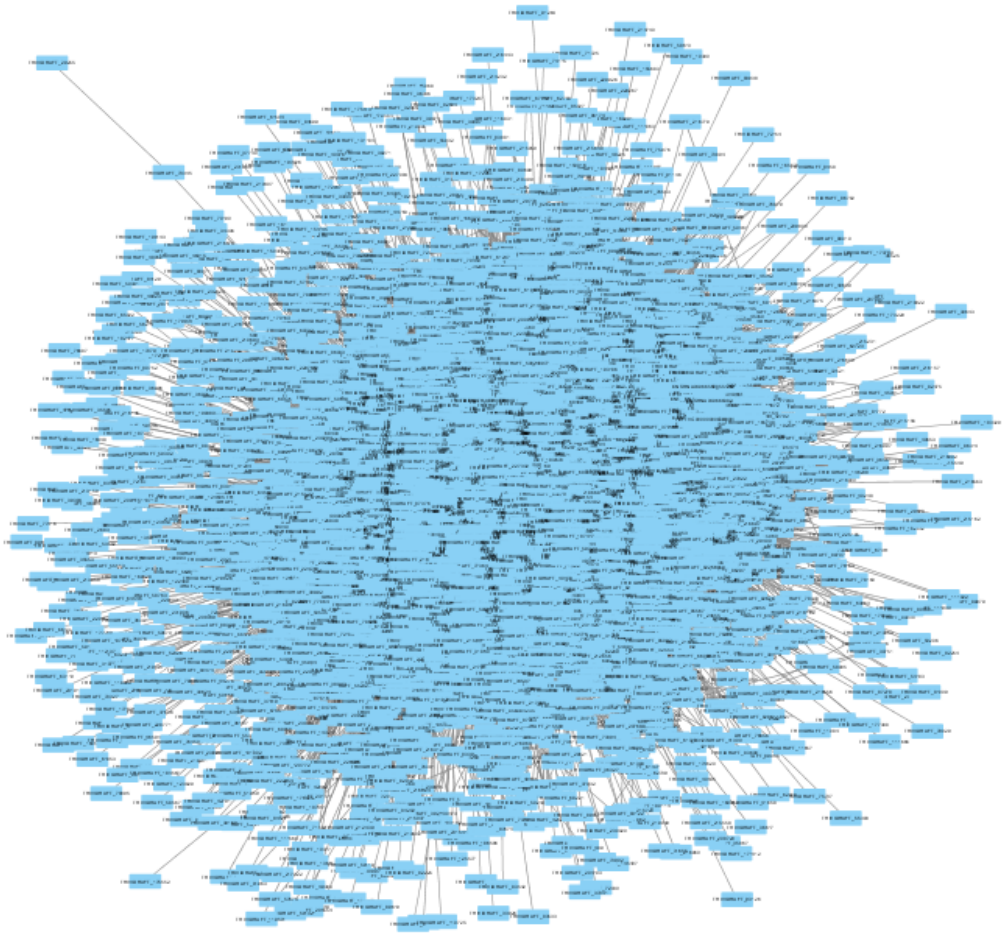

Figure 10. Visualization of the *T. virens* gene co-expression network. Each blue rectangle represents a single gene in the *T. virens* genome. The lines connecting genes, called edges, represent a high likelihood of co-expression.

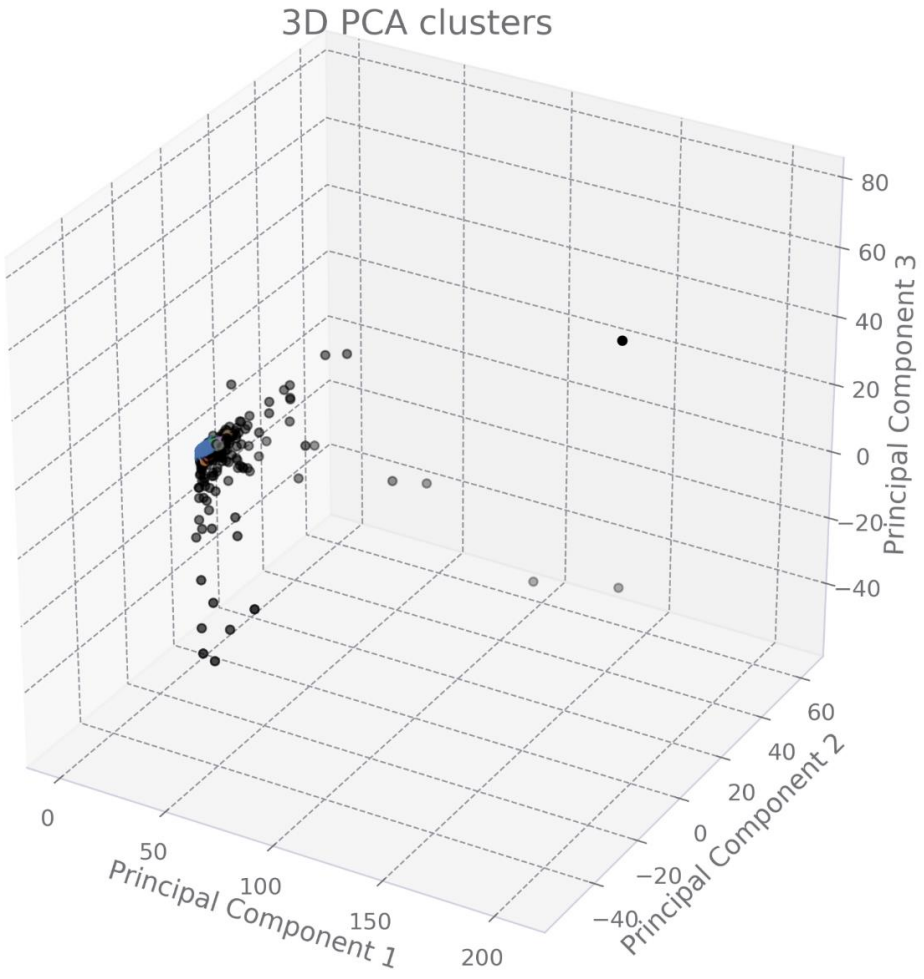

Figure 11. A three-dimensional plot of the top three principal components. Different colors represent different clusters as determined by the DBSCAN algorithm. Many clusters are not visible due to the density of the data points.

Analysis of ΔSm1/ΔSir1 transcriptome data

In addition to the time course dataset, an additional dataset from a previous experiment consisting of the transcriptomic response of *Sm1* and *Sir1* mutant strains in the presence of maize roots at 6 and 30 hpi was analyzed by differential expression analysis

compared to the wild-type fungus in the presence of maize roots. Initial DEG analysis revealed a significantly larger number of unique up and downregulated genes in the *Sir1* mutant compared to the *Sm1* mutant at 6 hpi (*Sir1*: 312 and 99; *Sm1*: 47 and 59; Figure 12). Interestingly, there were a larger number of unique downregulated genes in the *Sm1* strain at 30 hpi (205 vs 89), but *Sir1* had a larger number of unique upregulated genes at 30 hpi (163 vs 93; Figure 12). Heatmap analysis of genes that were either up or downregulated for at least one timepoint showed that many of the genes that were upregulated at 6 hpi were downregulated at 30 hpi, and vice versa (Figure 13).

Many of the 6 hpi downregulated genes in the *Sir1* mutant were annotated as being involved in protein production and modification (Figure 14a). There was also a decrease in genes categorized as signal transduction and defense mechanisms. The 6 hpi downregulated genes in the *Sm1* mutant mostly were involved in carbohydrate transport/metabolism and energy production (Figure 14a). Both mutants had a large number of genes that only had general function predictions.

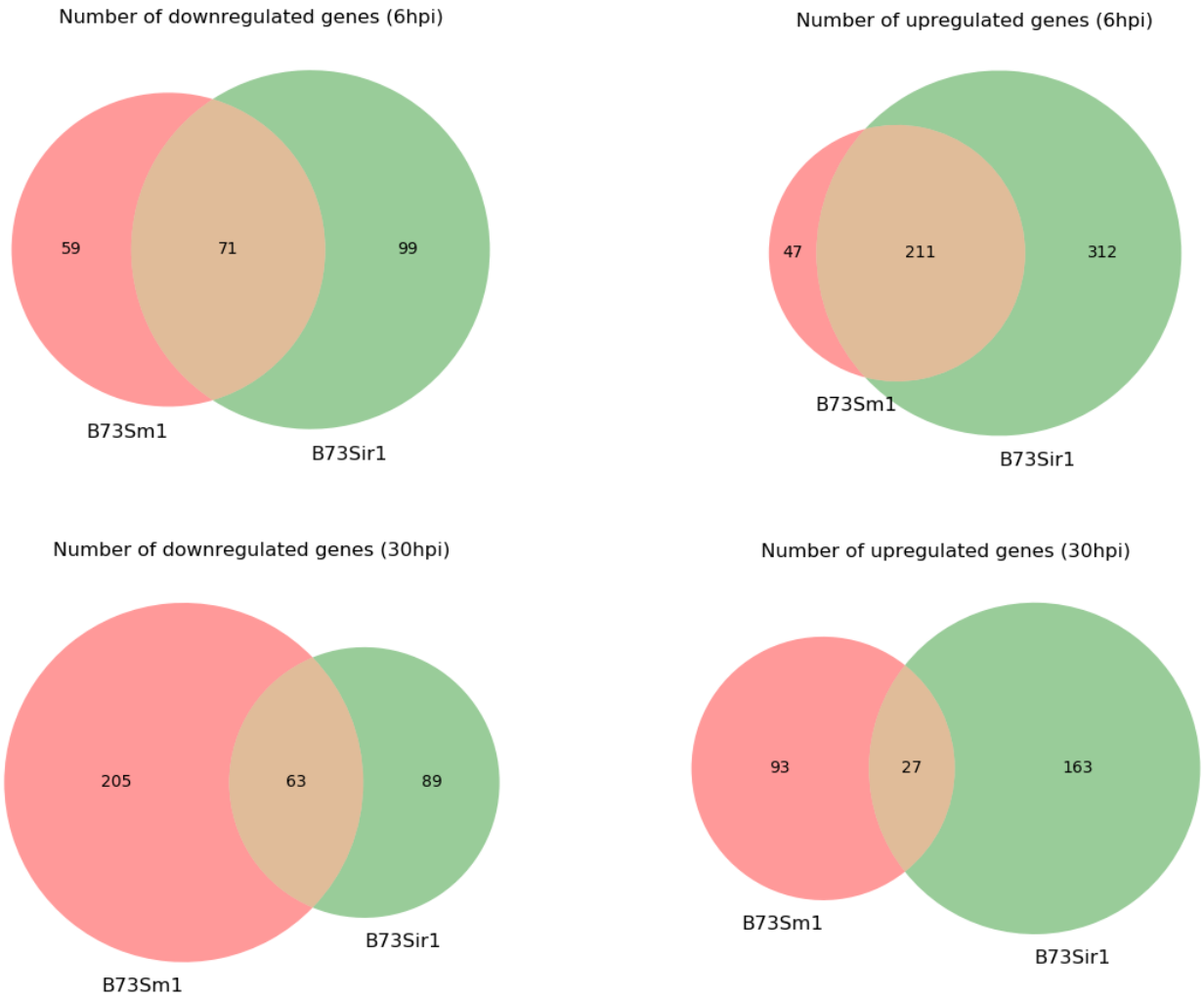

Figure 12. The number of unique genes differentially expressed in Sm1 or Sir1 deletion mutants at 6 and 30 hpi.

In contrast to the genes that were downregulated in the *Sm1* mutant at 6 hpi, the Sir1 mutant had a large number of carbohydrate transport/metabolism genes upregulated at 6 hpi (Figure 14b). There were also a significant number of signal transduction mechanism, secondary metabolism, and general function prediction genes upregulated at 6 hpi in the *Sir1* mutant.

The 30 hpi genes downregulated in the *Sm1* mutant was similar in both number and category to the *Sir1* mutant at 6 hpi: many genes involved in protein production and modifications (Figure 14c). The *Sir1* mutant displayed a spike in the number of signal transduction mechanism genes downregulated at 30 hpi (Figure 14c). Again, both mutants had a significant number of genes with only general function predictions downregulated at 30 hpi.

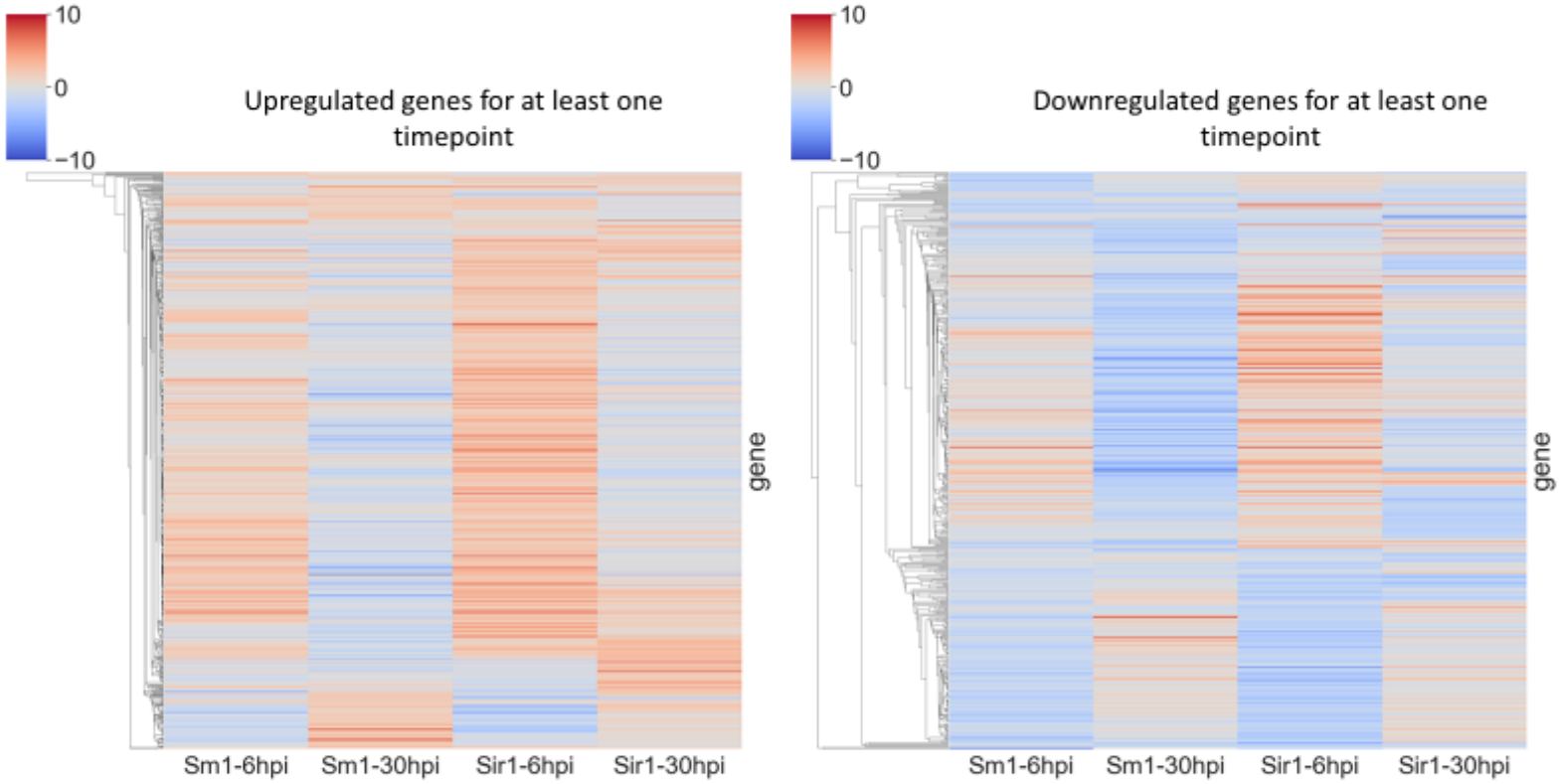

Figure 13. Heatmap comparison of differential gene expression from Sm1 or Sir1 mutants at 6 and 30 hpi.

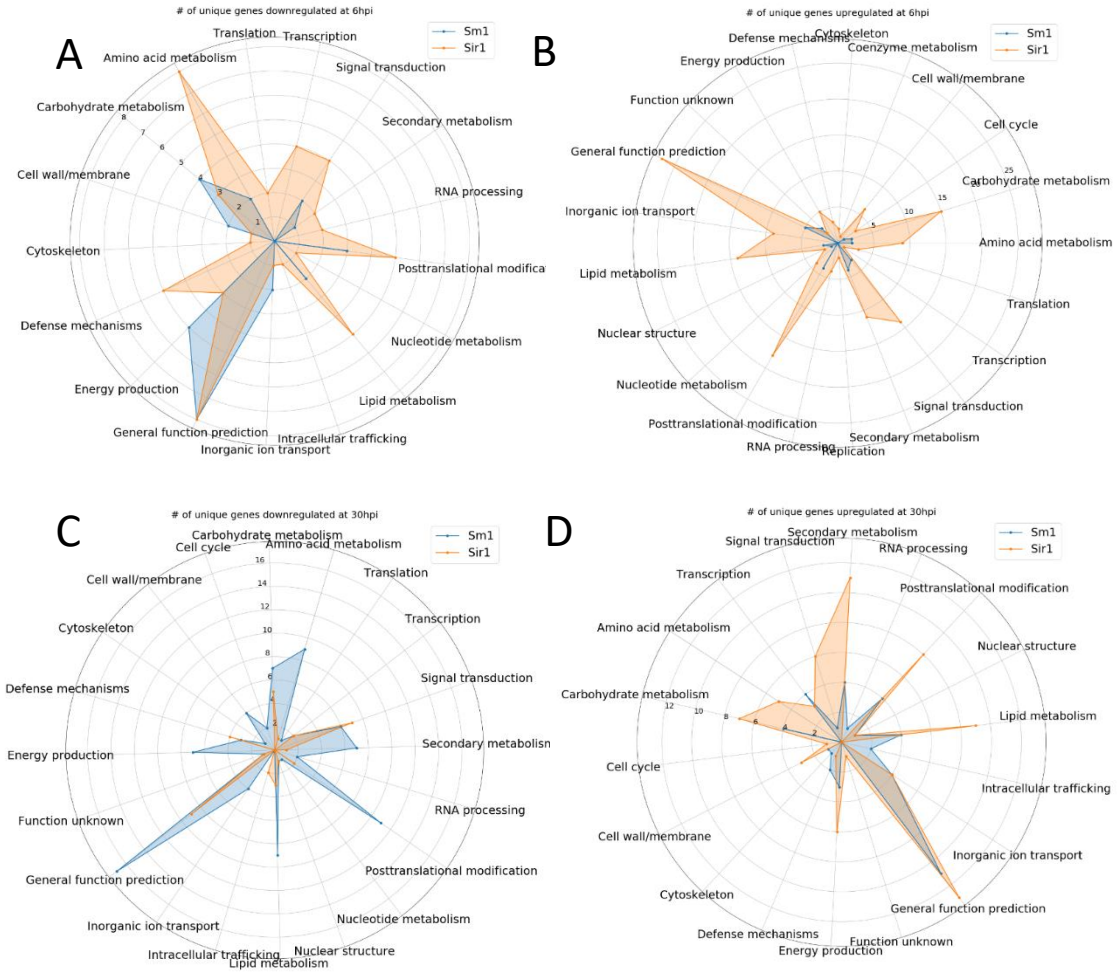

Figure 14. The number of unique genes up or downregulated in each strain at 6 or 30 hpi. Gene annotation categories were not filtered. Only those with at least one unique gene were included for comparison.

The pattern of upregulated *Sir1* mutant genes at 30 hpi is mostly similar to 6 hpi; however, there was a notable increase in the number of genes involved in energy production (Figure 14d). The *Sm1* mutant had a higher number of upregulated genes involved in transcription at this time point (Figure 14d). As with most of the other comparisons, there were a significant number of upregulated genes with general function predictions for each mutant at 30 hpi.

For all comparisons, there were a large number of unique genes with only general function predictions. These genes were examined in more detail. The majority of 6 hpi downregulated *Sir1* mutant genes were predicted to be major facilitator superfamily transporters, whereas the majority for the *Sm1* mutant were broad substrate reductases (Table 2). The *Sir1* mutant had a large number of predicted zinc-finger proteins upregulated at 6 hpi. In addition, there were many metal-dependent hydrolases, predicted hydrolases, and major facilitator superfamily transporters also upregulated in the *Sir1* mutant (Table 3). There were very few unique *Sm1* genes upregulated at 6 hpi, and no discernable pattern to the annotations (Table 3).

Table 2. Downregulated general function genes at 6hpi.

Downregulated genes 6hpi	# DEGs in category	
Predicted function	ΔSm1	ΔSir1
Aldehyde reductase	1	0
Aldo/keto reductase family proteins	1	0
FOG: Ankyrin repeat	1	1
FOG: RRM domain	0	1
Glucose dehydrogenase/choline dehydrogenase/mandelonitrile lyase (GMC oxidoreductase family)	0	1
Predicted dehydrogenase	1	0
Predicted fumarylacetoacetate hydralase	1	0
Predicted transporter (major facilitator superfamily)	1	3
Reductases with broad range of substrate specificities	2	1
Synaptic vesicle transporter SVOP and related transporters (major facilitator superfamily)	0	1

Sm1 mutants had a significant number of predicted transporters and other metabolism related genes that were downregulated at 30 hpi (Table 4). *Sir1* mutants followed a similar pattern, but to a lesser degree (Table 4).

Genes that were upregulated at 30 hpi for both *Sm1* and *Sir1* were mostly annotated as transporters of different varieties (Table 5). *Sir1* mutants also had several hydrolases and methyltransferases upregulated at this time point (Table 5).

Table 3. Upregulated general function genes at 6hpi.

Upregulated genes 6hpi	# DEGs in category	
Predicted function	ΔSm1	ΔSir1
Aldehyde reductase	0	1
C4-type Zn-finger protein	0	1
FOG: Zn-finger	0	4
Glucose dehydrogenase/choline dehydrogenase/mandelonitrile lyase (GMC oxidoreductase family)	0	1
Glyoxylase	0	1
Hydroxyindole-O-methyltransferase and related SAM-dependent methyltransferases	1	0
Large RNA-binding protein (RRM superfamily)	0	1
Monodehydroascorbate/ferredoxin reductase	0	1
Multifunctional pyrimidine synthesis protein CAD (includes carbamoyl-phophate synthetase, aspartate transcarbamylase, and glutamine amidotransferase)	1	0
Predicted Zn-finger protein	0	1
Predicted fumarylacetoacetate hydralase	0	1
Predicted hydrolases or acyltransferases (alpha/beta hydrolase superfamily)	0	2
Predicted kinase	0	1
Predicted metal-dependent hydrolase of the TIM-barrel fold	0	3
Predicted short chain-type dehydrogenase	1	0
Predicted transporter (major facilitator superfamily)	0	3
Reductases with broad range of substrate specificities	1	2
Synaptic vesicle transporter SV2 (major facilitator superfamily)	0	1
Synaptic vesicle transporter SVOP and related transporters (major facilitator superfamily)	1	2
WD40 repeat-containing protein	0	1

Table 4. Downregulated general function genes at 30hpi.

Downregulated genes 30hpi	# DEGs in category	
Predicted function	ΔSm1	ΔSir1
Acetyltransferase, (GNAT) family	1	0
FAD-dependent oxidoreductase	1	0
FOG: Ankyrin repeat	0	1
FOG: RRM domain	0	1
FOG: Transposon-encoded proteins with TYA, reverse transcriptase, integrase domains in various combinations	1	0
FOG: Zn-finger	0	1
Glucose dehydrogenase/choline dehydrogenase/mandelonitrile lyase (GMC oxidoreductase family)	2	1
Hydroxyindole-O-methyltransferase and related SAM-dependent methyltransferases	1	0
Metallopeptidase	1	0
Predicted ATPase	0	1
Predicted NAD-dependent oxidoreductase	1	0
Predicted metal-dependent hydrolase of the TIM-barrel fold	1	0
Predicted steroid reductase	2	0
Predicted transporter (major facilitator superfamily)	3	2
Reductases with broad range of substrate specificities	1	1
Synaptic vesicle transporter SVOP and related transporters (major facilitator superfamily)	2	1

Table 5. Upregulated general function genes at 30hpi.

Upregulated genes 30hpi	# DEGs in category	
Predicted function	ΔSm1	ΔSir1
C2H2-type Zn-finger protein	1	0
FOG: Ankyrin repeat	1	0
FOG: Zn-finger	1	0
Hydroxyindole-O-methyltransferase and related SAM-dependent methyltransferases	0	2
Large RNA-binding protein (RRM superfamily)	1	0
Multifunctional pyrimidine synthesis protein CAD (includes carbamoyl-phophate synthetase, aspartate transcarbamylase, and glutamine amidotransferase)	1	0
Permease of the major facilitator superfamily	1	0
Predicted haloacid-halidohydrolase and related hydrolases	0	1
Predicted short chain-type dehydrogenase	0	3
Predicted transporter (major facilitator superfamily)	2	4
Reductases with broad range of substrate specificities	1	1
Synaptic vesicle transporter SVOP and related transporters (major facilitator superfamily)	2	2

Discussion

There have been several studies that sought to elucidate fungal transcriptome or proteome during the colonization process in a hydroponic setting (Lamdan *et al.*, 2015a; Morán-Diez *et al.*, 2015; Malinich *et al.*, 2019). All of these studies estimated the colonization process (i.e. growth and ingress within the root) required longer than 24 hours to occur. Our results demonstrate that internal colonization in a setting that favors fungal growth can occur as early as 12 hpi, but more completely by 15 hpi. By bracketing the time points of a transcriptomic study around 15 hpi, an unprecedented level of detail of the colonization process was captured.

Malinich *et al*. analyzed in detail the broad patterns of gene expression exhibited by *T. virens* in the presence of maize (Malinich *et al.*, 2019). This study focused on identifying a subset of genes involved in the interactions between *T. virens* and maize by filtering the differentially expressed genes based on secretion signal predictions and functional annotation.

The upregulation of genes involved in signal transduction appears to coincide with increased fungal colonization. The noted drop in upregulation at 36 hpi may indicate that penetration and maximum growth within the root system has occurred. One of the genes that had a peak between 15 and 24 hpi was annotated as a ceramidase. Ceramidases catalyze the breakdown of ceramide into sphingosine, that, in addition to being a precursor to sphingolipids, may have its own signaling activities (Sayre *et al.*, 2015). Sphingolipids have roles in signaling and cellular organization (Michaelson *et al.*, 2016). Expression of

the putative adhesin gene, 10277, suggests that it may be aiding the attachment of hyphae to plant cell walls. GLEYA domain containing proteins are known to bind to carbohydrates, which adds support to this hypothesis (Willaert, 2018). The expression of other known signal transduction mechanisms increased up to 24 hpi, after which expression dropped off significantly. This suggests that the time between the initiation of hyphal penetration and expansion is critical for plant-fungal interaction, whereas communication seems to decrease after 24 hpi. This conclusion is supported by the expression pattern of a putative CFEM domain protein, 81869. CFEM domain proteins are commonly associated with virulence in pathogenic fungi, however, in the case of *T. virens* they are likely to be involved in colonization (Zhu *et al.*, 2017).

The pattern of carbohydrate transport and metabolism gene expression shows an interesting trend of low numbers of upregulated genes prior to a spike only at 24 hpi. The 24 hpi spike and 36 hpi downregulation coincides with the peak in signaling related genes. Interestingly, the majority of the DEGs in this category were chitinases. One of these chitinases contained a LysM domain (66683). Based on its expression pattern and domain annotation, this protein is likely involved in prevention of the plant PAMP response to chitin. The other chitinases showed varying patterns of expression with little consensus between them. This could be due to regulation of the synergism of chitinases as suggested by Malinich *et al.* (Gutiérrez-Román *et al.*, 2014; Malinich *et al.*, 2019).

Secondary metabolism related genes continue the trend of increasing expression up to 24 hpi and starkly decreasing at 36 hpi. The fungus may be producing a larger number of secondary metabolites during the early phases of colonization in order to defend

against potential competitors. Also, the medium in which the fungus and plants were cultivated favors fungal growth, so the ideal growing conditions may have contributed to production of additional secondary metabolites that were not necessary once internal colonization of the plant had occurred. In addition to the dehydrogenases and cytochrome P450 genes, among the upregulated genes, there were also multicopper oxidases and an amine oxidase that may have contributed to nutrient scavenging (Levasseur *et al.*, 2010).

Defense mechanisms appeared to be largely unchanged throughout the time course, with three identified upregulated DEGs. One of the DEGs was a putative myrosinase precursor. Myrosinases are involved in plant defense against pathogens and herbivores (Szucs *et al.*, 2018). The other two defense related genes upregulated by the fungus were von Willebrand factor domain proteins. Interestingly, proteins in this family are involved in maintaining the health of insect cuticles (Han *et al.*, 2017). Han *et al.* claim that these proteins are often targets of entomopathogenic fungi, so perhaps *T. virens* utilizes these proteins to recruit potential entomopathogenic fungi as a source of nutrition.

The lipid transport and metabolism category was examined to potentially find genes associated with plant lipoxygenase pathways associated with defense and ISR. All of the identified genes appeared to be involved in standard membrane maintenance mechanisms, including a cytochrome P450 gene likely to be involved in ergosterol synthesis (Yoshida, 1988).

A notable gene in the energy production and conversion category was a protein containing a FAD binding domain that was highly upregulated at the very early timepoints (6 and 12 hpi) and then expressed similarly to the wild-type strain afterwards. This gene

was likely involved in the metabolism of a simple sugar such as glucose or sucrose, which were both present in the growth medium (Yoshida *et al.*, 2015). A second FAD binding domain gene showed a completely different pattern of expression: downregulation at every time point with a spike at 24 hpi. These two FAD binding domain genes are likely binding different substrates. It is possible that the second gene is binding a compound only found within the maize apoplast.

There are several genes with annotations in the general function and function unknown categories. One of particular interest is a defense-related protein containing SCP domain. Proteins with this domain have been involved in human and plant defense against fungi (Darwiche *et al.*, 2017). Specifically in plants, the major defense related gene PR-1 is an SCP domain containing protein (Darwiche *et al.*, 2017).

Overall, these data suggest that 24 hpi is a key timepoint in the colonization process and seems to be the point at which symbiosis between the plant and fungus begins and internal expansion by the fungus ceases. Multiple key categories show increasing numbers of upregulated genes up to 24 hpi, after which many genes are downregulated. Heatmap analysis supported this hypothesis, as many of the identified genes showed spikes in either direction of expression at 24 hpi. The next step would be to examine if these same gene patterns exhibited in our hydroponic system are found at any time point in soil systems.

A gene co-expression network was generated from the TMM normalized read counts using Netminer software that had been modified to accept input from HiSAT2. Many coexpression networks are generated using only a single algorithm (Amrine *et al.*,

2015; Sun *et al.*, 2017; Mandal *et al.*, 2020). Netminer is useful as it generates a consensus network from three separate network construction algorithms, thus improving the likelihood of correct correlations.

Principal component analysis (PCA) was utilized to reduce the dimensionality of the dataset from 30 dimensions down to the top three dimensions that account for the largest amount of variance in the dataset. The top three principal components were used to cluster genes into groups that were expressed similarly. This clustering step allowed for additional dimensional reduction by limiting the number of genes that were being analyzed at a time. Each gene in each cluster was queried against the generated network to identify its betweenness centrality. Betweenness centrality is the measure of distance between a node (gene) and every other node in the network. Those with the shortest distance values are assigned a higher score. The genes with the highest score in each cluster were selected as putative enriched targets for future study. This analysis operates on the assumption that a node/gene with a higher centrality score will be more important to the network, and its removal will induce large phenotypic changes. Nearly 40% of the enriched targets identified by this analysis would not have been found using the rack-and-stack method previously employed in our laboratory.

One of the most important targets revealed by this analysis pipeline was 111830 or *Sm2*. This gene has been previously demonstrated as having roles in both colonization and induced systemic resistance, and is a paralog of the well-known elicitor *Sm1* (Crutcher *et al.*, 2015; Gaderer *et al.*, 2015). The identification of *Sm2* as a target by this pipeline demonstrates its effectiveness in enriching target gene selections.

Another promising candidate that has not previously been characterized is 50666. This protein was previously found in maize root apoplastic space, in the same region as Sm1 (Nogueira-Lopez *et al.*, 2018). The algorithmic identification of 50666 as an enriched target and its demonstrated presence in plant apoplastic spaces bolsters the efficacy of the presented pipeline.

Additionally, one-third of the enriched targets were small, secreted cysteine-rich proteins. Most effectors and elicitors share this trait, including SM1 and SM2. The likelihood of the involvement of these types of proteins in plant-microbe interactions is high (Lu and Edwards, 2016; Wang *et al.*, 2020a). Another common trait in proteins involved in plant-microbe interactions is the carbohydrate binding domain. This analysis revealed a gene (214993) whose only annotation was a carbohydrate binding domain. Many elicitors and effectors contain this domain and, in some instances, cannot function properly without it (Djonović *et al.*, 2006a; Djonović *et al.*, 2007; Brotman *et al.*, 2008).

Based on the traits discussed here, this pipeline is a very promising tool for the enrichment of targets involved in plant-microbe interactions. We are currently conducting characterization experiments with several of the genes listed in Table 1 for confirmation of roles in the *T. virens*-maize interaction.

As strains of *T. virens* are noted for their ability to induce host defense responses, we sought to analyze a transcriptomic study that incorporated a mutant that lacked the elicitor SM1 and a mutant that enhanced ISR (*ΔSir1*). Interestingly, *Sir1* mutants showed a significantly larger change in expression patterns compared to *Sm1* mutants. This was unexpected as we had hypothesized that *Sm1* had a larger role than *Sir1* in plant-fungal

interactions. Based on this analysis, it would appear that *Sir1* actually regulates much of the fungal response to the presence of the plant. Also, it is possible that many of the DEGs in this mutant were due to overexpression of the *Sm1* gene as shown in Wang *et al.* (2020). Many of the DEGs in the *Sir1* mutant were involved in signaling, transport, carbohydrate metabolism, and secondary metabolism. *Sm1* displayed significant changes to downregulated gene expression at 30 hpi, and intriguingly the expression pattern was similar to that of the *Sir1* mutant at 6 hpi. *Sir1* protein production has been previously demonstrated to be significantly reduced in the presence of maize roots, and plants treated with deletion mutants exhibited smaller foliar lesions upon pathogen attack (Lamdan *et al.*, 2015b). However, another "sir" group protein, 92810, was found in the apoplast of maize roots (Nogueira-Lopez *et al.*, 2018). This protein had a similar reduction in abundance and mutant phenotype as *ΔSir1* (Lamdan *et al.*, 2015b). Based on these similarities, SIR1 may also be present in the apoplast or even translocated into maize cells and unable to be liberated by the methods used in Nogueira-Lopez *et al.* Alternatively, SIR1 may remain outside of the plant apoplast and serve as a signaling protein, where it can induce a response from the plant causing the cascade of gene expression observed in this study.

Another interesting pattern was observed during heatmap analysis where genes that were up or downregulated at one time point would behave oppositely at the other timepoint (Figure 13). This could be due to the length of time between the time points (6 and 30 hpi). The early period time course demonstrated that much of the interaction occurs between 6-24 hpi, with significant changes in expression at 36 hpi. The combination of

this dataset with the time course dataset generated in this study would substantially increase the predictive power of the gene co-expression network and target enrichment pipeline.

In conclusion, our results here demonstrate that the early phases of colonization are important for the establishment of symbiosis between the plant and fungus. Additionally, further work is planned to characterize several of the targets generated from our pipeline, starting with the putative bicupin protein, 50666. These mutants will be characterized for their ability to colonize maize roots and induce systemic resistance against a foliar pathogen. Finally, *Sir1* appears to be the major regulator of the fungal response to the presence of a potential host. These findings provide the basis for future studies into the response of *T. virens* when establishing a symbiotic relationship with a potential plant host.

CHAPTER III

A CLASS I HYDROPHOBIN IN *TRICHODERMA VIRENS* INFLUENCES PLANT-MICROBE INTERACTIONS THROUGH ENHANCEMENT OF ENZYME ACTIVITY AND MAMP RECOGNITION

Introduction

The filamentous plant symbiotic fungus *Trichoderma virens* is recognized for its ability to colonize plant roots and provide benefits to its hosts through the induction of systemic resistance, protection against fungal root pathogens, and growth promotion (Howell, 1987; Pieterse *et al.*, 2014; Saldajeno *et al.*, 2014). During the colonization process, a large number of secreted fungal proteins are involved in the subroutines of evading the plant defenses, initially penetrating roots, and fungal growth within the root system by hyphal expansion (Djonović *et al.*, 2006a; Morán-Diez *et al.*, 2015; Lamdan *et al.*, 2015b). In addition to fungal proteins that are secreted into intercellular spaces, others localize to the outer cell wall of the fungus. Here they can serve a wide variety of functions such as receptors for specific stimuli, protect against antimicrobial compounds, and aid in physical interactions including attachment to surfaces (Zampieri *et al.*, 2010; Bignell, 2012; Kim *et al.*, 2016; Correia *et al.*, 2017). Much effort has been extended to discover and understand proteins involved in *Trichoderma*-plant interactions, with a major emphasis on small, secreted cysteine-rich proteins hypothesized to function as effectors (Lamdan *et al.*, 2015a; Morán-Diez *et al.*, 2015; Guzmán-Guzmán *et al.*, 2017; Ramírez-Valdespino *et al.*, 2019). The best-known example of this type of protein is SM1, which belongs to the cerato-platanin family and is required for induced systemic resistance (ISR)

mediated by *T. virens* (Djonović *et al.*, 2006a; Djonović *et al.*, 2007). In sharp contrast, the role of other protein families in *Trichoderma*-plant interactions are much less understood. Of these families, hydrophobin proteins are of particular interest due to their diverse suite of functions.

Hydrophobins are small cysteine-rich, secreted proteins that self-assemble at hydrophilic/hydrophobic interfaces (Wösten, 2001) and are unique to fungi. They contain a conserved motif of cysteine residues, which suggest they may act as effectors involved in plant-fungal interactions (Ruocco *et al.*, 2015; Guzmán-Guzmán *et al.*, 2017). As secreted proteins, hydrophobins are highly variable in function. Some hydrophobins may cover the surface of spores of fungal pathogens, helping to evade host defenses (Bayry *et al.*, 2012). Others may aid fungal morphogenesis by enabling hyphae to penetrate air/water interfaces. The unique properties of hydrophobins are suited for a variety of applications in industrial and scientific techniques. The fusion of a hydrophobin to a protein of interest can significantly boost the yield of the purified protein (Joensuu *et al.*, 2010; Mustalahti *et al.*, 2013). Hydrophobins are also industrially used as emulsifiers and agents to alter surface characteristics of substrates (Bayry *et al.*, 2012).

Hydrophobins are currently organized into two classes (I and II) based on solubility, the spacing between cysteines, and hydrophobicity (Wösten, 2001). Class II hydrophobins are more soluble than class I and have more conserved spacing between cysteines, whereas class I hydrophobins are very insoluble, requiring harsh acids to dissolve, and can have highly variable cysteine spacing (Wösten and de Vocht, 2000; Wösten, 2001; Bayry *et al.*, 2012). Class I hydrophobins typically localize to the outer cell

wall of fungal hyphae and/or spores where they form monolayers or self-assemble into amyloid fibrils. This differs from class II hydrophobins, which tend to be freely secreted into the environment. A limited number of hydrophobins from other *Trichoderma* species have been functionally characterized. A class I hydrophobin, TASHYD1 from *T. asperellum,* was found to aid in the attachment of conidia and hyphae to roots for more efficient colonization of cucumber plants (Viterbo and Chet, 2006). A class II hydrophobin, HYTLO1 from *T. longibrachiatum,* was shown to exhibit direct antifungal effects and induce systemic resistance when applied to plant leaves (Ruocco *et al.*, 2015). Additionally, a class II hydrophobin from *T. virens* was demonstrated to have a role in root colonization and mycoparasitism activity (Guzmán-Guzmán *et al.*, 2017). Class I hydrophobins have been identified in *T. virens,* but are fewer in number (three) than class II hydrophobins (eight), and no distinctive role in plant interactions has been demonstrated (Seidl-Seiboth *et al.*, 2011). One class I hydrophobin, HFB9A from *T. virens,* has been described which shares significant homology with TasHyd1 (Viterbo and Chet, 2006). Based on this homology and the typical characteristics of hydrophobins, we hypothesized that HFB9A would have a role in *T. virens*-plant interactions. In this study, we demonstrate the role of the *HFB9a* gene in root colonization and induction of systemic resistance in maize as well as the enhancement of enzyme activity on cell wall components.

Materials and Methods

Bioinformatic analysis

The protein sequences of selected proteins were subjected to a BLAST search of the NCBI database for homologs. The resulting matches were aligned using CLUSTAL Omega software. Additionally, the DNA sequence of the promoter and terminator regions of the hydrophobin were queried through the Joint Genome Institute BLAST (https://mycocosm.jgi.doe.gov/pages/blast-query.jsf?db=TriviGv29_8_2) search of the *T. virens Gv29-8* genome.

Strains and conditions

The root pathogens, *Pythium ultimum* and *Rhizoctonia solani,* and the wild-type strain of *T. virens* [Gv29-8 (WT)] were maintained on potato dextrose agar (PDA, BD Biosciences) at 27 ºC. The maize foliar pathogen *Colletotrichum graminicola* was maintained under an 14:10 light:dark light regime at room temperature on PDA plates for sporulation. Chlamydospores of *T. virens* were harvested from 14-day old cultures of *T. virens* grown in Fernbach flasks containing 1 L of molasses medium (30g molasses and 5g yeast extract per liter of water) by vacuum filtration and dried overnight. The dried chlamydospore mats were ground in a Wiley mill with a #60 sieve. *Zea mays* (Silver queen hybrid, Burpee) were grown in plastic cone containers in Metromix soilless medium or in a hydroponic system (Lamdan *et al.,* 2015b). The hydroponic system consisted of mason jars (500ml, wide mouth) with a shaker clamp placed inside. The jar was filled to the top of the clamp (~220ml) with 0.5x Murashige-Skoog basal medium containing Gamborg's vitamins and supplemented with 0.5% sucrose. The unit was covered with a glass petri

dish bottom and autoclaved. Plastic mesh (7 holes/linear inch) previously cut into discs to fit within the jars was autoclaved separately. After sterilization, the mesh discs were placed on top of the clamps, and pregerminated seeds with roots approximately 2 cm long were threaded through the mesh to contact the growth medium. The glass petri dish bottoms were replaced with sterile plastic petri dish bottoms, as they ensure a tighter fit. All plants were grown under lamps (Sun Blaze T5) with 6500K and 3000K lights at room temperature under a 14:10 light:dark regime.

RNA isolation and Expression assays

Total RNA was extracted from cultures of *T. virens* grown in potato dextrose broth (PDB, Difco) that were inoculated with approximately $3x10^9$ conidia. The fungal biomass was collected every 24 hours over the course of 7 days. To determine the expression of *hfb9a* in plant-fungal interactions, *T. virens* was grown in a hydroponic system in the presence of maize roots, and fungal tissue samples were collected at 6, 30, and 54 hours. All samples were extracted using the Direc-zol RNA miniprep kit (Zymo Research, USA) following manufacturer's instructions. Extracted RNA was converted to cDNA using the high capacity cDNA reverse transcription kit (Applied Biosystems) according to manufacturer's instructions. The resulting cDNA was analyzed by RT-PCR using gene specific primers and primers amplifying Histone H3 as a loading control (Supplementary Table 1).

Deletion of HFB9a

HFB9a was targeted for deletion through homologous recombination using a vector generated via the OSCAR method (Paz *et al.*, 2011) modified for use in *T. virens*.

Primers were designed to amplify approximately 1kb of upstream and downstream regions flanking the open reading frame of the gene and contained appropriate Gateway sites for recombination. The flanks amplified from *T. virens* genomic DNA were purified by adding 90 µl of combined PCR product, 270 µl TE buffer, and 180 µl 30% PEG 8000/30mM $MgCl_2$ to a microfuge tube. This solution was vortexed thoroughly, and then centrifuged for 15 minutes at maximum speed in the table-top centrifuge. The pellet was resuspended in 15 µl of sterile water. A 5 µl clonase reaction was performed using 20 ng of combined flanks, 60 ng pA-Hyg-OSCAR, 60 ng pOSCAR, and 1 µl of BP clonase (Invitrogen) with incubation in a thermocycler overnight at 25 ºC. The reaction was stopped the next morning by adding 0.5 µl of proteinase K and incubating at 37 ºC for 10 minutes. The entire reaction was used to transform *E. coli* DH5α cells and positive clones were screened as described in Paz et al (2011).

The resulting vector (pHFB9a) was electroporated into *A. tumefaciens* AGL1 and confirmed through colony PCR using primers to amplify both flanks and the hygromycin resistance gene (*hph*). Overnight cultures of AGL1 containing the vector were pelleted and resuspended to an OD_{600} of 0.15 in induction medium (M9 minimal medium; 100 ml 5x M9 salts, 3.9g MES, 0.45g glucose, 0.25 ml glycerol, to 500 ml with H2O, pH 5.3) with and without 200 µM acetosyringone and allowed to incubate for 6 hours at 27 ºC. Conidia of *T. virens* were collected from 4-day old PDA plates, diluted to $5x10^5$ conidia/ml, and mixed with bacteria in a 1:1 ratio. Several sterile cellophane squares (~$1cm^2$) were placed on co-cultivation plates (M9 minimal medium with 500 µM acetosyringone and 1.5% agar) and 20 µl of the mixed conidia/bacteria solution were

placed on each square. The plates were allowed to incubate for 60 hours before transferring the cellophane to PDA selection plates containing hygromycin, tetracycline, and chloramphenicol. Positive transformants were transferred to 2 ml PDA slants containing the same antibiotics. Once cultures began to sporulate, they were successively transferred to PDA + antibiotics, PDA, and back to PDA + antibiotics to ensure stability of the integration. Stable transformants were grown in PDB for 2 days and genomic DNA extracted for PCR analysis. Primers specific to the ORF of the gene and primers outside the 5' flank and inside of *hph* were used to confirm deletion.

Phenotypic analysis of mutants

Some number of mutants and the WT were assayed for differences in general morphology and radial growth rate by plating a 3 mm radius plug of actively growing fungus on four PDA plates each and measured every day for four days. The strains were also tested for differences in mycoparasitic ability in confrontation with *P. ultimum*. Plugs of each fungus were placed on opposite sides of a PDA plate 1 cm away from the edge of the plate and allowed to grow toward each other for seven days. The length of the growth front of WT or mutants was measured from the plug and recorded for comparison. Each experiment was repeated twice with four independent plates per experiment. Biocontrol activity was measured as in Djonović et al. using *R. solani* as the pathogen rather than *P. ultimum* (Djonović *et al.*, 2006b). Contact angle measurement was performed as in Crutcher et al. (Crutcher *et al.*, 2015).

Oxidative stress assay

Oxidative stress tolerance was measured by growth on VMS agar plates containing 10 µM sodium menadione bisulfite. Agar plugs (3 mm radius) of each strain were placed in the middle of the plates. Radial growth was measured every 24 hours for three days.

Root colonization and Induced Systemic Resistance assays

Maize seedlings were grown in a hydroponic system as described previously. Once the roots had reached sufficient length (approx. 3-5 cm), 1 g of tissue from WT or mutant *T. virens* strains was placed in the liquid growth medium and gently stirred to distribute. The seedlings and fungal biomass were incubated for 3 days shaking at 50 rpm. The roots were then harvested and thoroughly rinsed in tap water. The collected roots were ground in liquid nitrogen and genomic DNA was extracted using the same protocol described above. The samples were analyzed via the ΔΔCt method of qPCR with actin and phenylalanine ammonia lyase primers to determine the ratio of fungal to maize DNA, respectively. The maize samples were treated as the endogenous control and the WT:Maize DNA ratio was normalized to one relative abundance unit and used as the basis of comparison. Mutants were investigated for changes in ISR activity against the foliar pathogen *Colletotrichum graminicola* following the protocol of Djonović et al. (Djonović *et al.*, 2007) using Silver Queen hybrid plants instead of the B73 inbred line. The area of individual lesions was measured using ImageJ (Schneider *et al.*, 2012). *C. graminicola* was utilized due to its status as a top maize pathogen and the consistency of the lesions that it causes. The shoot height of treated plants was measured with a meter stick after removing the plants from the ‘conetainers’ starting at the seed and ending at the longest

leaf tip after straightening. After shoot measurements, the roots of the plants were cleaned under running water to remove attached soil and dried in an oven overnight. The combined dry weight of roots and shoots from each plant was recorded.

Confocal microscopy and staining

Colonized sections of roots harvested from the hydroponic system after two days incubation with strains of *T. virens* were cleared by treatment with 10% KOH for 1 hour at 95C. The samples were equilibrated in PBS (pH 7.4) for 1 hour. The equilibrated samples were infiltrated in a solution of 5 mg/ml WGA-Alexa-fluor 488 and 10 mg/ml propidium iodide in PBS (pH 7.4) for 15 minutes under vacuum and destained in PBS for an additional 15 minutes. The stained samples were immediately visualized on an Olympus FV3000 confocal microscope.

Enzymatic activity assay of cell wall degrading enzymes

Six replicates of 3 mm radius plugs of each strain were grown in 2 ml of VMS broth in a 24 well plate for 48 hours at 27 C. 150 µl of broth from each well was added to a PCR tube along with 150 µl of Bradford reagent and incubated at room temperature for 5 minutes. To determine total protein concentrations, the absorbance of the samples was measured at 595 nm and compared to absorbance values of a standard BSA curve. Samples from each well were diluted to a total protein concentration of 10 µg/ml. These diluted samples were used for enzyme activity assays.

To measure cellulolytic activity, 40 µl of each sample were transferred to a well of a 96 well microplate and repeated for a total of 3 technical replicates per sample. A 60 µl aliquot of 50 mM sodium acetate buffer at a pH of 4.8 was added to the well along with

10 µl of 1% carboxymethyl cellulose. The plate was sealed with adhesive film and incubated in a thermocycler at 50 C for 60 minutes. A 50 µl aliquot of solution from each well was transferred to a new 96 well plate and 100 µl of dinitrosalicylic acid solution was added. The new plate was then incubated at 95 C for 5 minutes to allow color to develop. 40 µl of the developed solution was added to a 96 well plate, diluted with 160 µl H_2O, and absorbance measured at 540nm in a microplate reader.

To measure chitinase activity, 20 µl of sample was added to a well of a flat bottom 96 well plate. To this, 80 µl of the same sodium acetate buffer used above and 5 µl of 0.5 mg/ml 4-methylumbelliferyl β-D-N, N', N"-triacetylchitotrioside as a substrate was added. This mixture was incubated for 15 minutes at 40 C, and fluorescence was measured in a microplate reader.

Protein expression and extraction

Primers were designed to amplify the 423bp coding sequence from cDNA with *Nde*I and *Hind*III restriction sites prepended to the 5' and 3' primers, respectively. The amplicon and pET30b(+) were double digested with *Nde*I and *Hind*III for 30 minutes at 37 C. The digested products were cleaned with a Qiagen PCR cleanup kit (Qiagen, US) and ligated at a 3:1 amplicon:plasmid ratio with t4 DNA ligase (NEB, US) overnight at 16 C. 5 µl of the ligase mix was transformed into DH5α competent cells via heat shock. Following a recovery period of one hour in SOC medium, 200 µl were plated on an LBA plate containing 50 µg/ml kanamycin and incubated overnight at 37 C. Resulting colonies were screened by PCR for amplification of the ORF of *hfb9a* and positive colonies were

digested with *Nde*I and *Hind*III to determine insert size. Several vectors were then sequenced for confirmation of the correct insertion.

The confirmed vector was transformed into BL21(DE3) (Invitrogen, USA) via heat shock. Four resulting colonies were inoculated into 3 ml of LB broth containing 50 µg/ml kanamycin. The cultures were shaken at 225 rpm in a 37 C incubator until the OD600 reached approximately 0.6 (roughly 5 hours). Expression was induced by adding 0.75 mM IPTG to the cultures with further incubation at 37 C for 4 hours. The cultures were transferred to 2 ml Eppendorf tubes and centrifuged for 5 minutes at 4500xg. The resulting pellet was washed with 500 µl of phosphate buffered saline (PBS, pH 7), and subsequently resuspended in 500 µl of PBS. The cells were lysed by repeated freeze-thaw cycles with liquid nitrogen. A 100 µl sample of the solution was collected in a 1.5 ml Eppendorf tube to represent the combined soluble and insoluble fractions of the lysate. The remainder was centrifuged for 5 minutes at full speed in a tabletop centrifuge. A 100 µl sample was taken to represent the soluble fraction of the lysate. Each sample was diluted with protein running buffer and placed in a boiling water bath for 5 minutes. 10 µl of each sample were loaded into a 15% SDS-PAGE gel and run at 35 milliamps for 1 hour.

To assess the presence of the protein of interest, a dot blot was performed using anti-His antibodies conjugated to alkaline phosphatase. 3 µl of each protein extract and a positive control were dotted onto a nitrocellulose membrane. After drying, the membrane was blocked using 5% skim milk powder in TTBS for 30 minutes. The membrane was rinsed briefly with TTBS, and the dilute antibody solution was added and allowed to incubate for 1 hour. The antibody solution was drained off, and the membrane was

thoroughly rinsed with TTBS. 10 ml of BCIP/NBT solution was added to the membrane and incubated for 20 minutes, until color developed.

An overnight culture of the expressing strain of *E. coli* was used to start a 2 L culture. The culture was centrifuged for 50 minutes at 16,000 rpm with the pellet resuspended in lysis buffer (20 mM Tris pH 7.5, 100 mM NaCl) and 2 M urea. Then 25 µl of 1 M $MgCl_2$ and 25 µl of DNaseI were added following resuspension, the solution was lysed using a French press, and centrifuged at 16,000 rpm for 50 minutes to obtain a pellet. The supernatant was decanted into a separate container for later blotting. The pellet was washed twice by resuspending in lysis buffer + 2 M urea and spun at 16000 rpm for 20 minutes. The final pellet was resuspended in lysis buffer + 8 M urea. The suspension was spun once more at 16,000 rpm for 20 minutes. The supernatant containing solubilized inclusion bodies was passed through a HisTrap HP (GE, USA) chromatography column using a peristaltic pump. The column was then attached to an FPLC where the bound proteins could be refolded by passing lysis buffer containing a slow gradient from 8 M to 0 M urea with 5 mM reduced glutathione and 0.5 mM oxidized glutathione. Following refolding, a gradient from 0-400 mM imidazole containing buffer was passed through the column to elute the bound protein. The fractions containing eluted protein were combined and run on SDS-PAGE gel, as well as subject to a dot blot with anti-his antibodies to confirm the presence of the protein.

SM1 production determination

Cultures of each strain were grown in 1 L VMS shaken at 150 rpm and 27C for one week. The cultures were filtered through Whatman #4 filter paper and the filtrate

collected. Proteins were precipitated from the filtrate with ammonium sulfate (~80% saturation) and collected by centrifugation. Levels of SM1 production were determined by immunoblotting as in Djonovic *et al*. 2006a.

Arabidopsis MAPK phosphorylation assay

Arabidopsis seedlings were grown on plates of 0.5x Murashige-Skoog basal medium with Gamborg's vitamins for ten days. Several seedlings were placed in wells of a 12 well plate with 500 ul of sterile water and incubated overnight. The seedlings were then treated with chitin, purified HFB9A, the protein suspension buffer, or purified SM1. The proteins were added to a concentration of 100 nM. After 15 or 30 minutes, the seedlings were collected, and flash frozen in liquid nitrogen. The frozen seedlings were ground in protein extraction buffer (Li *et al.*, 2015) and run on a 10% SDS-PAGE gel. The proteins were transferred and blotted with anti-pERK1/2 antibodies and detected by enhanced chemiluminescence.

Statistical analysis

All data was analyzed for statistical significance using the ANOVA, Tukey's HSD, and/or Kruskal-Wallis functions in R.

Results

The T. virens genome encodes two canonical type I hydrophobins

NCBI PSI-BLAST search using the protein sequences of HFB9A (Genbank Accession: EHK16816.1) revealed a characterized homolog within the *T. asperellum* genome, TASHYD1. A second similar hydrophobin was found in the *T. virens* genome, but has not yet been characterized. With MEGA software, a phylogenetic tree was

constructed using selected top hits of the NCBI PSI-BLAST, with HFB9A serving as the query sequence (Figure 15). The tree diverged into two main clades representing proteins that were more similar to HFB9A or HFB3A. The only characterized hydrophobin in the phylogeny was TASHYD1, which aligned near HFB9A, indicating that the two proteins may share similar characteristics and roles in the fungus. Additionally, PFAM database scanning revealed a hydrophobin domain with an N-terminal signal peptide and no other conserved domains. The protein sequence of HFB9A was used for predictive modeling of protein structure with the I-TASSER software (Yang *et al.*, 2015). The predicted structure of HFB9a (Figure 16) shared structural homology with human defensin and cell adhesion proteins and exhibited the predicted ability to bind a peptide as a ligand. The structure of TASHYD1 was predicted using the same software for comparison with the predicted structure of HFB9A and the solved structure of DEWA from *Aspergillus nidulans* (Morris *et al.*, 2013). All three were similar with a core of 2-3 beta-sheets, however DEWA exhibited significantly more secondary structure on the outward facing chains with multiple alpha-helices and beta-sheets throughout.

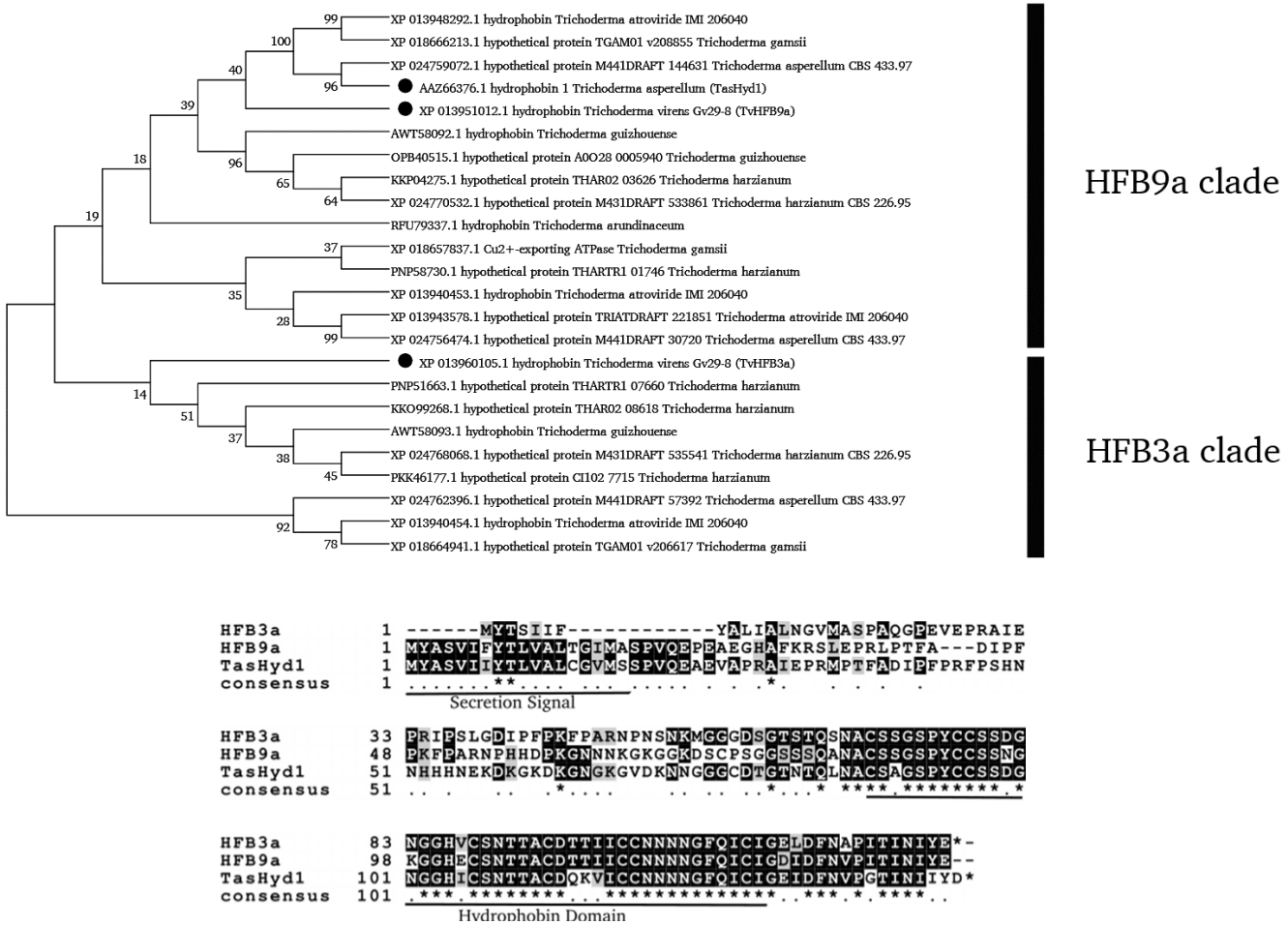

Figure 15. Phylogenetic comparison of hydrophobins from *Trichoderma spp.* Top: A phylogenetic tree of class I hydrophobins from *Trichoderma spp.* produced with MEGA software. Bottom: A clustal-omega alignment of the amino acid sequences of two *T. virens* class I hydrophobins (HFB9a and HFB3a) and TasHyd1 from *T. asperellum.* Identical residues between all three sequences are labeled with an asterisk.

HFB9a is induced during fungal association with maize roots

To develop an expression profile for *hfb9a*, cDNA generated from RNA of WT collected at predetermined time points either in the presence of living maize roots (6, 30, and 54 hpi) or in shaken culture of potato dextrose broth (PDB, collected every day for 7 days) was subjected to RT-PCR. Expression was observed only in samples from the hydroponic system collected 54 hours post inoculation, indicating expression of the gene between 30 and 54 hpi (Figure 17a). Expression of the gene from mycelial samples grown in PDB was not detected until 72 hpi but remained constant in the remainder of the samples. In the hydroponic system, attachment of the WT and each mutant to the root system of maize seedlings was recorded at approximately 6 hpi, with the entirety of the root system enveloped by fungus at 54 hpi. The initial expression results were further confirmed by whole transcriptome sequencing data (Figure 17b, 17c, Malinich *et al.*, 2019, Taylor et al. *unpublished*). In early time points (6-24 hpi, Figure 17b, 17c), the normalized transcript counts are near 0, while starting at 30 hours post inoculation transcript counts rapidly increase.

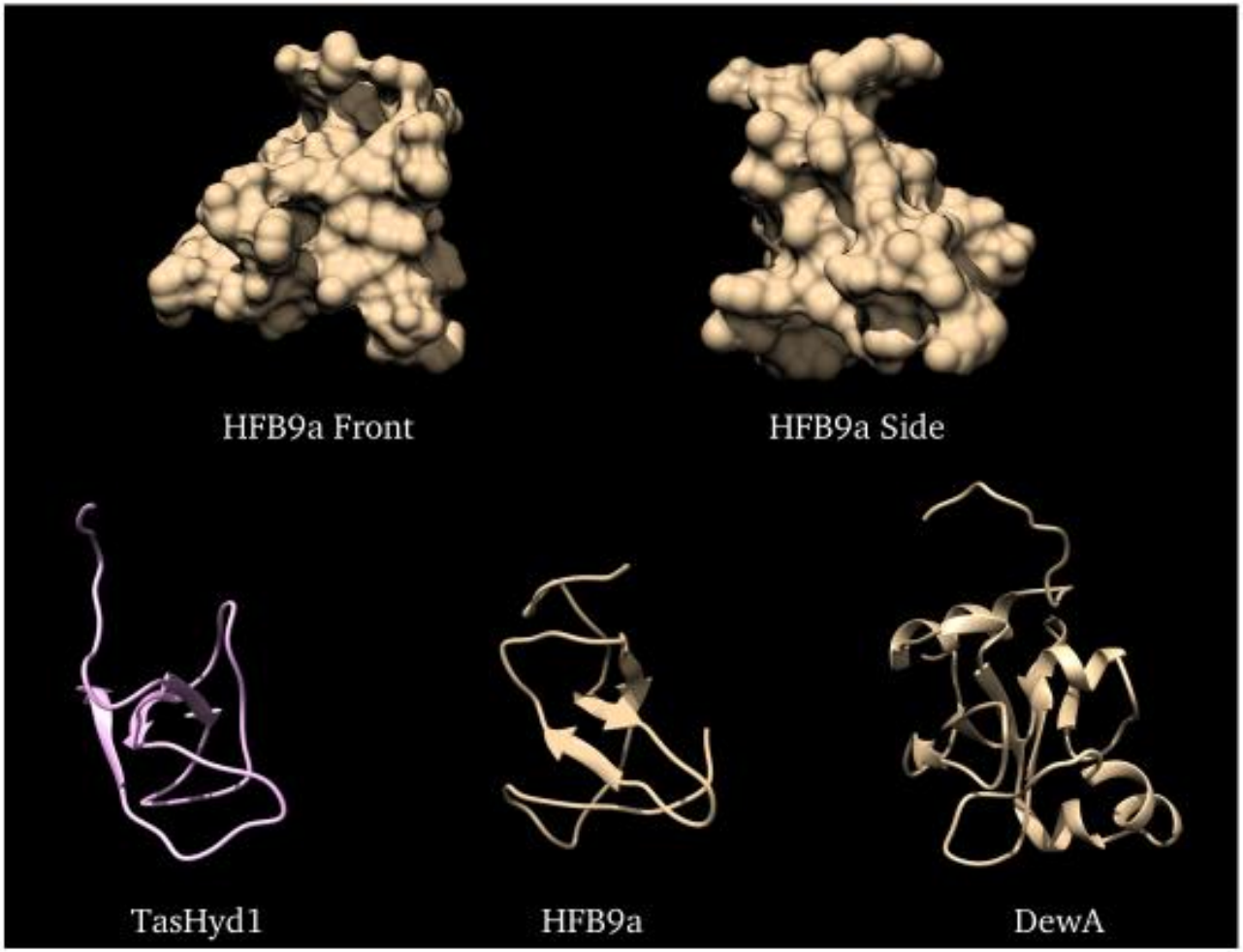

Figure 16. A comparison of the predicted protein structures of TASHYD1, HFB9A, and the solved structure of DEWA, a class I hydrophobin from *Aspergillus nidulans.*

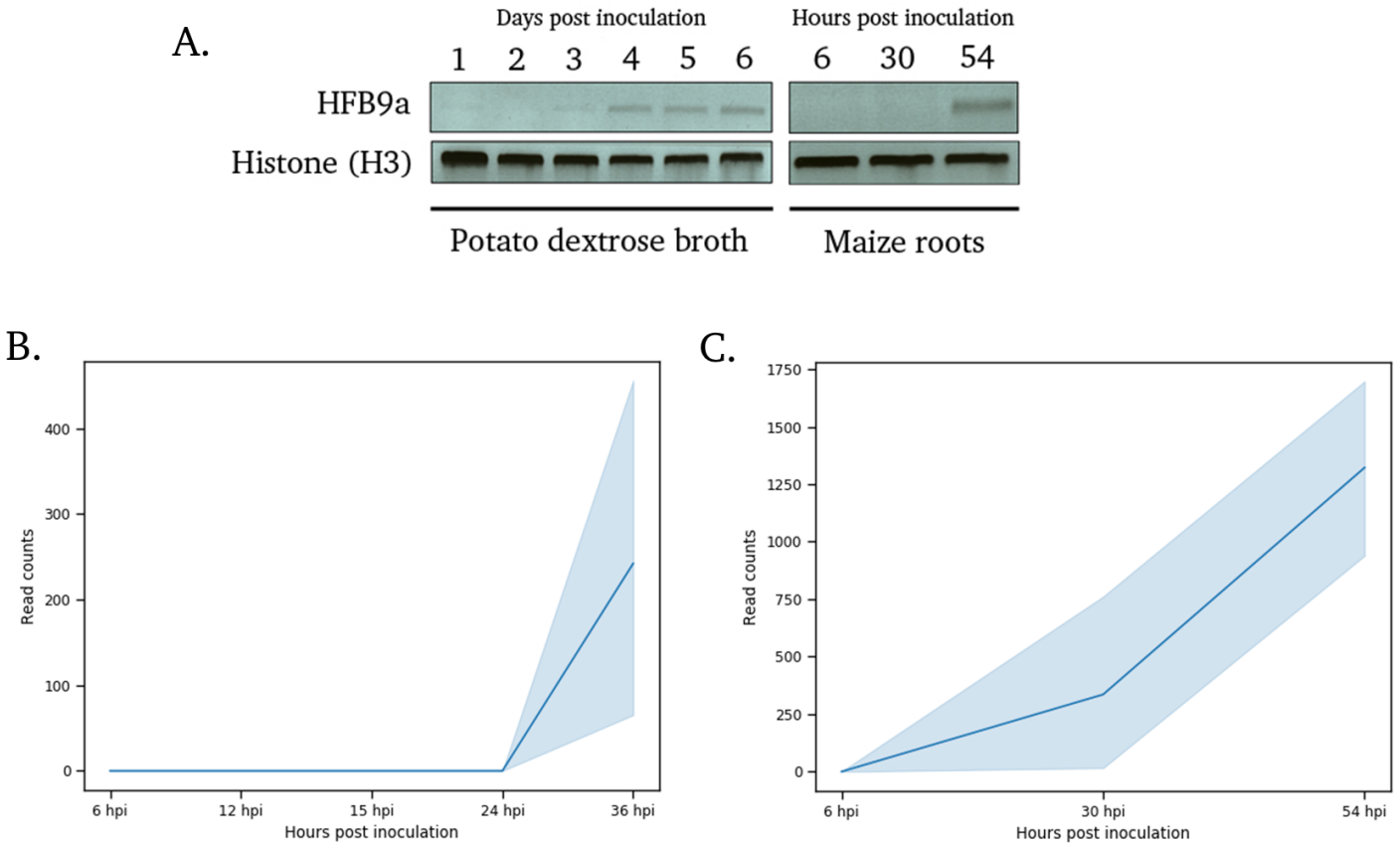

Figure 17. A. HFB9a expression in potato dextrose broth and in the presence of maize roots as measured by RT-PCR. Histone (H3) was used as a loading control. B and C. Normalized read counts from RNA-seq based transcriptomic datasets (B: Taylor *et al.* unpublished, C: Malinich *et al.*, 2019). The light colored, shaded regions along the line graph represent the standard deviation at each time point.

HFB9a is required for normal hydrophobicity and oxidative stress response

The gene encoding HFB9A was deleted via *Agrobacterium*-mediated transformation with a homologous recombination cassette (Appendix B Figure 40a). The knockouts were confirmed and screened for wild- type copies of the gene by PCR (Appendix B Figure 40b). *ΔHFB9a* mutants demonstrated a statistically significant difference in hyphal surface hydrophobicity as measured by contact angle of a water droplet on the surface of an agar plug (Figure 18a). There was no significant difference in radial growth on PDA between the mutants and wild type (Appendix B Figure 41). However, mutant strains grew significantly slower under oxidative stress than WT (Figure 18b). The mutants grew similar as WT in confrontation with *P. ultimum* (Appendix B Figure 42a) and retained biocontrol activity against *R. solani* on cotton roots (Appendix B Figure 42b).

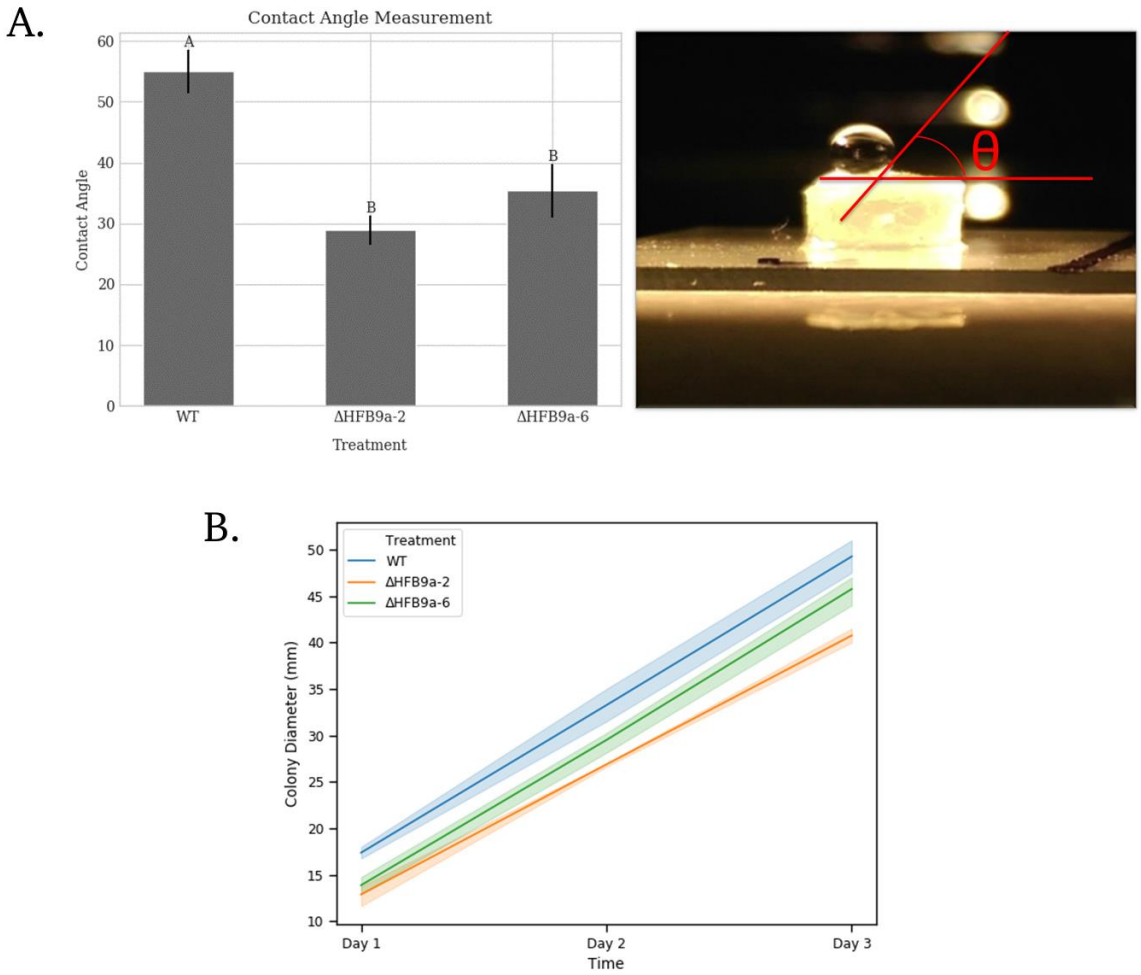

Figure 18. Surface hydrophobicity and oxidative stress response. A. Surface hydrophobicity of fungal mycelium as measured by contact angle of a water droplet. Different letters represent statistically different groups ($p < 0.05$) as determined by ANOVA and Tukey's HSD. B. Radial growth of each strain over the course of three days on PDA amended with sodium menadione bisulfite to induce oxidative stress**.**

HFB9a has a role in host root colonization and induction of systemic resistance

The ability of *ΔHFB9a* mutants to colonize maize roots was significantly reduced in the hydroponic system (Figure 19). Observations prior to harvest indicated a similar amount of each strain enveloping the roots. Interestingly, upon addition of pregerminated tissue to the hydroponic medium, individual colonies could be seen attaching to the roots as the biomass became dispersed. This was significantly faster than expected and did not support our initial hypothesis that the hydrophobin was involved in attachment of the fungus to the roots. Additionally, visualization of the colonized roots by confocal

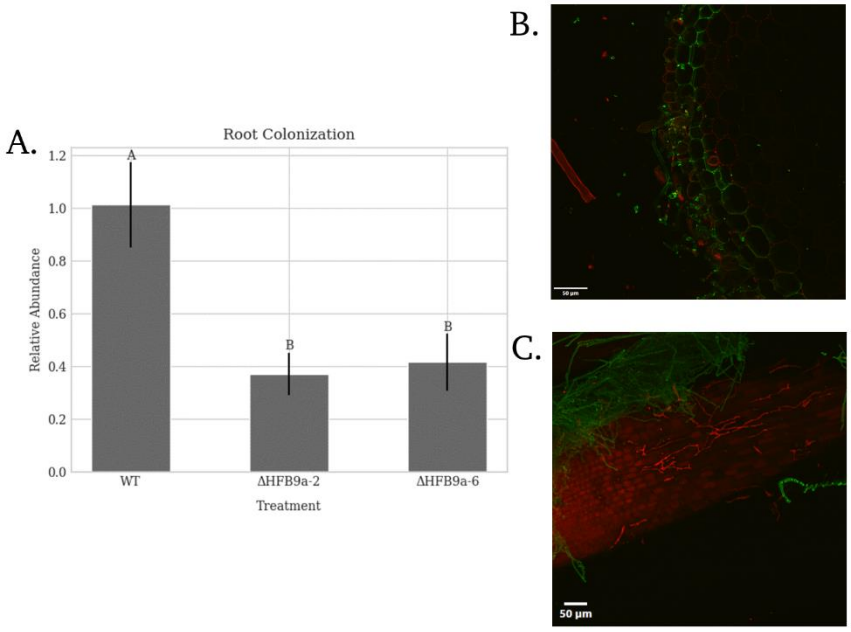

Figure 19. Root colonization of maize. A. Root colonization of maize roots in a hydroponic system by different strains of *T. virens*. Quantitative-PCR was used to determine the relative abundance of fungal DNA compared to maize DNA and normalized to the wild-type strain. Different letters represent statistically different groups ($p < 0.05$) as determined by ANOVA and Tukey's HSD. B and C. Confocal micrographs visualizing the wild-type strain (B) or HFB9a mutant strain (C) colonizing maize roots. Fungal tissue was stained with WGA-AlexaFluor-488 and maize tissue was stained with propidium iodide.

microscopy indicated attachment to the root epidermis by the mutant, but only WT was able to colonize internal portions of the root sections extensively (Figure 19b, 19c).

ΔHFB9a mutants were analyzed for their ability to induce systemic resistance against *C. graminicola* in maize plants. The average lesion area of the plants treated with ΔHFB9a mutants were significantly larger than the WT treated plants, indicating a lack of ISR (Figure 20a, 20b). Plants treated with *HFB9a* mutants did not differ significantly in height or dry weight compared to wild-type treated plants (data not shown). Western blot analysis was performed to determine whether the reduction of ISR was due to decreased production of the elicitor protein SM1. Total protein was extracted from WT and *ΔHFB9a* strains grown in PDB for 48 hours at 150 rpm. Each aliquot was diluted to 1 mg/ml and a western blot performed using anti-SM1 antibodies (Djonović *et al.*, 2006a). There was no appreciable difference in the amount of protein detected (Figure 21).

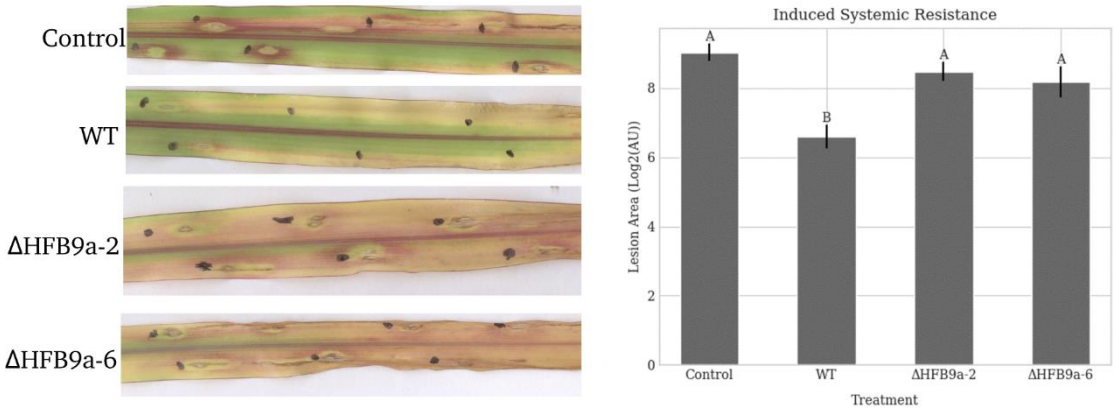

Figure 20. Induced systemic resistance of maize plants treated with the wild-type strain or HFB9a deletion mutants. Areas of individual lesions were measured in ImageJ. Different letters represent statistically different groups ($p < 0.05$) as determined by ANOVA and Tukey's HSD.

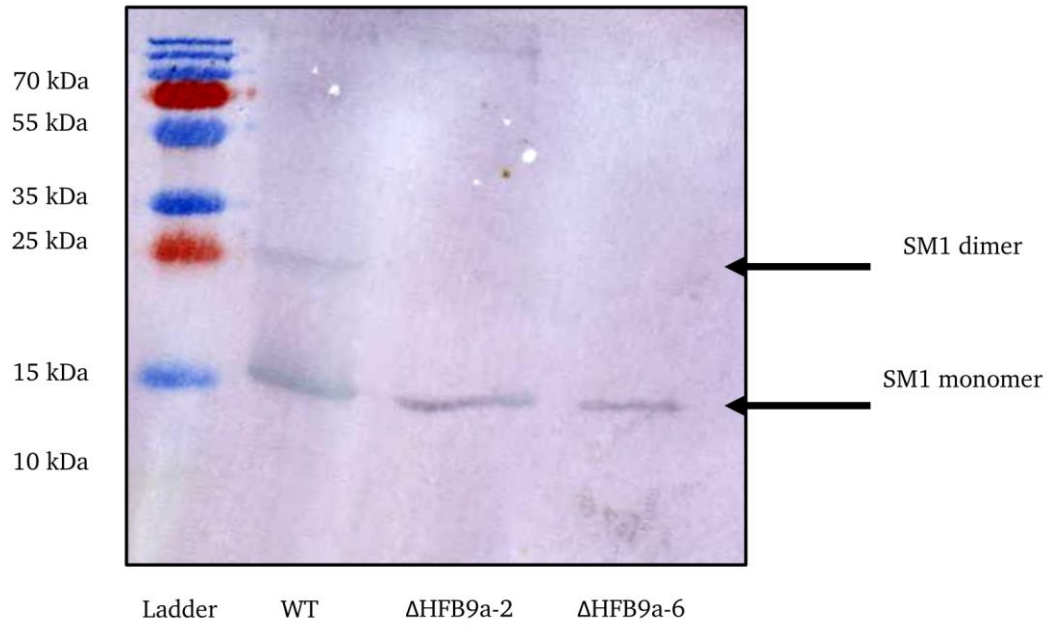

Figure 21. SM1 protein production. A western blot using antibodies specific to SM1 to determine the production of SM1 protein by the wild-type strain and deletion mutants. All lanes were loaded with one ug of protein.

HFB9a accelerates T. virens cellulase and chitinase activity

ΔHFB9a deletion mutants demonstrated significantly less cellulase activity compared to the wild type fungus (Figure 22a). To determine whether this effect was substrate specific, we duplicated the assay using colloidal chitin, pectin, and lignin. Chitinase activity on colloidal chitin was impacted by the loss of HFB9A (Figure 22b). However, no impact on pectin or lignin degradation was found with this assay.

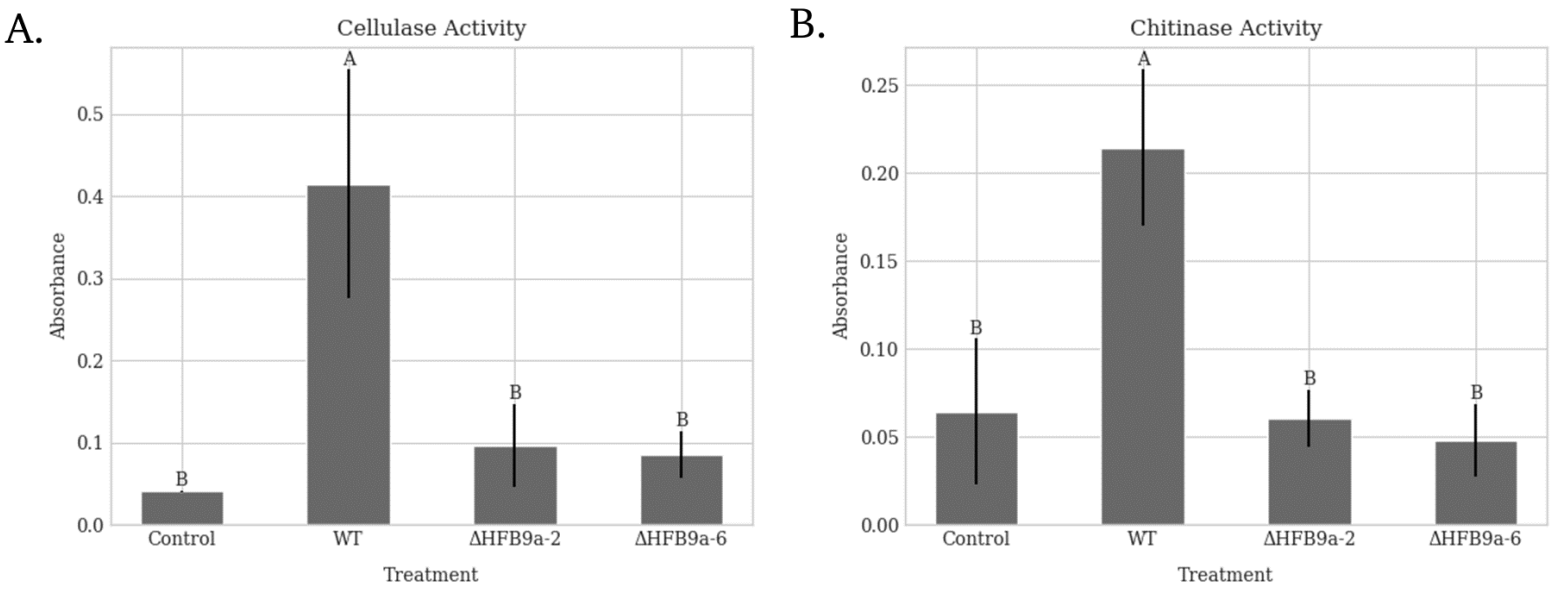

Figure 22. Cellulase (A) or chitinase (B) activity of culture filtrates from the wild-type strain and HFB9a deletion mutants as measured by the DNS assay. Different letters represent statistically different groups ($p < 0.05$) as determined by ANOVA and Tukey's HSD.

HFB9a protein complements enzyme activity of mutants

The *E. coli* expression vector pET30B(+) was used to produce recombinant HFB9A with a fused 6xHis tag at the C-terminal end. Expression following induction with IPTG was attempted at 30C overnight or 37C for four hours. Protein production was only detected with cultures incubated at 37C and present only in the insoluble fraction of the lysate.

The recombinant HFB9A protein was purified from solubilized inclusion bodies by metal affinity chromatography and refolded on the column. Following elution with imidazole, the fractions containing the protein of interest were identified with a dot blot. The positive fractions were pooled, assayed by western blotting (Figure 23), and the protein was stored at 4 C for future use. The protein was collected in a buffer with high salt and imidazole. We attempted to exchange the buffer by dialysis, but found that the protein aggregated and precipitated out of solution. To avoid aggregation and the resulting insolubility, the protein was rapidly precipitated using 4 volumes of ice-cold acetone; however, the protein remained insoluble. The protein was re-solubilized via treatment with formic acid followed by the addition of an equal volume of 30% H_2O_2 to produce performic acid (Wosten *et al.*, 1993). The protein immediately went into solution following evaporation of the acid. The new protein solution retained the same surface activity in comparison with samples dissolved in the original buffer and was used throughout the rest of the study.

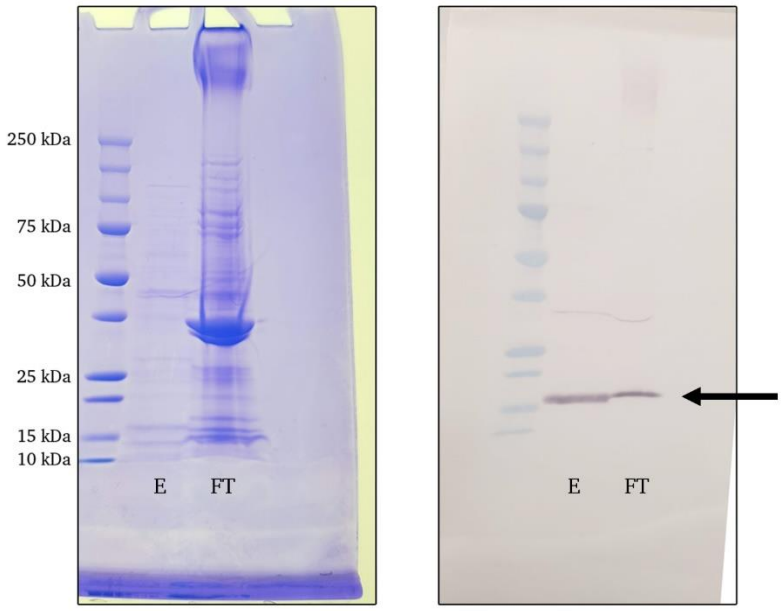

Figure 23. Detection of recombinant HFB9a. Coomassie Blue stained SDS-PAGE gel and western blot with antibodies specific to the H6 tag to detect recombinant HFB9a. E: eluted fraction, FT: column flowthrough prior to elution.

The purified protein was able to complement the cellulase activity of the mutants at 1 uM concentration. In addition to restoring the enzyme activity of the mutants to WT levels, addition of purified protein to the WT culture filtrate was able to enhance the cellulolytic activity against filter paper (Figure 24a). The protein on its own displays no enzymatic activity and requires an enzyme to have this function. The protein suspension buffer was also tested to ensure that there was no interaction in this assay and found no cellulolytic activity. Additionally, the pure protein at 1 uM was able to enhance the activity of commercially sourced cellulase (Figure 24b).

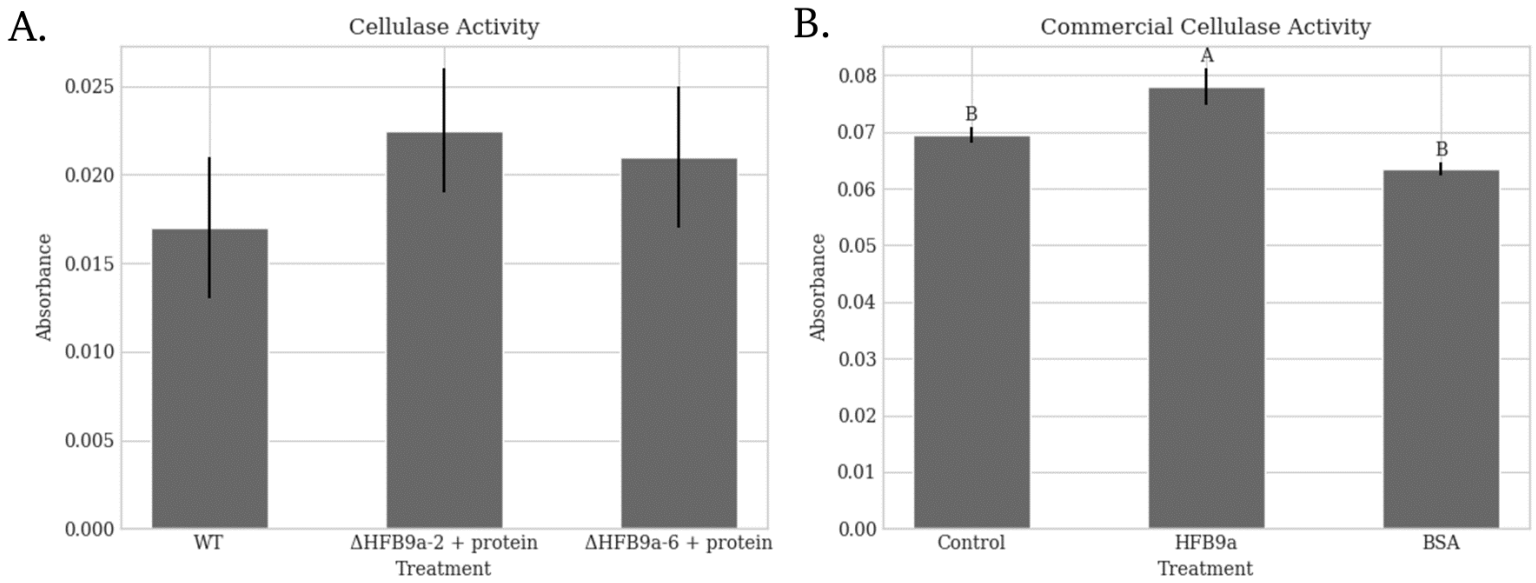

Figure 24. A. Complementation of HFB9a deletion mutant cellulase activity by addition of purified HFB9a protein. B. Enhancement of commercial cellulase with purified HFB9a protein. BSA treatment was included as a control. Different letters represent statistically different groups ($p < 0.05$) as determined by ANOVA and Tukey's HSD.

HFB9a induces phosphorylation of AtMAPK 3 and 4

Purified protein samples of HFB9A and SM1 were applied to Arabidopsis seedlings to determine whether the proteins could induce rapid activation of plant innate immunity commonly associated with microbe associated molecular patterns (MAMPs). HFB9A treated samples displayed phosphorylation of AtMAPK3 and 4 starting 30-minutes post inoculation, whereas SM1 and buffer control samples did not display phosphorylation 15- or 30-minutes post inoculation (Figure 25).

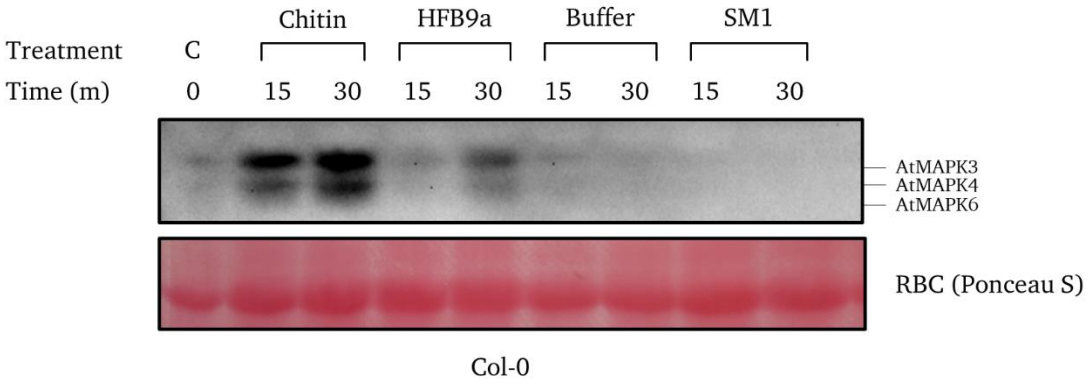

Figure 25. MAPK phosphorylation of *Arabidopsis* by addition of HFB9a over the course of 15 and 30 minutes. Phosphorylation was detected by antibodies specific to pERK1/2. Chitin was included as a positive control.

Discussion

Hydrophobins are known to self-assemble at hydrophobic/hydrophilic interfaces. The resulting hydrophobin monolayer can modify the properties of the surface to which it adheres. Alteration of surface properties of materials by hydrophobins enable fungi to interact with previously intractable material as well as adapt to environmental changes. In

this study, this phenomenon was demonstrated with *HFB9a*, as this hydrophobin is required for efficient colonization of maize roots and enhancement of cell wall degrading enzymes. Remarkably, induced systemic resistance in maize treated with mutant strains was reduced, and one potential mode of action of *HFB9a* on ISR may be due to the ability of the purified protein to induce activation of MAP kinase cascade, similar to other MAMPs such as chitin.

It is not unprecedented that a hydrophobin may act as an elicitor to influence plant health. HyTlo1 was demonstrated to have a role in induced systemic resistance when applied to leaves, as well as when expressed transgenically by tomato plants (Ruocco *et al.*, 2015). The hydrophobin HFB9a may be functioning in a similar manner as a MAMP. AtMAPK3/4 proteins associated with MAMP response and innate immunity were phosphorylated after treatment with purified HFB9A. The phosphorylation cascade starting with atMAPK3/4 activates WRKY transcription factors involved in plant innate immunity (Adachi *et al.*, 2015). The direct activation of these proteins by purified HFB9A suggests that the fungal protein has activity that is recognized by the plant as non-self, and induces defense responses. Another protein with putative MAMP activity from *Trichoderma spp.* is Swollenin from *T. asperellum* (Brotman *et al.*, 2008). Brotman *et al.* suggested that the carbohydrate binding domain of the protein acted as a MAMP, but they did not provide direct evidence, such as MAPK phosphorylation. Additionally, the production of SM1, a known elicitor, remained unchanged in the mutant strains in the presence of plant roots. This, paired with decreased ISR in plants treated with mutant strains, strongly suggests that HFB9A acts as a MAMP.

Our initial hypothesis was that HFB9A mediates attachment of hyphae to maize roots in a manner similar to TASHYD1 (Viterbo and Chet, 2006). However, based on observations of the attachment phenomenon in hydroponics and the timing of expression of the gene, this hypothesis is rejected. There is previous evidence that hydrophobins of both classes from *T. virens* enhance PET plastic degradation by cutinases (Przylucka *et al.*, 2014). The enzymatic enhancement property of HFB9A may aid the fungus in the degradation of plant cell walls, enhancing colonization. The demonstrated reduction in enzyme activity and colonization by the mutants suggest this may be an alternative role for some hydrophobins. The semi-selective nature of enzyme enhancement was a surprising discovery. The ability of the hydrophobin to enhance enzyme activity of cellulases and chitinases, but not other cell wall degrading enzymes such as pectinases may be due to the solubility of the substrates. Cellulose and chitin are both insoluble in water whereas pectin is highly soluble. We speculate that HFB9A may be modifying the hydrophobicity of the substrates that the enzymes are acting upon, promoting enzyme attack. Beyond its biological role in the fungus, HFB9A could present application in an industrial setting. Fungal hydrophobins are increasingly being used in commercial applications, such as in the protection of historic stonework from water damage (Winandy *et al.*, 2019). The enhancement activity of HFB9A makes it a viable candidate for industrial applications, e.g. as an additive to enzyme cocktails.

Interestingly, the reduction in chitinase activity in mutants of *HFB9a* did not influence the ability of the fungus to protect against *R. solani* infection of cotton roots, nor mycoparasitism of *P. ultimum* as measured by confrontation assays. This could be

explained by to the experimental conditions we used to measure chitinase activity. The major chitinases involved in mycoparasitism may not be expressed in minimal medium to the same degree as if a competing fungus or chitin substrate was present. Additionally, secondary metabolites such as gliotoxin and viridin have been demonstrated to have activity against both *R. solani* and *P. ultimum* (Howell *et al.*, 1993; Vargas *et al.*, 2014). The lowered activity of chitinases may be compensated by the activity of the antifungal secondary metabolites.

Overall, we demonstrate that *HFB9a* has an important role in the interaction between *T. virens* and its host. Induced systemic resistance is significantly reduced when HFB9a is not produced and the protein induces phosphorylation of MAPK proteins involved in immune responses, suggesting that HFB9A may function as a MAMP. Furthermore, the purified protein enhances several cell wall degrading enzymes and has potential industrial applications.

CHAPTER IV

DELETION OF THE *TRICHODERMA VIRENS* NRPS, TEX7, INDUCES ACCUMULATION OF THE ANTI-CANCER COMPOUND HEPTELIDIC ACID.

Introduction

Trichoderma virens, a mycoparasitic ascomycete with plant health promoting benefits, produces a unique and diverse array of compounds with pharmacological, industrial, and agricultural applications(Mukherjee *et al.,* 2012b; Gupta *et al.,* 2014; Zeilinger *et al.,* 2016). Currently, strains of *T. virens* are classified into two distinct groups, P- and Q-strains, based on their secondary metabolite profile(Howell *et al.*, 1993). The Q-strains produce gliotoxin and dimethylgliotoxin, P-strains synthesize gliovirin and heptelidic acid, and both strains generate viridin and viridiol. Heptelidic acid, also known as koningic acid, is a potent antibiotic with reported uses as an anticancer agent (Rahier *et al.*, 2015). In fungi, the genes responsible for the biosynthesis of secondary metabolites are chromosomally arranged in gene clusters that are typically initiated by either a non-ribosomal peptide synthetase (NRPS), polyketide synthetase (PKS), or terpene cyclase. The NRPS generates a precursor peptidic compound that is used as substrate by downstream members of the cluster through modifications and/or transport(Mukherjee *et al.*, 2012b). Disruption of the NRPS, PKS, or terpene cyclase ablates the function of the entire cluster and often enables the identification of the metabolite produced by the cluster(Vargas *et al.,* 2014). This methodology was adopted in *T. virens* for the characterization of the *Tex7* gene cluster (Mukherjee *et al.*, 2012a). Unexpectedly,

disruption of the *Tex7* gene cluster resulted in the dramatic over-production of heptelidic acid, a molecule previously undocumented in the Q-strains. In addition to finding heptelidic acid in the mutant strains, minute quantities of heptelidic acid were identified in the wild-type (WT) Gv29-8, suggesting that the current strain classification model needs revision. Finally, maize treated with *ΔTex7* mutants displayed reduced plant height, but retained the ability to express systemic resistance against plant pathogens.

Results and Discussion

The *Tex7* gene cluster consists of three genes, Tex7 NRPS (EHK18450.1, henceforth referred to as *Tex7*), an ATPase (EHK18452.1), and a member of the major facilitator superfamily (EHK18451.1). The *Tex7* gene consists of 20,946 nucleotides with a single 48 base pair intron close to its 3' end. The gene encodes a 6,965 amino acid polypeptide with five predicted amino acid adenylation domains, three S-adenosyl-L-methionine-dependent methyltransferase domains, five ACP-like domains, and six condensation domains. There is no predicted secretion signal, while it is presumed to localize to the cytoplasm. There are five predicted amino acid substrates putatively assembled by the protein based on its adenylation domains - leucine, leucine, phenylalanine, leucine, and proline. The *TEX7* amino acid sequence demonstrates homology with NRPS proteins that produce depsipeptides, which are large, cyclic antibiotic molecules composed of repeating units of carboxylic acids bound to an amino acid with either a peptide or ester bond (Prosperini *et al.*, 2017). Additionally, transcriptomic analysis demonstrated that the *Tex7* cluster is upregulated in the presence of maize roots (Malinich *et al.*, 2019). These predicted attributes led us to hypothesize that

Tex7 ultimately produces a depsipeptide that may serve as an antibiotic defense molecule involved in interactions with plants and microbes.

Thin layer chromatography (TLC) was used to develop a secondary metabolite profile for the WT and mutant strains grown in VMG media as part of our mutant characterization. A large band was visualized running above the band of a gliotoxin standard (Figure 26). The band was isolated from the plate by collecting the silica areas of the unknown band and resuspending in methanol for analysis by HPLC. This unknown analyte (designated Unk23.8min) eluted from the HPLC column at 23.8 minutes, close to viridin (Figure 27A**)**, but was distinctly different based on UV spectra (Figure 28**)**. An aliquot of the culture filtrate was subjected to untargeted LC-MS/MS analysis where a peak (retention time: ~ 6 min) corresponding to a compound with the molecular formula $C_{15}H_{20}O_5$ was present in the mutants in greater abundance. In addition to the unknown compound, a large quantity of viridin was produced by the mutant strains (Figures 27A and 28). The over-production of viridin by the mutant was also visible in LC-MS/MS analysis (Figure 27B). This finding is interesting, as previous transcriptomic analysis revealed that the viridin gene cluster was downregulated in the presence of maize roots (Malinich *et al.*, 2019). The overproduction of these two secondary metabolites may be due to regulation of other clusters by *TEX7* (Hidalgo *et al.*, 2014; Sheridan *et al.*, 2015).

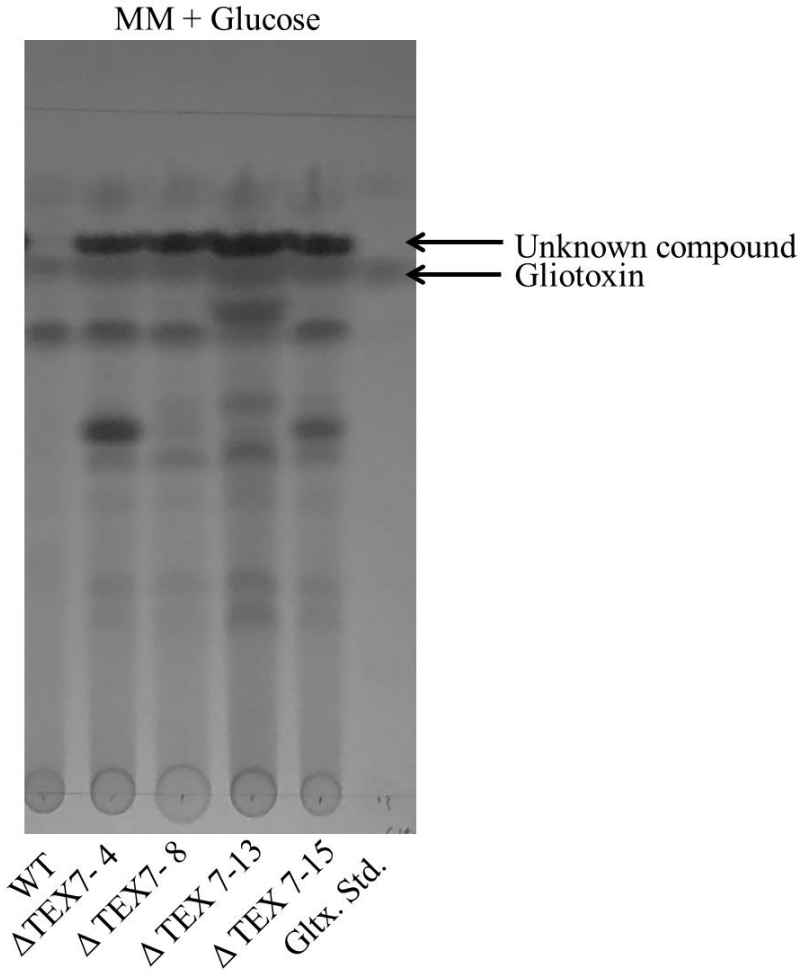

Figure 26. Thin layer chromatography profiles of *T. virens* strains. A comparison of the metabolite profile between the WT and mutant strains (Tex7-4, Tex7-8, Tex7-13, and Tex7-15) grown with glucose as a carbon source. A band corresponding to an unknown compound was detected above the characteristic gliotoxin band, indicated with arrows.

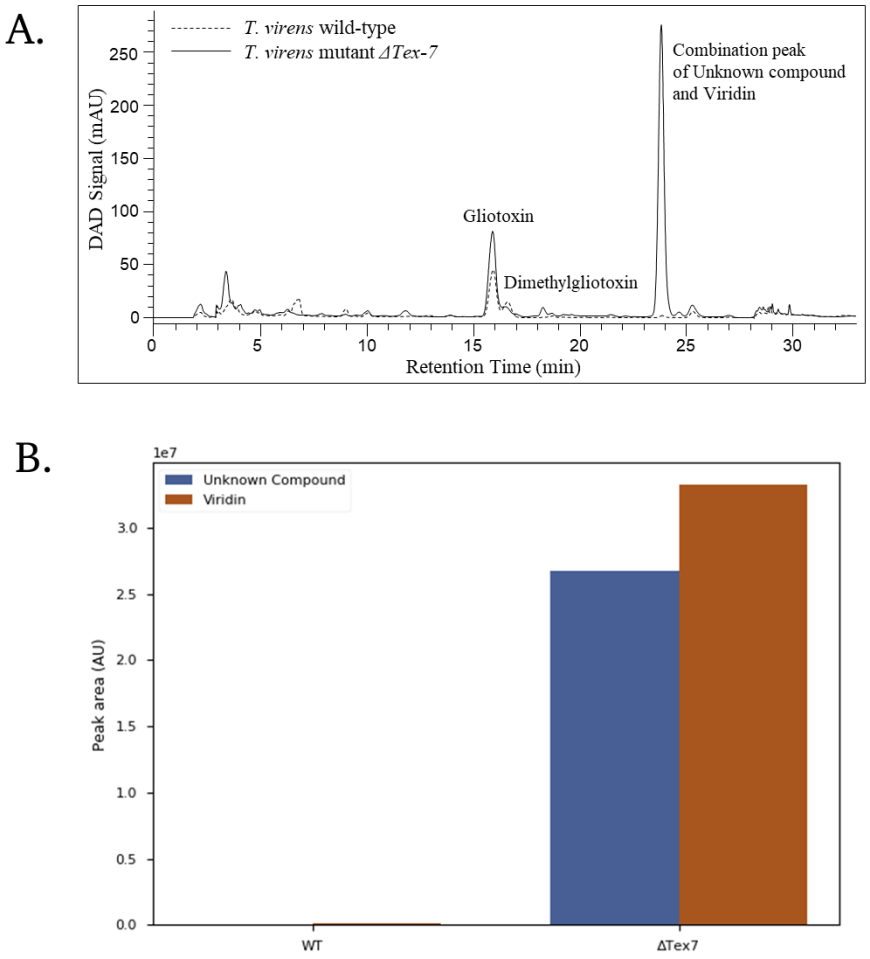

Figure 27. HPLC metabolite profile comparison. A) Representative spectra of secondary metabolite extractions from the WT (dotted) and a composite sample from Tex7 disruption strains (solid). There was a large peak detected at approximately 23.8 minutes comprised of viridin and heptelidic acid in the Tex7 strain composite sample, but not in the WT. B) LCMS peak area for HA and viridin in culture filtrate samples from WT or Tex7 mutant strains. Tex7 strains produced significantly more HA and viridin than the WT strain.

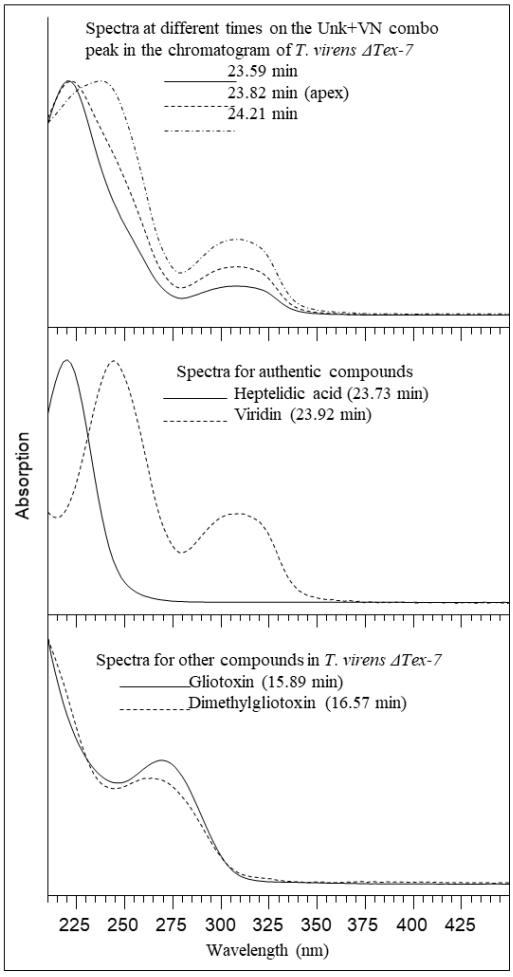

Figure 28. UV spectra comparison of HPLC resolved compounds. Top: Comparison of the UV spectra of the combination peak of heptelidic acid (HA) and viridin (VN) at three selected time points. Middle: Comparison of UV spectra of pure heptelidic acid and viridin demonstrates distinct differences, allowing for differentiation. Bottom: UV spectra of other common secondary metabolites produced by *T. virens*.

Ethyl acetate extracts from four 50-mL cultures of *T. virens Δtex7* strains were combined, evaporated, and then dissolved in 1 mL methanol. The sample was subjected to HPLC, and the Unk23.8min peak was manually collected from the HPLC eluent. The

collected sample yielded approximately 2 mg with 73% pure Unk23.8min as determined by HPLC.

Column chromatography was performed to purify Unk23.8 from a 500 mL *ΔTex7* culture extract. Sixty mL fractions were collected and subjected to HPLC revealing the presence of gliotoxin, dimethylgliotoxin, and viridin in fraction 1, high concentration and high purity of Unk23.8min in fractions 8-14, and low concentration and low purity Unk23.8min in fractions 15-16. The process yielded two Unk23.8min samples that were weighed and analyzed by HPLC; one sample was 64 mg of 61% Unk23.8min and the other consisted of 18 mg of 35% Unk23.8min.

The Unk23.8min samples were analyzed by TLC, and three bands appeared under 250 nm UV light of exposure. The middle band at Rf 0.21 contained Unk23.8min as confirmed by HPLC. The Unk23.8min bands on the plates were collected, the compound was extracted and dried, yielding a white, tacky solid. An attempt was made to dry the material further with ethanol, but the sample gained yellow color and HPLC revealed that some of the Unk23.8min compound had decomposed. The sample was again purified by TLC yielding 28 mg of 93.6% Unk23.8min. The Unk23.8min sample was crystallized yielding 7.7 mg of white crystals which were 96.6% pure; the mother liquor (8.9 mg) was 88.1% Unk23.8min.

The entire crystalline sample was dissolved in acetone-d_6 and analyzed using one-dimensional (1D) and two-dimensional (2D) liquid-state NMR spectroscopy with direct ^{1}H and ^{13}C detection. The assignment of ^{1}H and ^{13}C resonances of the unknown compound was carried out using the information about characteristic chemical shifts of specific

chemical groups, multiplicities, and integral intensities of spectral peaks. For example, ^{1}H-^{13}C single-bond and multiple-bond correlations were obtained from the 2D HMQC (Figure 29) and HMBC spectra (Figure 30), respectively. ^{1}H-^{1}H correlations were obtained from the 2D COSY and TOCSY spectra (data not shown). All ^{1}H and ^{13}C resonance assignments are indicated on the 1D ^{1}H and ^{1}H-decoupled ^{13}C spectra (Figure 31, A and B). Comparison of the ^{1}H and ^{13}C chemical shifts obtained in our experiments with those reported previously for heptelidic acid (HA) in chloroform-d(Riehs and Urban, 1997) (Table 6) enabled us to unambiguously identify the unknown compound as heptelidic acid.

This finding was unexpected because the WT strain used in this work and other Q-strains have never been reported to produce HA. The production of HA has served as one of the distinguishing factors to differentiate strains of *T. virens*, namely, P- and Q-strains. P-strains that typically produce HA do not produce gliotoxin. The Unk23.8min compound also was compared *via* HPLC with an authentic sample of heptelidic acid (Cayman Chemical Co., Ann Arbor, MI). The Unk23.8min compound and the authentic HA had the same retention time at 23.8 ± 0.1 min and the same UV-vis spectrum with a single λ_{max} at 219.8 ± 0.1 nm.

To determine the general yield of HA, a 250 mL volume of culture filtrate was extracted for quantification of the analyte by HPLC and revealed a concentration of 71.38 mg/L. This yield is significantly higher than the current published data from cultures grown in large batch fermenters (Rahier *et al.*, 2015). This could impact cancer research

due to the currently high costs of HA production and purification. With optimization and scaling, the yield could feasibly be increased even further.

During the process of identifying HA from the *ΔTex7* mutants, we also were able to detect a small amount of HA produced by the Gv29-8 strain. The amounts detected were negligible in comparison to the mutants and the P-strains (Howell *et al.*, 1993); however, as production of this compound is a hallmark in the classification of *T. virens* strains, this observation is crucial for fungal biology. Furthermore, due to the drastic overproduction of both viridin and HA in the absence of TEX7, there is a possibility that other secondary metabolite clusters may also influence regulation of HA through cross-talk (Hidalgo *et al.*, 2014; Sheridan *et al.*, 2015). Based on our data, we propose that production of HA is excluded as a defining characteristic for classifying strains of *T. virens*.

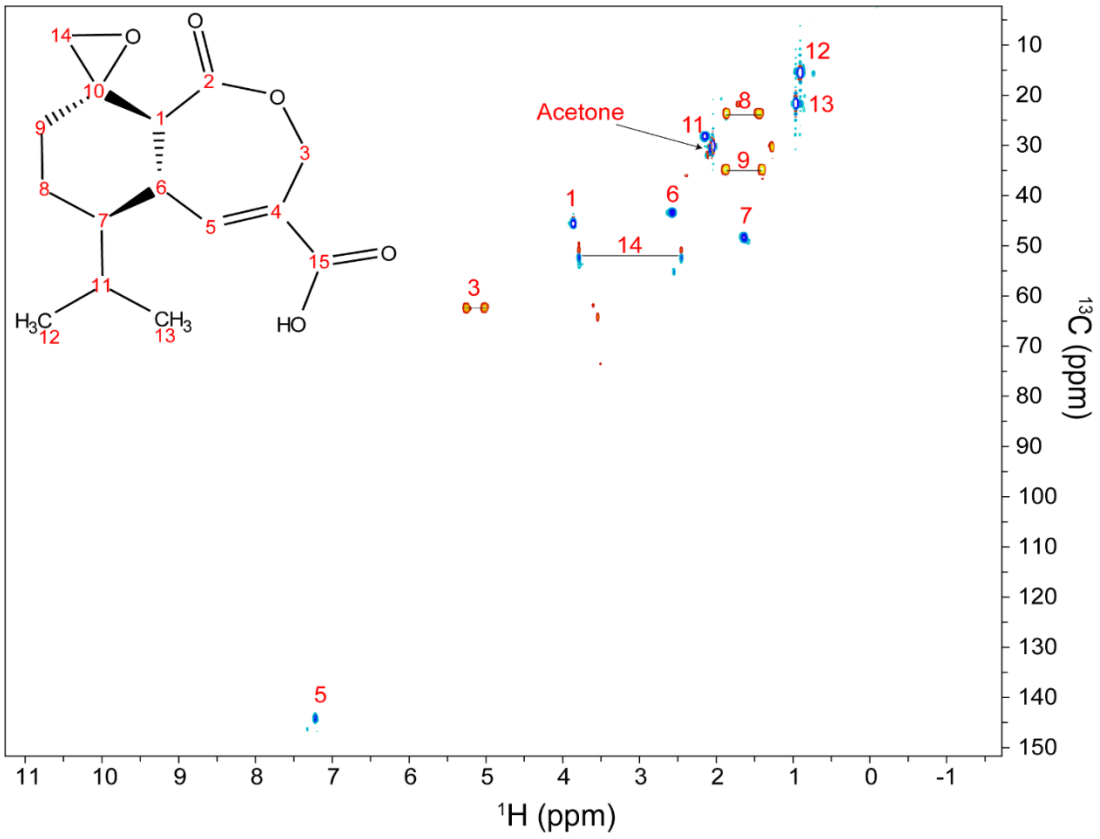

Figure 29. 2D [1H,13C] HMQC spectrum. The cross-peaks in the spectra indicate one-bond ^{1}H-^{13}C correlations. Horizontal lines connect two protons attached to the same carbon. Cross-peaks that have a positive phase (blue gradient) correspond to the CH and CH_3 groups; cross-peaks that have a negative phase (red gradient) belong to the CH_2 groups.

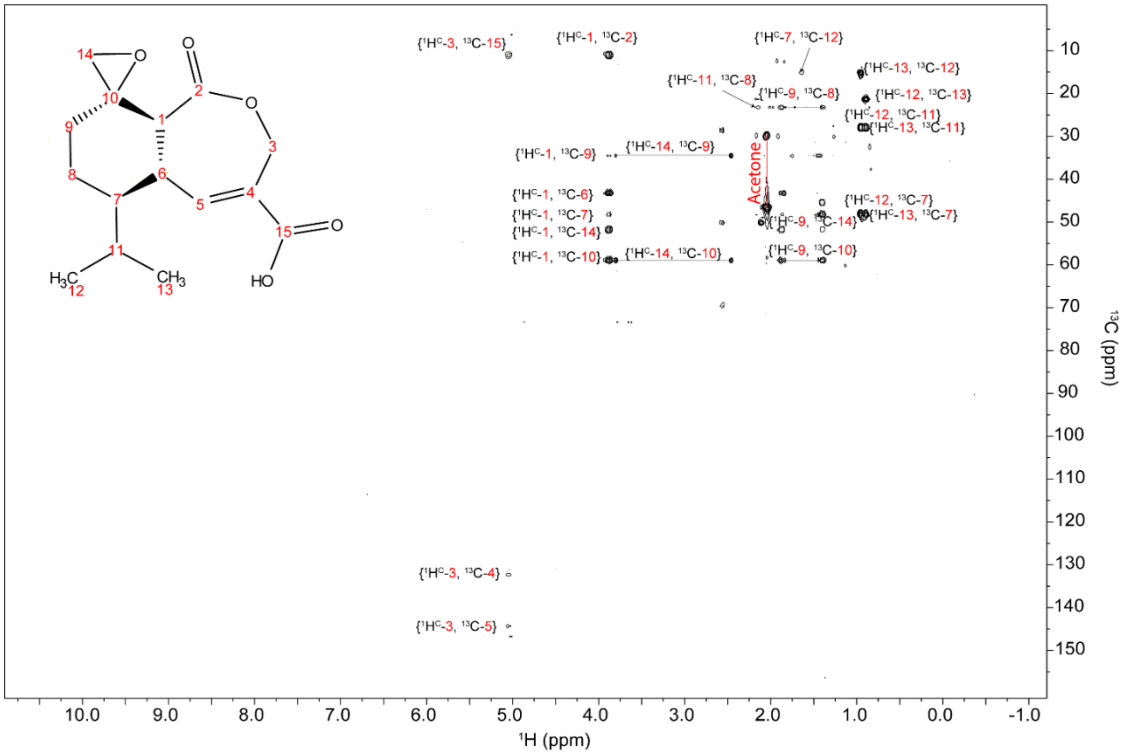

Figure 30. 2D [1H,13C] HMBC spectrum. The cross-peaks correspond to two- and three-bond ^{1}H-^{13}C correlations. The most upfield cross-peaks, H3-C15 and H1-C2, are aliased.

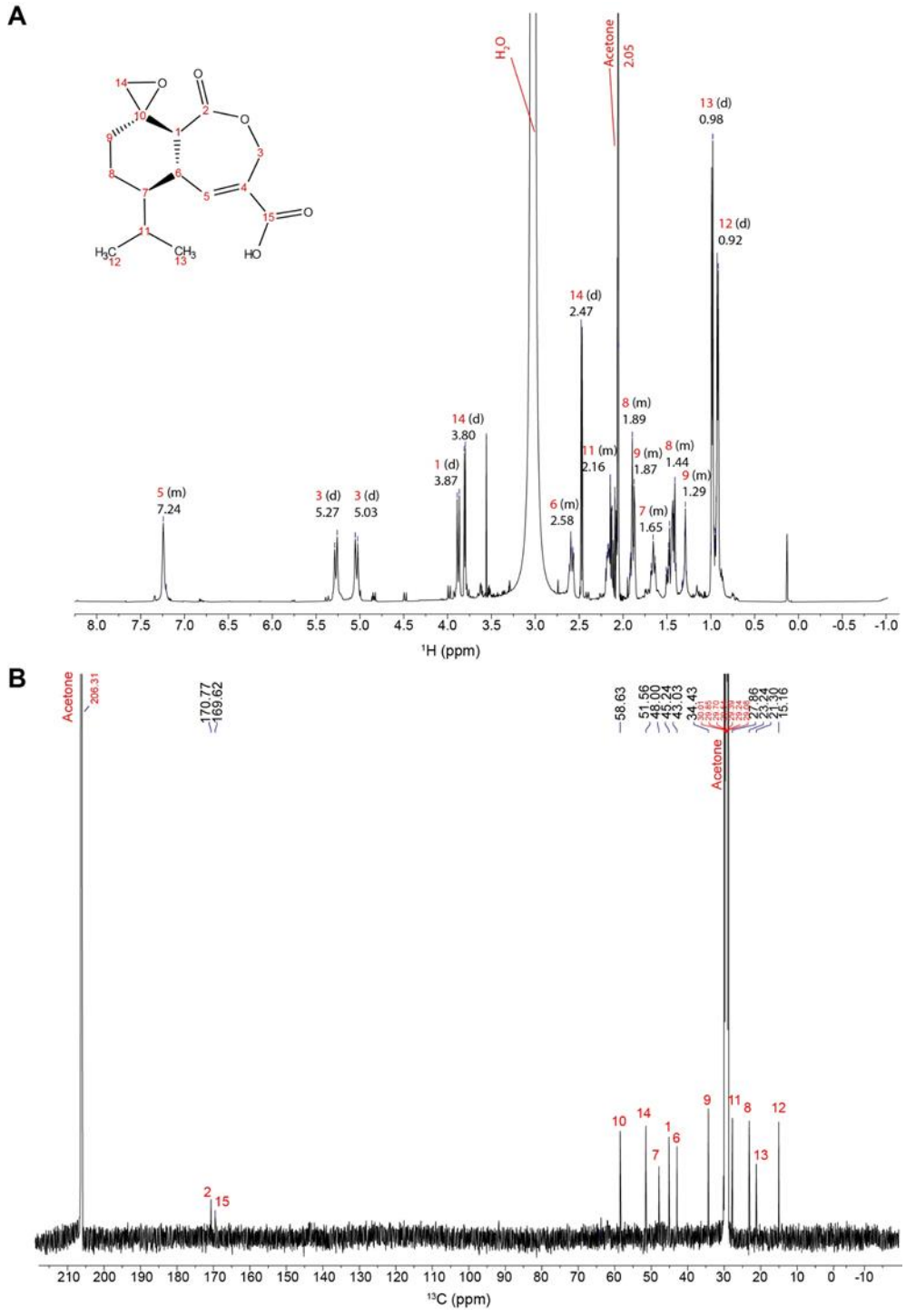

Figure 31. A) 1D ^{1}H NMR spectrum. All ^{1}H resonances are labeled according to the hydrogen position in the chemical structure (red), multiplicity in parenthesis, and the chemical shift value (black). ^{1}H peaks originating from residual protonated acetone and

water are also labeled. B) 1D ^{13}C NMR spectrum. All ^{13}C resonances are labeled according to the carbon position in the chemical structure. C4 and C3 are not detectable in the spectra likely due to unfavorable relaxation properties, but can be unambiguously identified in 2D [^{1}H,^{13}C] HMQC 2D [^{1}H,^{13}C] HMBC spectra, respectively.

Table 6. Comparison of the ^{1}H and ^{13}C chemical shifts and multiplicities for heptelidic acid in acetone-d^{6} (this work) and previously published values in chloroform-d^{11}:

Position		**δ_C (mult)**		**δ_H (intgt., mult, *J* in Hz)**	
This study	Ref.	This study	Ref.	This study	Ref.
1	*9a*	45.24 (CH)	*45.34*	3.87 (1H, d, 12.1)	*3.58 (1H, d, 12.2)*
2	*1*	169.62 (C)	*170.35*		
3	*3*	62.14 (CH2)	*61.09*	5.03 (1H, d, 14.8) 5.27 (1H, d, 14.8)	*5.03 (1H, d, 15.5)* *5.10 (1H, d, 15.5)*
4	*4*	132.18 (C)	*128.50*		
5	*5*	144.08 (CH)	*147.63*	7.24 (1H, m)	*7.39 (1H, d, 2.8)*
6	*5a*	43.03 (CH)	*42.26*	2.58 (1H, m)	*2.65 (1H, m)*
7	*6*	48.00 (CH)	*46.96*	1.65 (1H, m)	*1.43 (1H, s, 4.5)*
8	*7*	23.24 (CH2)	*22.34*	1.44 (1H, m) 1.89 (1H, m)	*1.47 (1H, m)* *1.82 (1H, m)*
9	*8*	34.43 (CH2)	*33.24*	1.25-1.34 (1H, m) 1.83-1.93 (1H, m)	*1.53-1.67(1H, m)* *1.93 (1H, m)*
10	*9*	58.63 (C)	*58.23*		
11	*i-Pr-CH*	27.86 (CH)	*27.43*	2.16 (1H, m)	*2.14 (1H, m)*
12	*i-Pr-CH_3*	15.16 (CH3)	*15.09*	0.92 (3H, d, 6.8)	*0.90 (3H, d, 6.8)*
13	*i-Pr-CH_3*	21.30 (CH3)	*21.09*	0.98 (3H, d, 6.8)	*0.99 (3H, d, 6.8)*
14	*epoxide*	51.56 (CH2)	*52.19*	2.47 (1H, d, 5.8) 3.80 (1H, d, 5.8)	*2.60 (1H, d, 4.7)*
15	*COOH*	171.77 (C)	*170.10*		

Following two weeks of exposure to *T. virens* strains, seedlings treated with *ΔTex7* mutants were significantly smaller in height compared with the WT-treated plants (Figure

32). Initially, we believed that the reduction in growth was due to the presence of HA. To explore this hypothesis, we tested maize germination after treatment with HA. For both the HA-treated and water-treated seeds (control), we observed 100% germination; thus, our hypothesis was rejected. The growth effect could instead be explained by the overproduction of viridin by the strains in conjunction with HA (Figure 27B**)**. Viridin is quickly reduced to viridiol, which has been previously demonstrated to be phytotoxic to a variety of plants, including maize (Jones and Hancock, 1987; Jones *et al.*, 1988). To explore a role of *TEX7* and HA in induced systemic resistance (ISR), plants colonized by WT or *ΔTex7* mutants were infected with the foliar pathogen, *Cochliobolus heterostrophus*. The *Δ*Tex7-treated plants did not show any difference in resistance phenotype compared to the WT (Figure 33). This finding suggests that despite reduced plant growth, *Δ*Tex7-treated plants are still receiving some of the symbiotic benefits from the fungus, and that these two fungus-derived benefits appear not to be correlated in plants. Our conclusion is supported by a previous study that revealed little correlation between percentage of plant growth enhancement and plant protection capability in a variety of other *Trichoderma* species (Fontenelle *et al.*, 2011).

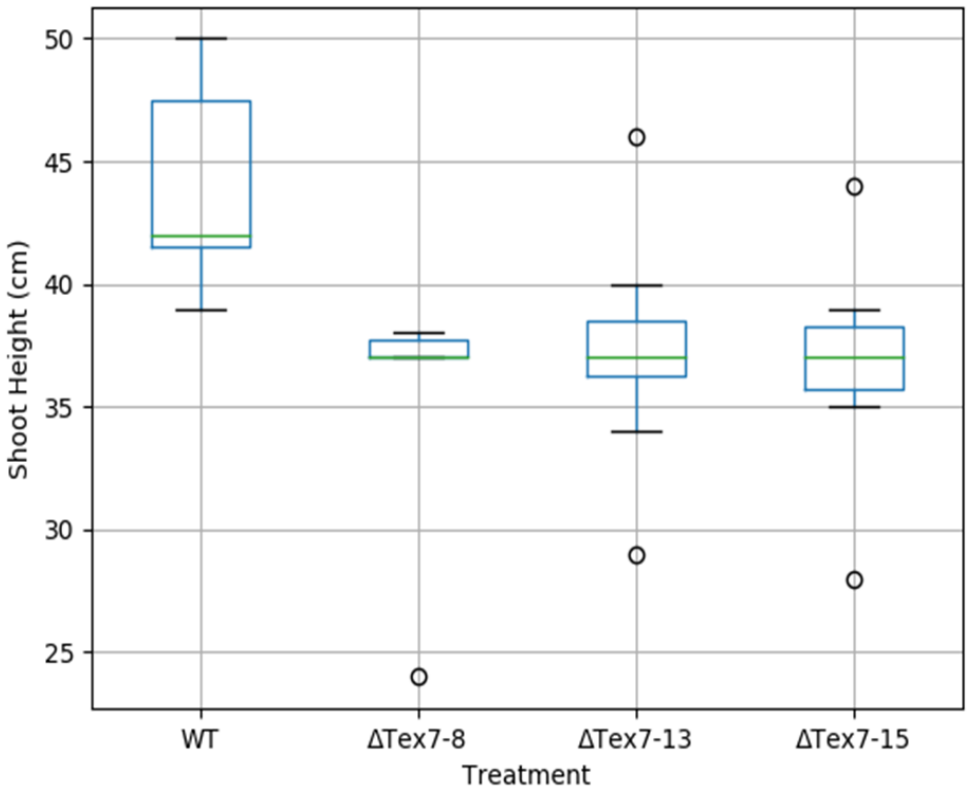

Figure 32. Growth inhibition of maize by *ΔTex7* disruption mutants. Plants treated with Tex7 disruption mutants were significantly shorter than those treated with the WT. Individual data points on the chart represent outliers. Treatments labeled with the different letters are significantly different at the 0.05 level by Tukey's HSD.

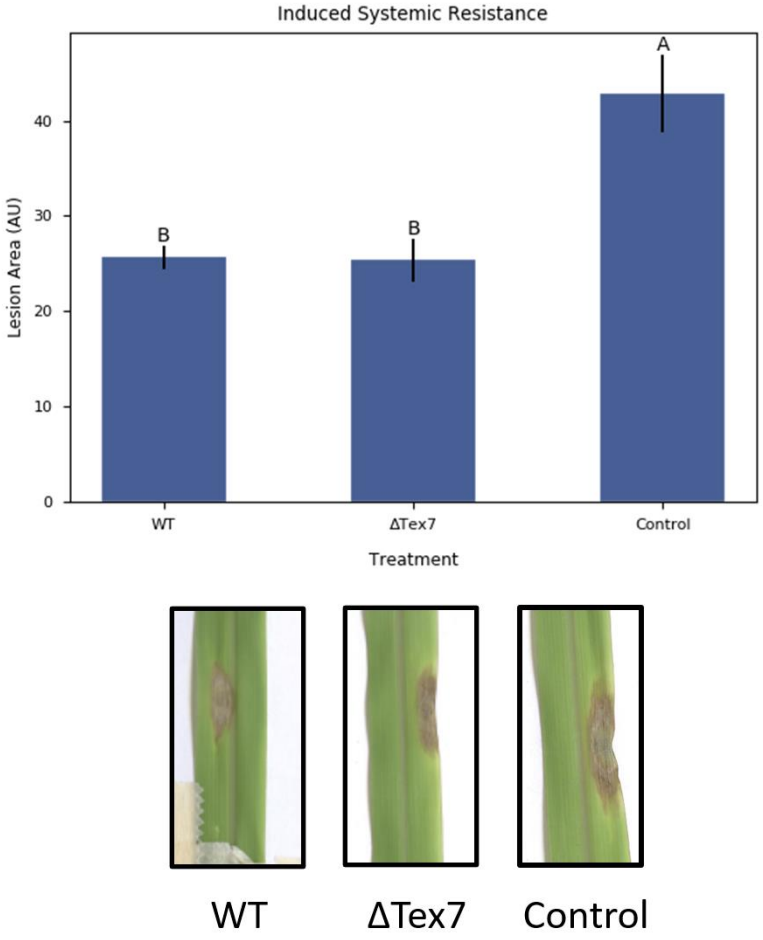

Figure 33. Induced systemic resistance. Plants treated with a *ΔTex7* strain showed no significant difference in lesion area compared to the WT strain, while untreated plants displayed larger lesion area on average. Treatments labeled with the different letters are significantly different at the 0.05 level by Tukey's HSD.

In conclusion, deletion of the *T. virens* NRPS, *Tex7*, resulted in the accumulation of large quantities of the bioactive anticancer compound heptelidic acid. The compound was purified using HPLC and identified using LC-MS/MS and solution NMR spectroscopy. We hypothesize that TEX7 regulates the production of HA and viridin through endogenous cross-talk. In addition to the biosynthesis of HA, the mutants inhibit

the growth of maize seedlings, likely due to the over-production and subsequent reduction of viridin to viridiol, a known phytotoxin. Finally, we noted the production of small amounts of heptelidic acid by the WT strain, suggesting that HA production is not an accurate distinguishing factor between *T. virens* strains.

Experimental Section

Strains and culture conditions

Trichoderma virens strain Gv 29-8 (WT) was cultured on potato dextrose agar (PDA) at 27°C. Strains were grown in liquid Vogel's minimal medium(Vogel, 1956) supplemented with glucose as a carbon source (VMG) for production of secondary metabolites. A single crossover strategy was implemented to generate Tex7 gene disruption mutants as a part of a previous study (Mukherjee *et al.*, 2012a). The maize foliar pathogen, *C. heterostrophus* was cultured on PDA at room temperature under a 14:10 hour light:dark regime.

Bioinformatic analysis

The nucleotide and protein sequences of *Tex7* were obtained from the Joint Genome Institute (JGI) database for *T. virens* (Kubicek *et al.*, 2011). The protein sequence was analyzed for conserved domains using the Interpro scan server (Jones *et al.*, 2014). The protein sequence was also analyzed for putative amino acid substrates of the NRPS using the Nonribosomal Peptide Synthase Substrate Predictor server (Prieto *et al.*, 2012).

Extraction of metabolites and TLC analysis

Flasks containing 50 mL of Vogel's minimal medium with 1.5% sucrose or glucose were inoculated with three, six mm diameter agar plugs of either the mutants or

WT cultures. The flasks were incubated at 27°C as still culture for four days. The cultures were filtered through No. 4 Whatman filter paper with two mL of the culture filtrate for each sample added to a test tube and mixed vigorously with an equal volume of ethyl acetate. The layers were allowed to separate, and the upper organic layer was collected in a 2-mL microcentrifuge tube and concentrated by evaporation under low pressure. After the concentration, the resulting residue was suspended in 20 µl methanol and used for thin layer chromatography (TLC).

TLC was used for separation of the constituent metabolites within each sample. A 10 x10 inch silica-coated aluminum TLC plate was pretreated by running the mobile phase (70:28:2 chloroform:methanol:formic acid) along the length of the plate to adjust the plate's pH. The plate was removed from the chamber and allowed to fully dry. The samples and gliotoxin standard were spotted on the plate approximately 1 cm apart and allowed to fully dry. The plate was then placed in the chamber and the mobile phase allowed to run approximately 90% of the plate length and the solvent front marked. The plate was fully dried before visualization with UV light to observe the analytes.

Preparation for HPLC and HPLC protocol

Five 100 mL cultures of the mutant strains were grown for four days at room temperature without shaking. The cultures were filtered and extracted as above, with an equal volume of ethyl acetate in a separatory funnel. The bottom aqueous layer was discarded, and the upper organic layer was passed through sodium sulfate to remove residual water during collection. The extract was transported to the Southern Plains Agricultural Research Center in College Station, Tx for HPLC analysis.

Extracts from *T. virens* culture or a sample from the isolation and purification procedures was rotoevaporated to dryness under a reduced vacuum at 30°C and then reconstituted in a recorded volume of methanol or acetonitrile. The sample was subjected to HPLC using an Agilent Technologies 1200 LC system equipped with a diode array detector (Santa Clara, CA). The HPLC method used an SGE ProteCol-GP125-C18 (4.6 x 250 mm, 5 µm) column (Trajan Scientific, Australia) maintained at 40°C and a gradient mobile phase of acetonitrile and water (both with 0.07% H_3PO_4) run at 1.25 mL/min. The acetonitrile % setpoints for the gradient are as follows: 25% (0 min), 25% (14 min), 32% (15 min), 32% (25 min), 80% (26 min), 80% (28 min), 25% (30 min), and 25% (33min). The chromatogram signal was obtained at 254 ± 10 nm (reference 550 ± 50 nm) and spectra for detected peaks were collected over 210 – 600 nm. Injection volumes varied from 5 to 25 µL.

Quantitation of the known compounds viridiol, gliotoxin, dimethylgliotoxin, gliovirin, and viridin in an extract was achieved using µg versus HPLC peak area curves determined from authentic material. During the isolation and purification procedures, the purity of the unknown analyte in any one sample was estimated from its peak area in relation to the summation of the areas of all peaks in the chromatogram (i.e., peak area percentage).

Purification of Unk23.8min (HA)

Ethyl acetate extracts from four 50 mL cultures of three individual *T. virens ΔTex7* strains were combined, rotoevaporated to dryness under reduced pressure at 30°C, and then reconstituted in 1 mL methanol. The sample was subjected to HPLC, using standard

analytical methods with a 50 µL injection volume. Afterwards, the Unk23.8min peak was manually collected from the HPLC eluent from each of the runs. The collected fraction was rotoevaporated to remove acetonitrile and then extracted three times with an equal volume of ethyl acetate. The ethyl acetate sample was rotoevaporated to dryness, weighed, and analyzed by HPLC.

An ethyl acetate extract from a 500 mL culture of *T. virens ΔTex7* was rotoevaporated to dryness under reduced pressure at 30 °C to obtain the dry weight of the extract (332 mg). The material was dissolved in 30 mL ethyl acetate. A 10 mL aliquot of the concentrated extract was dried onto 6 g Baker silica gel 40-140 mesh (Baker Mallinckrodt, Phillipsburg, NJ) and then loaded onto a 50 g silica gel column (2.5 x 34 cm). The sample was eluted with ca. 1000 mL of 50:50:20 (v:v:v) hexane:isopropyl alcohol:ethyl acetate. Fractions (60 mL) were collected and subjected to HPLC. Fractions with similar Unk23.8min content were combined to yield two samples which were then rotoevaporated to dryness and, along with fractions lacking Unk23.8min, stored at -20 °C. The isolation procedure was repeated for two more aliquots of the extract and the new fractions combined as appropriate into the three samples. The final two Unk23.8min samples were weighed and analyzed by HPLC.

The Unk23.8min samples were streaked onto multiple plates of Baker silica gel G/HR for TLC with zinc silicate phosphor (Sigma-Aldrich, St. Louis, MO) and developed in 85:15 chloroform:ethyl acetate (v:v). The Unk23.8min bands on the plates were collected, the compound was washed from the silica gel with ethyl acetate, and the washed sample was rotoevaporated to dryness. The sample was purified by TLC again. The

Unk23.8min sample was crystallized using hexane:ethyl acetate (1:1, v:v) at room temperature for several days.

NMR spectroscopy

The sample was prepared by dissolving 7.7 mg of compound in 550 µL of acetone-d_6. All spectra were collected on an NMR spectrometer (Avance III HD, Bruker Biospin) operating at the 1H Larmor frequency of 500 MHz (11.7 T) and equipped with a conventional 5 mm TXI probe. The temperature in all experiments was set to 25 ºC. The following NMR experiments were carried out: 1D ^{1}H, 1D ^{13}C (^{1}H decoupled), 1D ^{13}C DEPT-135, 2D [^{1}H,^{13}C] HMQC, 2D [^{1}H,^{13}C] HMBC, 2D [^{1}H,^{1}H] COSY, and 2D [^{1}H,^{1}H] TOCSY. Chemical shift referencing was done with respect to TMS.

Maize germination assay

Maize seeds were allowed to imbibe either water or 10 µM heptelidic acid for 2 hours. The seeds and remaining solutions (10 mL) were transferred to sterile petri plates lined with filter paper. The plates were sealed with parafilm and allowed to germinate for 3 days in the dark at 27 ºC.

Plant growth and ISR activity

For plant growth studies, 50 g of MetroMix 366 soil-less medium was infested with 0.1 g of either WT or mutant *T. virens* chlamydospores and transferred to a bleach sterilized container. Seeds of maize B73 inbred line were pre-germinated on 0.5x Murashige and Skoog basal medium with Gamborg's vitamins (Sigma, USA) plus 0.5% sucrose and 1.5% agar for three days. Uniform seedlings were selected to minimize differences in germination and planted into the infested soil approximately two cm deep.

The plants were grown for two weeks before the shoots were cut just above the seed and measured for total height and fresh weight. Induced systemic resistance was measured as in Djonovic et al. (Djonović *et al.*, 2007) using *C. heterostrophus* as the pathogen based on the consistency of lesion production.

CHAPTER V

CONCLUSION

The development of our comprehension of the colonization process of *T. virens* is paramount to enable a greater understanding of plant-microbe interactions. Advanced knowledge of these interactions has implications in both understanding how beneficial microbes attain symbiosis with plant hosts, but also how pathogens evade plant defenses to cause disease. This project expanded our knowledge of the colonization process and plant-microbe interactions through an RNA-seq transcriptomic profiling study of the early stage of colonization and of the effects of *Sm1* or *Sir1* gene deletion, characterization of HFB9a, a hydrophobin that is vital for colonization and induced systemic resistance, and characterization of the *Tex7* deletion mutant, which over produces heptelidic acid and viridin.

Through transcriptomic profiling of WT in association of maize in hydroponic systems at early time points (6, 12, 15, 24, and 36 hpi), 24 hpi was revealed as a key time with regard to plant-microbe interactions. Differentially expressed genes involved in signal transduction mechanisms, defense mechanisms, carbohydrate metabolism, and secondary metabolism all peaked in expression at 24 hpi. Some of the signal transduction genes discovered in this analysis included a ceramidase, adhesin gene, and a CFEM domain protein, all of which could be exciting targets for future study. Analysis of carbohydrate transport and metabolism genes revealed several chitinases, one of which contained a LysM domain and likely served as a tool for the fungus to avoid pathogen

associated molecular pattern recognition of chitin by the plant. Another gene of interest that only had a general function assigned, was a protein containing the SCP domain. This domain is involved in defense against fungi and related to the plant PR-1 gene.

A gene co-expression network was developed and utilized in a pipeline to select target genes with a higher likelihood of involvement in colonization and plant microbe interactions. This pipeline importantly identified SM2, a known elicitor protein. In addition, 40% of the genes identified by the pipeline were not found by the traditional method of target gene selection.

Analysis of RNA-seq based transcriptome profiles of *Sir1* and *Sm1* deletion mutants on maize plants demonstrated that Sir1 regulated much of the fungal side of the colonization process. *ΔSir1* mutants had significantly more unique differentially expressed genes compared to *ΔSm1.* Many of the unique genes were annotated as being involved in signal transduction, carbohydrate metabolism, and transport.

The *T. virens* hydrophobin, HFB9a, was demonstrated to have roles in root colonization and induced systemic resistance. The deletion mutants exhibited significantly less cell wall-degrading enzyme activity (complemented by addition of purified HFB9a protein), were unable to colonize maize roots as well as the wild-type strain, and were unable to induce systemic resistance. The pure protein was also found to activate phosphorylation of atMAPK3/4 which is associated with recognition as a MAMP.

Finally, deletion of the non-ribosomal peptide synthetase, *Tex7*, induced the accumulation of heptelidic acid and viridin. These mutants negatively affected maize plant growth, likely due to the overproduction of viridin and its consequent conversion to

viridiol, a phytotoxin. Production of hepteledic acid was a novel discovery for this strain, both in large amounts by the mutant, and in miniscule amounts by the wild-type strain. The current classification structure of *T. virens* strains separates strains by the secondary metabolites they produce, and the discovery of heptelidic acid production by the wild-type strain, breaks the mold of the current classification structure.

REFERENCES

Adachi, H., Nakano, T., Miyagawa, N., Ishihama, N., Yoshioka, M., Katou, Y., *et al.* (2015) Wrky transcription factors phosphorylated by mapk regulate a plant immune nadph oxidase in nicotiana benthamiana. *Plant Cell* **27**: 2645–2663.

Adav, S.S., and Sze, S.K. (2014) Trichoderma Secretome: An Overview. In *Biotechnology and Biology of Trichoderma*. pp. 103–114.

Altomare, C., Norvell, W.A., Björkman, T., and Harman, G.E. (1999) Solubilization of phosphates and micronutrients by the plant-growth- promoting and biocontrol fungus Trichoderma harzianum Rifai 1295-22. *Appl Environ Microbiol* **65**: 2926–2933.

Amrine, K.C.H., Blanco-Ulate, B., and Cantu, D. (2015) Discovery of core biotic stress responsive genes in Arabidopsis by weighted gene co-expression network analysis. *PLoS One* **10**.

Baek, J.M., Howell, C.R., and Kenerley, C.M. (1999) The role of an extracellular chitinase from Trichoderma virens Gv29-8 in the biocontrol of Rhizoctonia solani. *Curr Genet* **35**: 41–50 http://link.springer.com/10.1007/s002940050431. Accessed May 1, 2017.

Bayry, J., Aimanianda, V., Guijarro, J.I., Sunde, M., and Latgé, J.P. (2012) Hydrophobins-unique fungal proteins. *PLoS Pathog* **8**: e1002700 http://dx.plos.org/10.1371/journal.ppat.1002700. Accessed July 29, 2016.

Bignell, E. (2012) The Molecular Basis of pH Sensing, Signaling, and Homeostasis in Fungi. In *Advances in Applied Microbiology*. Academic Press Inc., pp. 1–18.

Boller, T., and He, S.Y. (2009) Innate immunity in plants: An arms race between pattern recognition receptors in plants and effectors in microbial pathogens. *Science (80-)* **324**: 742–743 http://science.sciencemag.org/content/324/5928/742.long. Accessed August 13, 2017.

Brotman, Y., Briff, E., Viterbo, A., and Chet, I. (2008) Role of swollenin, an expansin-like protein from Trichoderma, in plant root colonization. *Plant Physiol* **147**: 779–789 http://www.pubmedcentral.nih.gov/articlerender.fcgi?artid=2409044&tool=pmcentrez&rendertype=abstract. Accessed November 13, 2015.

Brotman, Y., Landau, U., Cuadros-Inostroza, Á., Takayuki, T., Fernie, A.R., Chet, I., *et al.* (2013) Trichoderma-Plant Root Colonization: Escaping Early Plant Defense Responses and Activation of the Antioxidant Machinery for Saline Stress Tolerance. *PLoS Pathog* **9**.

Chaverri, P., Samuels, G.J., and Stewart, E.L. (2001) Hypocrea virens sp. nov., the teleomorph of Trichoderma virens . *Mycologia* **93**: 1113–1124.

Choudhary, D.K., Prakash, A., and Johri, B.N. (2007) Induced systemic resistance (ISR) in plants: Mechanism of action. *Indian J Microbiol* **47**: 289–297 http://www.ncbi.nlm.nih.gov/pubmed/23100680. Accessed August 14, 2017.

Christensen, S.A., Nemchenko, A., Borrego, E., Murray, I., Sobhy, I.S., Bosak, L., *et al.* (2013) The maize lipoxygenase, ZmLOX10, mediates green leaf volatile, jasmonate and herbivore-induced plant volatile production for defense against insect attack. *Plant J* **74**: 59–73.

Constantino, N.N., Mastouri, F., Damarwinasis, R., Borrego, E.J., Moran-Diez, M.E.,

Kenerley, C.M., *et al.* (2013) Root-expressed maize lipoxygenase 3 negatively regulates induced systemic resistance to Colletotrichum graminicola in shoots. *Front Plant Sci* **4**: 510 http://www.ncbi.nlm.nih.gov/pubmed/24391653. Accessed May 2, 2017.

Contreras-Cornejo, H.A., Macías-Rodríguez, L., Cortés-Penagos, C., and López-Bucio, J. (2009) Trichoderma virens, a plant beneficial fungus, enhances biomass production and promotes lateral root growth through an auxin-dependent mechanism in arabidopsis. *Plant Physiol* **149**: 1579–1592 http://www.ncbi.nlm.nih.gov/pubmed/19176721. Accessed October 4, 2016.

Contreras-Cornejo, H.A., Macías-Rodríguez, L., López-Bucio, J.S., and López-Bucio, J. (2014) Enhanced Plant Immunity Using Trichoderma. In *Biotechnology and Biology of Trichoderma*. pp. 495–504.

Correia, I., Prieto, D., Alonso-Monge, R., Pla, J., and Román, E. (2017) The MAP Kinase Network As the Nervous System of Fungi. In *Reference Module in Life Sciences*. Elsevier, .

Creelman, R.A., and Mullet, J.E. (1997) Biosynthesis and Action of Jasmonates in Plants. *Annu Rev Plant Physiol Plant Mol Biol* **48**: 355–381 http://www.annualreviews.org/doi/10.1146/annurev.arplant.48.1.355. Accessed August 14, 2017.

Crutcher, F.K., Moran-Diez, M.E., Ding, S., Liu, J., Horwitz, B.A., Mukherjee, P.K., and Kenerley, C.M. (2015) A paralog of the proteinaceous elicitor SM1 is involved in colonization of maize roots by Trichoderma virens. *Fungal Biol* **119**: 476–486.

Darwiche, R., Mène-Saffrané, L., Gfeller, D., Asojo, O.A., and Schneiter, R. (2017) The

pathogen-related yeast protein Pry1, a member of the CAP protein superfamily, is a fatty acid-binding protein. *J Biol Chem* **292**: 8304–8314.

Degenkolb, T., Fognielsen, K., Dieckmann, R., Branco-Rocha, F., Chaverri, P., Samuels, G.J., *et al.* (2015) Peptaibol, secondary-metabolite, and hydrophobin pattern of commercial biocontrol agents formulated with species of the trichoderma harzianum complex. *Chem Biodivers* **12**: 662–684.

Delabona, P. da S., Farinas, C.S., Silva, M.R. da, Azzoni, S.F., and Pradella, J.G. da C. (2012) Use of a new Trichoderma harzianum strain isolated from the Amazon rainforest with pretreated sugar cane bagasse for on-site cellulase production. *Bioresour Technol* **107**: 517–521.

Djonović, S., Pozo, M.J., Dangott, L.J., Howell, C.R., and Kenerley, C.M. (2006a) Sm1, a proteinaceous elicitor secreted by the biocontrol fungus Trichoderma virens induces plant defense responses and systemic resistance. *Mol Plant-Microbe Interact* **19**: 838–853 http://apsjournals.apsnet.org/doi/abs/10.1094/MPMI-19-0838. Accessed August 31, 2016.

Djonović, S., Pozo, M.J., and Kenerley, C.M. (2006b) Tvbgn3, a β-1,6-glucanase from the biocontrol fungus Trichoderma virens, is involved in mycoparasitism and control of Pythium ultimum. *Appl Environ Microbiol* **72**: 7661–7670.

Djonović, S., Vargas, W.A., Kolomiets, M. V., Horndeski, M., Wiest, A., and Kenerley, C.M. (2007) A proteinaceous elicitor Sm1 from the beneficial fungus Trichoderma virens is required for induced systemic resistance in Maize. *Plant Physiol* **145**: 875–889 http://www.plantphysiol.org/cgi/doi/10.1104/pp.107.103689. Accessed October 4, 2016.

Dubey, M.K., Jensen, D.F., and Karlsson, M. (2014) Hydrophobins are required for conidial hydrophobicity and plant root colonization in the fungal biocontrol agent Clonostachys rosea. *BMC Microbiol* **14**: 18 http://bmcmicrobiol.biomedcentral.com/articles/10.1186/1471-2180-14-18. Accessed July 21, 2016.

Ellilä, S., Fonseca, L., Uchima, C., Cota, J., Goldman, G.H., Saloheimo, M., *et al.* (2017) Development of a low-cost cellulase production process using Trichoderma reesei for Brazilian biorefineries. *Biotechnol Biofuels* **10**: 1–17.

Fontenelle, A.D.B., Guzzo, S.D., Lucon, C.M.M., and Harakava, R. (2011) Growth promotion and induction of resistance in tomato plant against Xanthomonas euvesicatoria and Alternaria solani by Trichoderma spp. *Crop Prot* **30**: 1492–1500.

Gaderer, R., Lamdan, N.L., Frischmann, A., Sulyok, M., Krska, R., Horwitz, B.A., and Seidl-Seiboth, V. (2015) Sm2, a paralog of the Trichoderma cerato-platanin elicitor Sm1, is also highly important for plant protection conferred by the fungal-root interaction of Trichoderma with maize. *BMC Microbiol* **15**.

Gorman, Z., Christensen, S.A., Yan, Y., He, Y., Borrego, E., and Kolomiets, M. V. (2020) Green leaf volatiles and jasmonic acid enhance susceptibility to anthracnose diseases caused by Colletotrichum graminicola in maize. *Mol Plant Pathol* **21**: 702–715 https://bsppjournals.onlinelibrary.wiley.com/doi/full/10.1111/mpp.12924.

Gupta, V.K., Schmoll, M., Herrera-Estrella, A., Upadhyay, R.S., Druzhinina, I., and Tuohy, M.G. (2014) *Biotechnology and Biology of Trichoderma*. .

Gutiérrez-Román, M.I., Dunn, M.F., Tinoco-Valencia, R., Holguín-Meléndez, F.,

Huerta-Palacios, G., and Guillén-Navarro, K. (2014) Potentiation of the synergistic activities of chitinases ChiA, ChiB and ChiC from Serratia marcescens CFFSUR-B2 by chitobiase (Chb) and chitin binding protein (CBP). *World J Microbiol Biotechnol* **30**: 33–42.

Guzmán-Guzmán, P., Alemán-Duarte, M.I., Delaye, L., Herrera-Estrella, A., and Olmedo-Monfil, V. (2017) Identification of effector-like proteins in Trichoderma spp. and role of a hydrophobin in the plant-fungus interaction and mycoparasitism. *BMC Genet* **18**: 16 http://www.ncbi.nlm.nih.gov/pubmed/28201981. Accessed September 17, 2018.

Han, F., Lu, A., Yuan, Y., Huang, W., Beerntsen, B.T., Huang, J., and Ling, E. (2017) Characterization of an entomopathogenic fungi target integument protein, *Bombyx mori* single domain von Willebrand factor type C, in the silkworm, *Bombyx mori*. *Insect Mol Biol* **26**: 308–316 http://doi.wiley.com/10.1111/imb.12293. Accessed May 12, 2020.

Heil, M., and Bostock, R.M. (2002) Induced systemic resistance (ISR) against pathogens in the context of induced plant defences. *Ann Bot* **89**: 503–12 http://www.ncbi.nlm.nih.gov/pubmed/12099523. Accessed August 11, 2017.

Hermosa, R., Belén Rubio, M., Cardoza, R.E., Nicolás, C., Monte, E., and Gutiérrez, S. (2013) The contribution of Trichoderma to balancing the costs of plant growth and defense. *Int Microbiol* **16**.

Hidalgo, P.I., Ullán, R. V., Albillos, S.M., Montero, O., Fernández-Bodega, M.Á., García-Estrada, C., *et al.* (2014) Molecular characterization of the PR-toxin gene cluster in Penicillium roqueforti and Penicillium chrysogenum: Cross talk of secondary

metabolite pathways. *Fungal Genet Biol* **62**: 11–24.

Howell, C.R. (1987) Relevance of Mycoparasitism in the Biological Control of Rhizoctonia solani by Gliocladium virens. *Phytopathology* **77**: 992–994.

Howell, C.R. (2003) Mechanisms Employed by *Trichoderma* Species in the Biological Control of Plant Diseases: The History and Evolution of Current Concepts. *Plant Dis* **87**: 4–10 http://apsjournals.apsnet.org/doi/abs/10.1094/PDIS.2003.87.1.4. Accessed October 4, 2016.

Howell, C.R., Hanson, L.E., Stipanovic, R.D., and Puckhaber, L.S. (2000) Induction of Terpenoid Synthesis in Cotton Roots and Control of *Rhizoctonia solani* by Seed Treatment with *Trichoderma virens*. *Phytopathology* **90**: 248–252 http://apsjournals.apsnet.org/doi/10.1094/PHYTO.2000.90.3.248. Accessed August 11, 2017.

Howell, C.R., Stipanovic, R.D., and Lumsden, R.D. (1993) Antibiotic production by strains of *Gliocladium virens* and its relation to the biocontrol of cotton seedling diseases. *Biocontrol Sci Technol* **3**: 435–441 http://www.tandfonline.com/doi/abs/10.1080/09583159309355298. Accessed June 6, 2019.

Huang, P.-C. (2017) Oxylipin signals govern drought and salt tolerance and resistance to pathogens. .

Joensuu, J.J., Conley, A.J., Lienemann, M., Brandle, J.E., Linder, M.B., and Menassa, R. (2010) Hydrophobin fusions for high-level transient protein expression and purification in Nicotiana benthamiana. *Plant Physiol* **152**: 622–33

http://www.ncbi.nlm.nih.gov/pubmed/20018596. Accessed March 31, 2017.

Jones, P., Binns, D., Chang, H.Y., Fraser, M., Li, W., McAnulla, C., *et al.* (2014) InterProScan 5: Genome-scale protein function classification. *Bioinformatics* **30**: 1236–1240.

Jones, R.W., and Hancock, J.G. (1987) Conversion of viridin to viridiol by viridin-producing fungi. *Can J Microbiol* **33**: 963–966.

Jones, R.W., Lanini, W.T., and Hancock, J.G. (1988) Plant Growth Response to the Phytotoxin Viridiol Produced by the Fungus Gliocladium virens . *Weed Sci* **36**: 683–687.

Junaid, J.M., Dar, N.A., Bhat, T.A., Hussain Bhat, A., and Bhat, M.A. (2013) Commercial Biocontrol Agents and Their Mechanism of Action in the Management of Plant Pathogens. *Int J Mod Plant Anim Sci J Mod Plant Anim Sci* **1**: 39–57 www.ModernScientificPress.com/Journals/IJPlant.aspx. Accessed February 26, 2020.

Kazan, K., and Lyons, R. (2014) Intervention of Phytohormone Pathways by Pathogen Effectors. *Plant Cell* **26**.

Kim, K.T., Jeon, J., Choi, J., Cheong, K., Song, H., Choi, G., *et al.* (2016) Kingdom-wide analysis of fungal small secreted proteins (SSPs) reveals their potential role in host association. *Front Plant Sci* **7**.

Kovács, K., Szakacs, G., and Zacchi, G. (2009) Comparative enzymatic hydrolysis of pretreated spruce by supernatants, whole fermentation broths and washed mycelia of Trichoderma reesei and Trichoderma atroviride. *Bioresour Technol* **100**: 1350–1357.

Kubicek, C.P., Baker, S.E., Gamauf, C., Kenerley, C.M., Druzhinina, I.S., Wessels, J., *et al.* (2008) Purifying selection and birth-and-death evolution in the class II hydrophobin

gene families of the ascomycete Trichoderma/Hypocrea. *BMC Evol Biol* **8**: 4 http://bmcevolbiol.biomedcentral.com/articles/10.1186/1471-2148-8-4. Accessed July 26, 2016.

Kubicek, C.P., Herrera-Estrella, A., Seidl-Seiboth, V., Martinez, D.A., Druzhinina, I.S., Thon, M., *et al.* (2011) Comparative genome sequence analysis underscores mycoparasitism as the ancestral life style of Trichoderma. *Genome Biol* **12**: R40 http://www.ncbi.nlm.nih.gov/pubmed/21501500. Accessed August 31, 2016.

Lamdan, N.-L., Shalaby, S., Ziv, T., Kenerley, C.M., and Horwitz, B.A. (2015a) Secretome of the biocontrol fungus Trichoderma virens co-cultured with maize roots: role in induced systemic resistance. *Mol Cell Proteomics* **14**: 1054–1063 http://www.mcponline.org/content/14/4/1054.abstract?etoc.

Lamdan, N.-L., Shalaby, S., Ziv, T., Kenerley, C.M., and Horwitz, B.A. (2015b) Secretome of Trichoderma interacting with maize roots: role in induced systemic resistance. *Mol Cell Proteomics* **14**: 1054–63 http://www.ncbi.nlm.nih.gov/pubmed/25681119. Accessed November 30, 2016.

Levasseur, A., Saloheimo, M., Navarro, D., Andberg, M., Pontarotti, P., Kruus, K., and Record, E. (2010) Exploring laccase-like multicopper oxidase genes from the ascomycete Trichoderma reesei: A functional, phylogenetic and evolutionary study. *BMC Biochem* **11**: 1–10.

Li, B., Jiang, S., Yu, X., Cheng, C., Chen, S., Cheng, Y., *et al.* (2015) Phosphorylation of trihelix transcriptional repressor ASR3 by MAP KINASE4 negatively regulates arabidopsis immunity. *Plant Cell* **27**: 839–856.

Lu, S., and Edwards, M.C. (2016) Genome-wide analysis of small secreted cysteine-rich proteins identifies candidate effector proteins potentially involved in fusarium graminearum-wheat interactions. *Phytopathology* **106**: 166–176.

Lumsden, R.D., Ridout, C.J., Vendemia, M.E., Harrison, D.J., Waters, R.M., and Walter, J.F. (1992) Characterization of major secondary metabolites produced in soilless mix by a formulated strain of the biocontrol fungus *Gliocladium virens*. *Can J Microbiol* **38**: 1274–1280 http://www.nrcresearchpress.com/doi/10.1139/m92-210. Accessed January 16, 2020.

Malinich, E.A., Wang, K., Mukherjee, P.K., Kolomiets, M., and Kenerley, C.M. (2019) Differential expression analysis of Trichoderma virens RNA reveals a dynamic transcriptome during colonization of Zea mays roots. *BMC Genomics* **20**: 280 https://bmcgenomics.biomedcentral.com/articles/10.1186/s12864-019-5651-z. Accessed August 13, 2019.

Mandal, S., Ji, W., and McKnight, T.D. (2020) Candidate Gene Networks for Acylsugar Metabolism and Plant Defense in Wild Tomato Solanum pennellii. *Plant Cell* **32**: 81–99.

Mendoza-Mendoza, A., Zaid, R., Lawry, R., Hermosa, R., Monte, E., Horwitz, B.A., and Mukherjee, P.K. (2018) Molecular dialogues between Trichoderma and roots: Role of the fungal secretome. *Fungal Biol Rev* **32**: 62–85 https://www.sciencedirect.com/science/article/pii/S1749461317300738. Accessed April 5, 2018.

Michaelson, L. V., Napier, J.A., Molino, D., and Faure, J.D. (2016) Plant sphingolipids: Their importance in cellular organization and adaption. *Biochim Biophys Acta - Mol Cell*

Biol Lipids **1861**: 1329–1335.

Monfil, V.O., and Casas-Flores, S. (2014) Molecular Mechanisms of Biocontrol in Trichoderma spp. and Their Applications in Agriculture. In *Biotechnology and Biology of Trichoderma*. .

Morán-Diez, M.E., Trushina, N., Lamdan, N.L., Rosenfelder, L., Mukherjee, P.K., Kenerley, C.M., and Horwitz, B.A. (2015) Host-specific transcriptomic pattern of Trichoderma virens during interaction with maize or tomato roots. *BMC Genomics* **16**: 8 http://www.ncbi.nlm.nih.gov/pubmed/25608961. Accessed August 31, 2016.

Morris, V.K., Kwan, A.H., and Sunde, M. (2013) Analysis of the Structure and Conformational States of DewA Gives Insight into the Assembly of the Fungal Hydrophobins. *J Mol Biol* **425**: 244–256 https://www.sciencedirect.com/science/article/pii/S0022283612008546?via%3Dihub. Accessed February 20, 2018.

Mukherjee, P.K., Buensanteai, N., Moran-Diez, M.E., Druzhinina, I.S., and Kenerley, C.M. (2012a) Functional analysis of non-ribosomal peptide synthetases (NRPSs) in Trichoderma virens reveals a polyketide synthase (PKS)/NRPS hybrid enzyme involved in the induced systemic resistance response in maize. *Microbiology* **158**: 155–165 http://mic.microbiologyresearch.org/content/journal/micro/10.1099/mic.0.052159-0. Accessed June 6, 2019.

Mukherjee, P.K., Horwitz, B.A., and Kenerley, C.M. (2012b) Secondary metabolism in Trichoderma - A genomic perspective. *Microbiology* **158**: 35–45.

Mukherjee, P.K., Hurley, J.F., Taylor, J.T., Puckhaber, L., Lehner, S., Druzhinina, I., *et*

al. (2018) Ferricrocin, the intracellular siderophore of Trichoderma virens, is involved in growth, conidiation, gliotoxin biosynthesis and induction of systemic resistance in maize. *Biochem Biophys Res Commun* https://linkinghub.elsevier.com/retrieve/pii/S0006291X18321090.

Mustalahti, E., Saloheimo, M., and Joensuu, J.J. (2013) Intracellular protein production in Trichoderma reesei (Hypocrea jecorina) with hydrophobin fusion technology. *N Biotechnol* **30**.

Nawrocka, J., and Małolepsza, U. (2013) Diversity in plant systemic resistance induced by Trichoderma. *Biol Control* **67**.

Nogueira-Lopez, G., Greenwood, D.R., Middleditch, M., Winefield, C., Eaton, C., Steyaert, J.M., and Mendoza-Mendoza, A. (2018) The Apoplastic Secretome of Trichoderma virens During Interaction With Maize Roots Shows an Inhibition of Plant Defence and Scavenging Oxidative Stress Secreted Proteins. *Front Plant Sci* **9**: 409 http://journal.frontiersin.org/article/10.3389/fpls.2018.00409/full. Accessed June 6, 2019.

Park, Y.-H., Kenerley, C.M., and Stack, J.P. (1992) Inoculum dynamics of Gliocladium virens associated with roots of cotton seedlings. *Microb Ecol* **23**: 169–179 http://link.springer.com/10.1007/BF00172638. Accessed October 4, 2017.

Paz, Z., García-Pedrajas, M.D., Andrews, D.L., Klosterman, S.J., Baeza-Montañez, L., and Gold, S.E. (2011) One Step Construction of Agrobacterium-Recombination-ready-plasmids (OSCAR), an efficient and robust tool for ATMT based gene deletion construction in fungi. *Fungal Genet Biol* **48**: 677–684.

Pieterse, C.M.J., Zamioudis, C., Berendsen, R.L., Weller, D.M., Wees, S.C.M. Van, and Bakker, P.A.H.M. (2014) Induced Systemic Resistance by Beneficial Microbes. *Annu Rev Phytopathol* **52**.

Prieto, C., García-Estrada, C., Lorenzana, D., and Martín, J.F. (2012) NRPSsp: non-ribosomal peptide synthase substrate predictor. *Bioinformatics* **28**: 426–427 https://academic.oup.com/bioinformatics/article-lookup/doi/10.1093/bioinformatics/btr659. Accessed November 8, 2019.

Prosperini, A., Berrada, H., Ruiz, M.J., Caloni, F., Coccini, T., Spicer, L.J., *et al.* (2017) A review of the mycotoxin enniatin B. *Front Public Heal* **5**.

Przylucka, A., Ribitsch, D., Herrero-Acero, E., Gübitz, G., Kubicek, C.P., and Druzhinina, I. (2014) Hydrophobins class I versus class II: Trichoderma virens HFB9a and HFB9b (class I) are more effective as enhancing agents in enzymatic PET hydrolysis and surface modulators compared to HFB4 and HFB7 (class II). *N Biotechnol* **31**: S190 https://www.sciencedirect.com/science/article/pii/S1871678414009972?via%3Dihub. Accessed August 17, 2018.

Rahier, N.J., Molinier, N., Long, C., Deshmukh, S.K., Kate, A.S., Ranadive, P., *et al.* (2015) Anticancer activity of koningic acid and semisynthetic derivatives. *Bioorg Med Chem* **23**: 3712–3721 https://www.sciencedirect.com/science/article/pii/S0968089615003016?via%3Dihub. Accessed August 13, 2019.

Ramírez-Valdespino, C.A., Casas-Flores, S., and Olmedo-Monfil, V. (2019) Trichoderma as a model to study effector-like molecules. *Front Microbiol* **10**: 1030.

Riehs, G., and Urban, E. (1997) EPC Synthesis of (+)-Heptelidic Acid. *Monatshefte fur Chemie* **128**: 281–289.

Ruocco, M., Lanzuise, S., Lombardi, N., Woo, S.L., Vinale, F., Marra, R., *et al.* (2015) Multiple Roles and Effects of a Novel Trichoderma Hydrophobin. *Mol Plant-Microbe Interact* **28**: 167–179.

Salas-Marina, M.A., Silva-Flores, M.A., Uresti-Rivera, E.E., Castro-Longoria, E., Herrera-Estrella, A., and Casas-Flores, S. (2011) Colonization of Arabidopsis roots by Trichoderma atroviride promotes growth and enhances systemic disease resistance through jasmonic acid/ethylene and salicylic acid pathways. *Eur J Plant Pathol* **131**: 15–26 http://link.springer.com/10.1007/s10658-011-9782-6. Accessed August 21, 2017.

Saldajeno, M.G.B., Naznin, H.A., Elsharkawy, M.M., Shimizu, M., and Hyakumachi, M. (2014) *Enhanced Resistance of Plants to Disease Using Trichoderma spp.* .

Samuels, G.J. (2006) The Nature and Application of Biocontrol Microbes II: Trichoderma spp. Trichoderma: Systematics, the Sexual State, and Ecology. **96**: 195.

Saravanakumar, K., Fan, L., Fu, K., Yu, C., and Wang, M. (2016) Cellulase from Trichoderma harzianum interacts with roots and triggers induced systemic resistance to foliar disease in maize. *Nat Publ Gr* .

Sayre, R., Wallace, I.S., Wu, X., Yao, N., F-c, B., J-x, W., *et al.* (2015) An Arabidopsis neutral ceramidase mutant ncer1 accumulates hydroxyceramides and is sensitive to oxidative stress. www.frontiersin.org. Accessed May 12, 2020.

Schneider, C.A., Rasband, W.S., and Eliceiri, K.W. (2012) NIH Image to ImageJ: 25 years of image analysis. *Nat Methods* **9**: 671–675.

Seidl-Seiboth, V., Gruber, S., Sezerman, U., Schwecke, T., Albayrak, A., Neuhof, T., *et al.* (2011) Novel Hydrophobins from Trichoderma Define a New Hydrophobin Subclass: Protein Properties, Evolution, Regulation and Processing. *J Mol Evol* **72**: 339–351 http://link.springer.com/10.1007/s00239-011-9438-3. Accessed July 21, 2016.

Shaw, S., Cocq, K. Le, Paszkiewicz, K., Moore, K., Winsbury, R., Torres Zabala, M. de, *et al.* (2016) Transcriptional reprogramming underpins enhanced plant growth promotion by the biocontrol fungus Trichoderma hamatum GD12 during antagonistic interactions with Sclerotinia sclerotiorum in soil. *Mol Plant Pathol* .

Sheridan, K.J., Dolan, S.K., and Doyle, S. (2015) Endogenous cross-talk of fungal metabolites. *Front Microbiol* **5** http://journal.frontiersin.org/article/10.3389/fmicb.2014.00732/abstract. Accessed January 12, 2020.

Shoresh, M., Yedidia, I., and Chet, I. (2005) Involvement of Jasmonic Acid/Ethylene Signaling Pathway in the Systemic Resistance Induced in Cucumber by *Trichoderma asperellum* T203. *Phytopathology* **95**: 76–84 http://apsjournals.apsnet.org/doi/10.1094/PHYTO-95-0076. Accessed August 21, 2017.

Steyaert, J.M., Weld, R.J., Mendoza-Mendoza, A., and Stewart, A. (2010) Reproduction without sex: Conidiation in the filamentous fungus Trichoderma. *Microbiology* **156**: 2887–2900 http://www.ncbi.nlm.nih.gov/pubmed/20688823. Accessed February 26, 2020.

Sun, W., Wang, B., Yang, J., Wang, W., Liu, A., Leng, L., *et al.* (2017) Weighted Gene Co-expression Network Analysis of the Dioscin Rich Medicinal Plant Dioscorea

nipponica. *Front Plant Sci* **8**: 789 http://journal.frontiersin.org/article/10.3389/fpls.2017.00789/full. Accessed May 13, 2020.

Szucs, Z., Plaszkó, T., Cziáky, Z., Kiss-Szikszai, A., Emri, T., Bertóti, R., *et al.* (2018) Endophytic fungi from the roots of horseradish (Armoracia rusticana) and their interactions with the defensive metabolites of the glucosinolate - myrosinase - isothiocyanate system. *BMC Plant Biol* **18**.

Taylor, J.T., Horwitz, B.A., and Kenerley, C.M. (2017) Characterization of Tvhyd1, a Trichoderma virens hydrophobin (Abstr.). *Phytopathology* **107**: S3.12.

Trdá, L., Boutrot, F., Claverie, J., Brulé, D., Dorey, S., and Poinssot, B. (2015) Perception of pathogenic or beneficial bacteria and their evasion of host immunity: pattern recognition receptors in the frontline. *Front Plant Sci* **6**: 219 http://www.ncbi.nlm.nih.gov/pubmed/25904927. Accessed September 18, 2017.

Vargas, W.A., Crutcher, F.K., and Kenerley, C.M. (2011) Functional characterization of a plant-like sucrose transporter from the beneficial fungus Trichoderma virens. Regulation of the symbiotic association with plants by sucrose metabolism inside the fungal cells. *New Phytol* **189**: 777–789 http://doi.wiley.com/10.1111/j.1469-8137.2010.03517.x. Accessed March 29, 2020.

Vargas, W.A., Mandawe, J.C., and Kenerley, C.M. (2009) Plant-Derived Sucrose Is a Key Element in the Symbiotic Association between Trichoderma virens and Maize Plants. *Plant Physiol* **151** http://www.plantphysiol.org/content/151/2/792.long. Accessed August 23, 2017.

Vargas, W.A., Mukherjee, P.K., Laughlin, D., Wiest, A., Moran-Diez, M.E., and Kenerley, C.M. (2014) Role of gliotoxin in the symbiotic and pathogenic interactions of Trichoderma virens. *Microbiology* **160**.

Viterbo, A., and Chet, I. (2006) TasHyd1 , a new hydrophobin gene from the biocontrol agent Trichoderma asperellum , is involved in plant root colonization. *Mol Plant Pathol* **7**: 249–258 http://doi.wiley.com/10.1111/j.1364-3703.2006.00335.x. Accessed August 2, 2016.

Viterbo, A., Wiest, A., Brotman, Y., Chet, I., and Kenerley, C. (2007) The 18mer peptaibols from Trichoderma virens elicit plant defence responses. *Mol Plant Pathol* **8**: 737–746 http://www.ncbi.nlm.nih.gov/pubmed/20507534. Accessed March 29, 2020.

Vogel, H. (1956) A convenient growth medium for Neurospora (Medium N). *Microbiol Genet Bull* **13**: 42–43.

Wang, D., Tian, L., Zhang, D., Song, J., Song, S., Yin, C., *et al.* (2020a) Functional analyses of small secreted cysteine-rich proteins identified candidate effectors in *Verticillium dahliae*. *Mol Plant Pathol* **21**: 667–685 https://onlinelibrary.wiley.com/doi/abs/10.1111/mpp.12921. Accessed May 19, 2020.

Wang, K. Der, Borrego, E.J., Kenerley, C.M., and Kolomiets, M. V. (2020b) Oxylipins Other Than Jasmonic Acid Are Xylem-Resident Signals Regulating Systemic Resistance Induced by Trichoderma virens in Maize. *Plant Cell* **32**: 166–185.

Wilhite, S.E., Lumsden, R.D., and Straney, D.C. (2001) Peptide Synthetase Gene in Trichoderma virens. *Appl Environ Microbiol* **67**: 5055–5062.

Willaert, R.G. (2018) Adhesins of yeasts: Protein structure and interactions. *J Fungi* **4**.

Winandy, L., Schlebusch, O., and Fischer, R. (2019) Fungal hydrophobins render stones impermeable for water but keep them permeable for vapor. *Sci Rep* **9**: 6264 http://www.nature.com/articles/s41598-019-42705-w. Accessed July 12, 2019.

Wösten, H. a (2001) Hydrophobins: multipurpose proteins. *Annu Rev Microbiol* **55**: 625–646.

Wosten, H., Vries, O. De, and Wessels, J. (1993) Interfacial Self-Assembly of a Fungal Hydrophobin into a Hydrophobic Rodlet Layer. *Plant Cell* **5**: 1567–1574 http://www.ncbi.nlm.nih.gov/pubmed/12271047. Accessed April 3, 2017.

Wösten, H.A., and Vocht, M.L. de (2000) Hydrophobins, the fungal coat unravelled. *Biochim Biophys Acta* **1469**: 79–86 http://www.ncbi.nlm.nih.gov/pubmed/10998570. Accessed January 12, 2017.

Yan, Y., Borrego, E., and Kolomiets, M. V. (2013) Jasmonate Biosynthesis, Perception and Function in Plant Development and Stress Responses. In *Lipid Metabolism*. InTech, http://www.intechopen.com/books/lipid-metabolism/jasmonate-biosynthesis-perception-and-function-in-plant-development-and-stress-responses. Accessed August 14, 2017.

Yang, J., Yan, R., Roy, A., Xu, D., Poisson, J., and Zhang, Y. (2015) The I-TASSER Suite: protein structure and function prediction. *Nat Methods* **12**: 7–8 http://www.nature.com/articles/nmeth.3213. Accessed April 4, 2018.

Yoshida, H., Sakai, G., Mori, K., Kojima, K., Kamitori, S., and Sode, K. (2015) Structural analysis of fungus-derived FAD glucose dehydrogenase. *Sci Rep* **5**: 1–13.

Yoshida, Y. (1988) Cytochrome P450 of fungi: primary target for azole antifungal agents. *Curr Top Med Mycol* **2**: 388–418.

Yu, X., Feng, B., He, P., and Shan, L. (2017) From Chaos to Harmony: Responses and Signaling upon Microbial Pattern Recognition. *Annu Rev Phytopathol* **55**: 109–137 http://www.annualreviews.org/doi/10.1146/annurev-phyto-080516-035649. Accessed March 29, 2020.

Zampieri, F., Wösten, H.A.B., and Scholtmeijer, K. (2010) Creating surface properties using a palette of hydrophobins. *Materials (Basel)* **3**: 4607–4625.

Zeilinger, S., Gruber, S., Bansal, R., and Mukherjee, P.K. (2016) Secondary metabolism in Trichoderma - Chemistry meets genomics. *Fungal Biol Rev* **30**.

Zhu, W., Wei, W., Wu, Y., Zhou, Y., Peng, F., Zhang, S., *et al.* (2017) BcCFEM1, a CFEM Domain-Containing Protein with Putative GPI-Anchored Site, Is Involved in Pathogenicity, Conidial Production, and Stress Tolerance in Botrytis cinerea. *Front Microbiol* **8**: 1807 http://journal.frontiersin.org/article/10.3389/fmicb.2017.01807/full. Accessed May 19, 2020.

APPENDIX A

PRELIMINARY RESULTS FOR HFB3A CHARACTERIZATION

Genomic description and expression

HFB3a encodes a 133 amino acid protein whose sequence is very similar to both HFB9a and TasHyd1 (Figure 34a). The inter-cysteine spacing is consistent with class I hydrophobins and the hydrophobicity plot is nearly identical to that of HFB9a, but with a shift of several residues to the left where (Figure 34b). These observations make HFB3a an interesting target for characterization. Gene expression is initiated between 30 and 54 hours post inoculation in the presence of maize roots and approximately 72 hours post inoculation in potato dextrose broth, which is similar to the expression of HFB9a (Figure 35a). This is supported by read counts from whole transcriptome analyses (Figure 35b and 35c, Taylor *et al.* unpublished, Malinich *et al.*, 2019).

Generation of knockout and overexpressing strains

The HFB3a gene was deleted from the *T. virens* genome by homologous recombination. *Agrobacterium tumefaciens* was used to transform *T. virens* conidia with the generated knockout vector with putative deletion transformants confirmed by PCR. A construct to overexpress the HFB3a gene was also generated by restriction cloning between the constitutive *T. virens* GPD promoter and terminator. This vector was also confirmed by PCR and sequencing and transformed into the fungus by PEG mediated protoplast transformation. Overexpression in stable transformants was confirmed by

qPCR using gene specific primers. Two mutants were selected that demonstrated 5- and 15-fold increased expression of the gene compared to WT.

HFB3a is involved in limiting ingress of T. virens into maize roots and required for induction of systemic resistance

Maize seedlings treated with *ΔHFB3a* mutants were significantly more colonized compared to those treated with the WT strain (Figure 36). This directly contradicted the hypothesis that HFB3a mediated attachment of fungal hyphae to plant cells and thus enhanced colonization. Instead, the protein appears to act as a limiter of colonization. This is also opposite the effect that was seen with HFB9a deletion mutants, which demonstrated significantly reduced colonization compared to the wild-type strain.

The ability of *T. virens* strains to induce systemic resistance in maize plants was examined by foliar treatment with *C. heterostrophus* to determine if increased colonization influenced fungal derived plant benefits. Plants treated with mutant strains exhibited significantly larger lesions compared to WT treated plants (Figure 37). The ability of the overexpressing strains to induce systemic resistance was also tested to understand if the effect observed in the knockout strains was due to over-colonization by the fungus or the lack of an HFB3a derived signal. Plants treated with overexpressing strains had significantly smaller lesions than both the control and WT treated plants (Figure 38).

HFB3a enhances plant growth

Maize plants treated with ΔHFB3a strains were significantly shorter than untreated plants and those treated with the WT strain (Figure 39a). The opposite effect

was observed with overexpression strains, wherein plants treated with overexpression strains were significantly larger than the WT treated and untreated strains (Figure 39b).

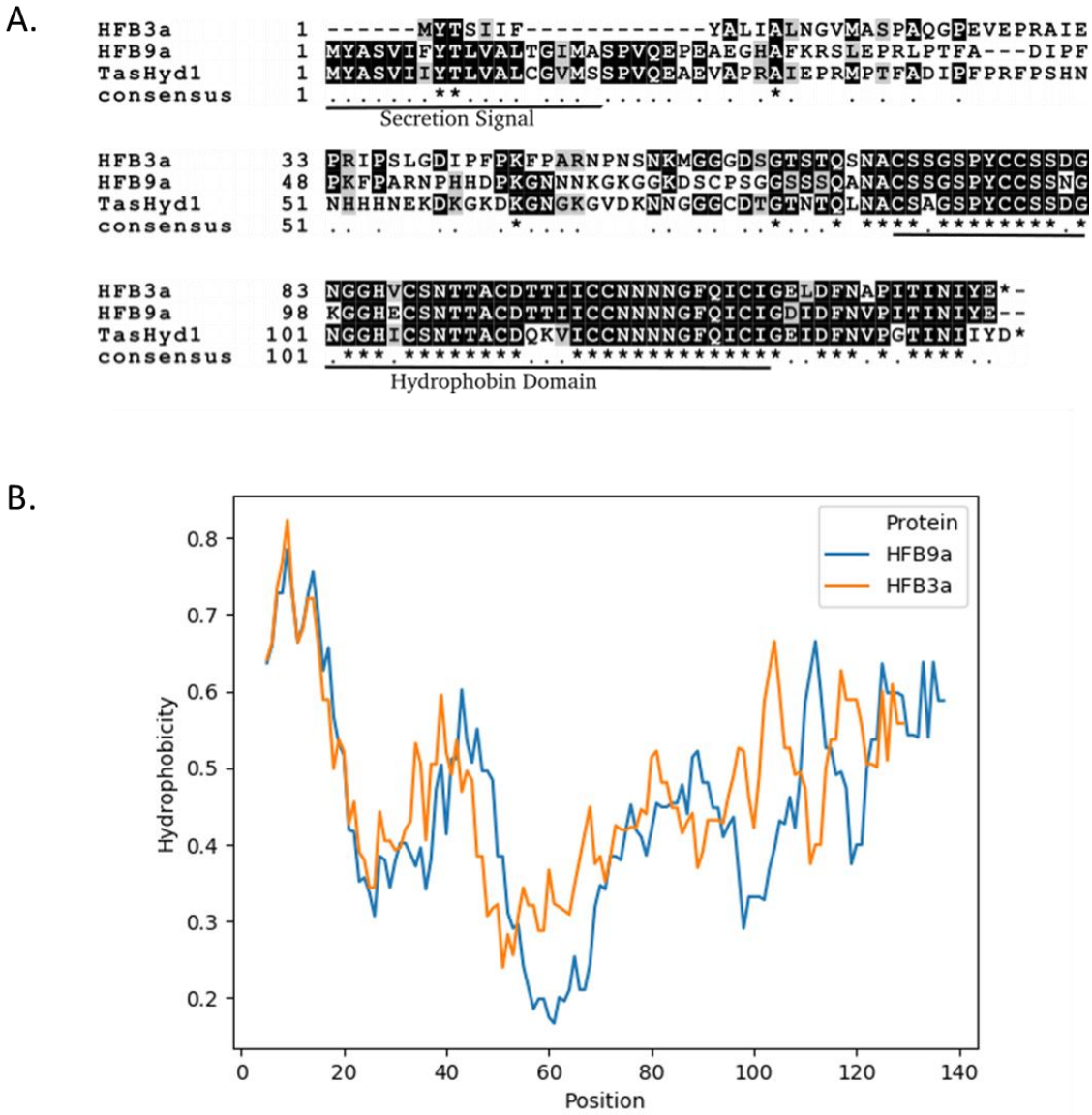

Figure 34. A. Clustal omega alignment of amino acid sequences of HFB9a and HFB3a from *T. virens*, and TasHyd1 from *T. asperellum*. B. Hydrophobicity plot of amino acid sequences from HFB9a and HFB3a. Hydrophobicity of a five-residue window is represented on the Y-axis and the amino acid number in of the central amino acid in the window is represented on the X-axis.

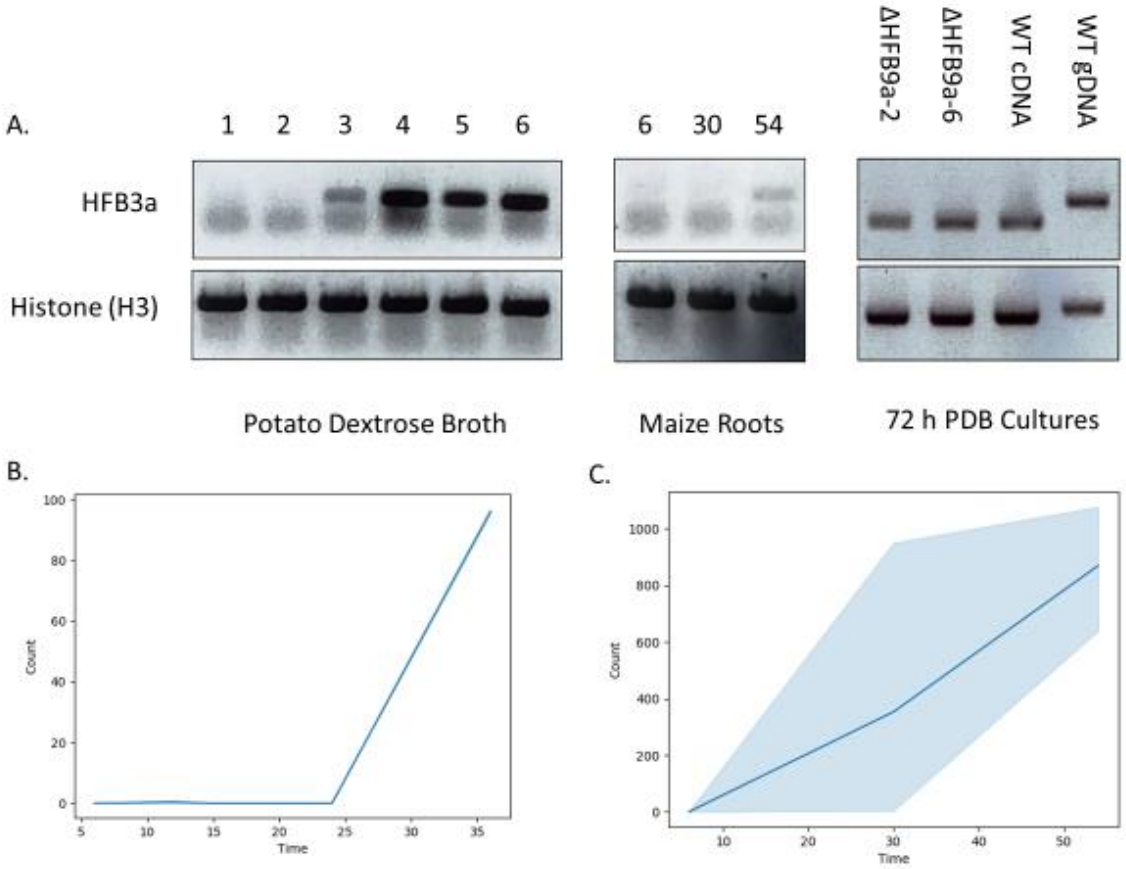

Figure 35. A. RT-PCR profile of HFB3a expression in potato dextrose broth and maize roots, and expression of HFB3a in HFB9a mutants and wild-type strains. B. Normalized read counts from an RNA-seq transcriptomic study with timepoints at 6, 12, 15, 24, and 36 hpi. C. Normalized read counts from an RNA-seq transcriptomic study with timepoints at 6, 30, and 54 hpi.

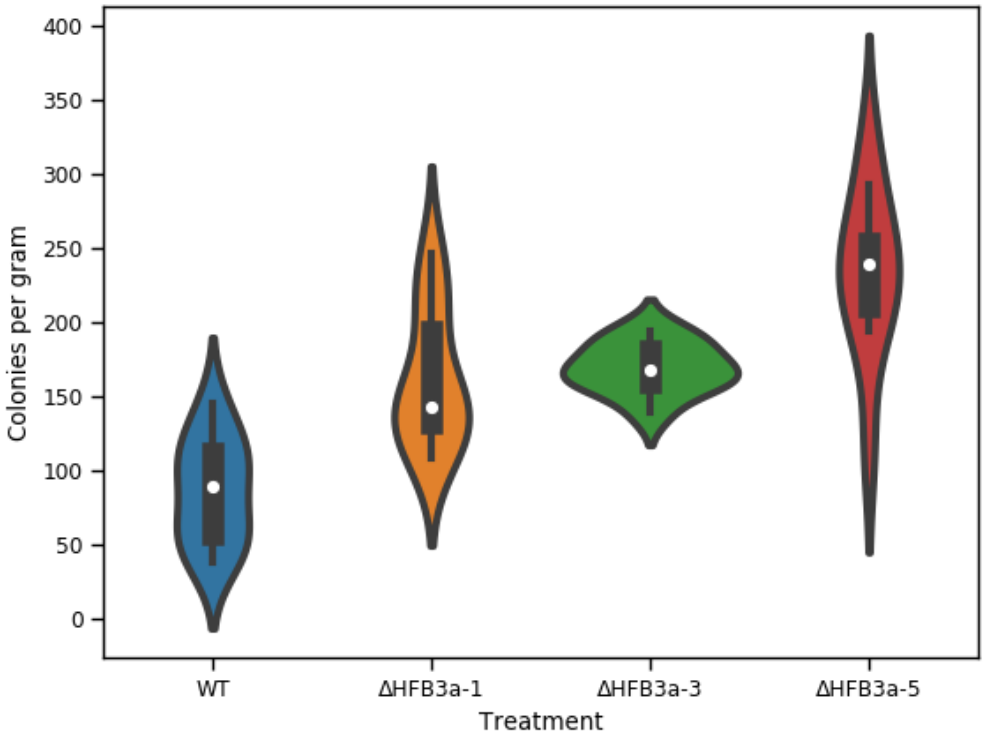

Figure 36. Root colonization of maize by HFB3a mutant strains and the wild-type strain.

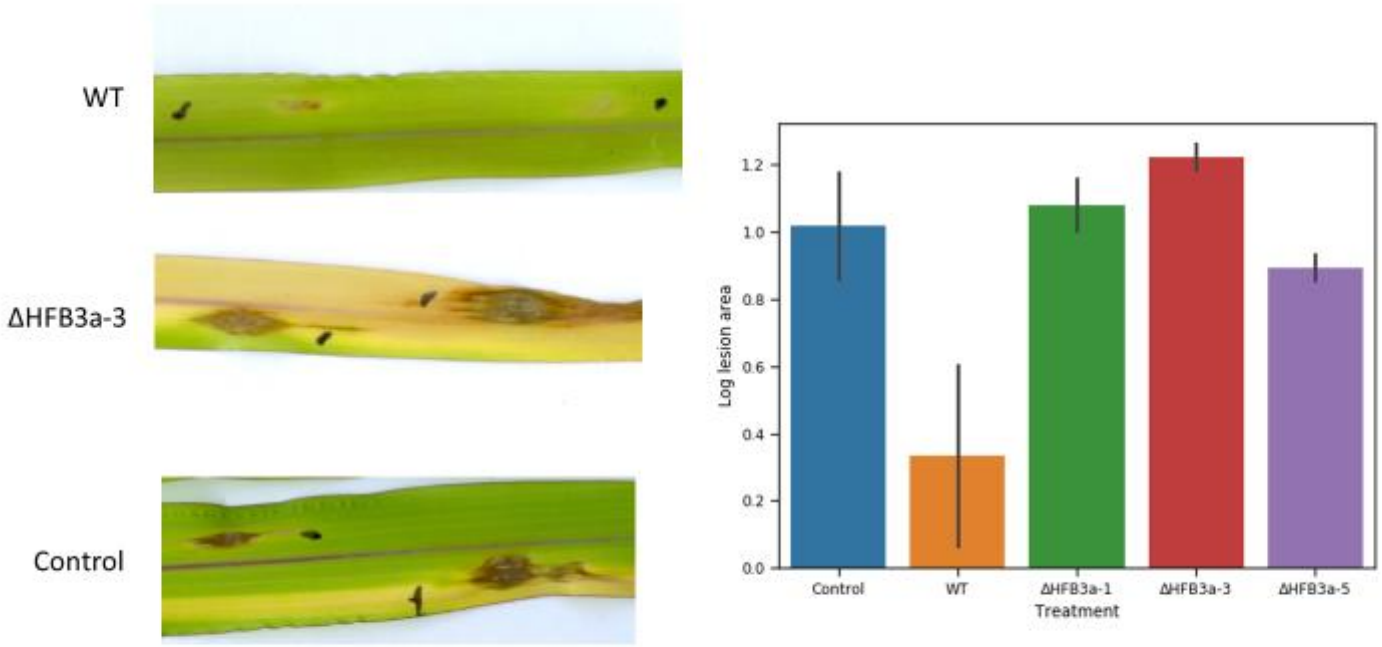

Figure 37. Induced systemic resistance against *Cochliobolus heterostrophus* of plants treated with HFB3a deletion mutants or the wild-type strain.

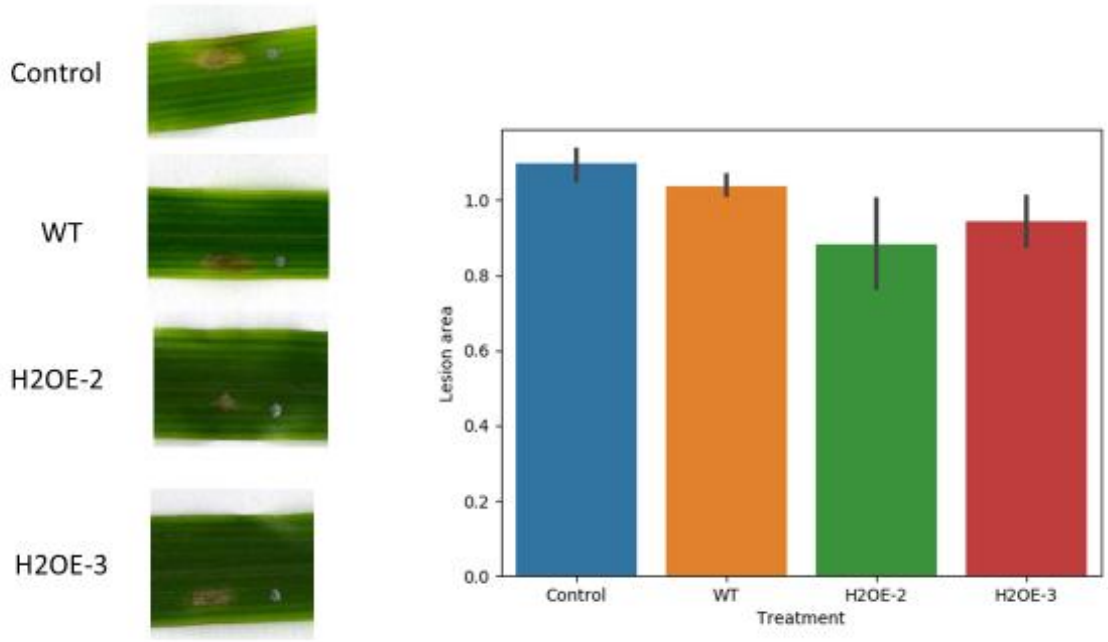

Figure 38. Induced systemic resistance against *Cochliobolus heterostrophus* of overexpression and the wild-type strains.

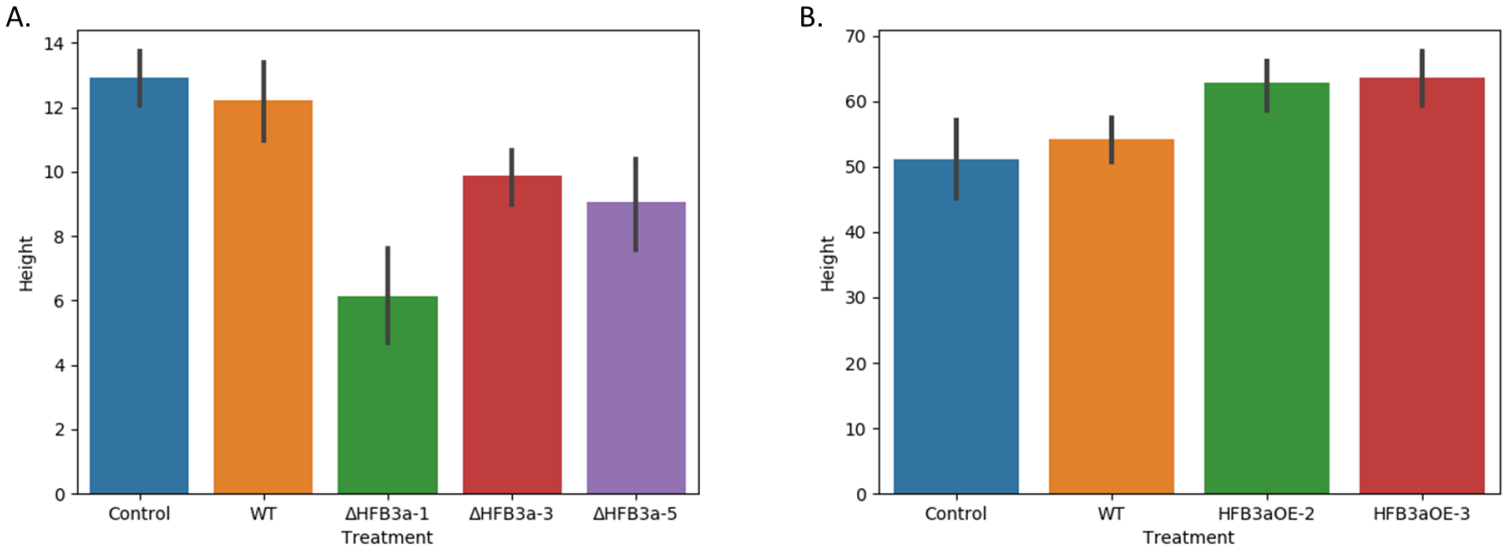

Figure 39. Heights of plants treated with either HFB3a deletion mutants, HFB3a overexpression mutants, or the wild-type strain.

APPENDIX B

SUPPLEMENTARY FIGURES FOR CHAPTER III

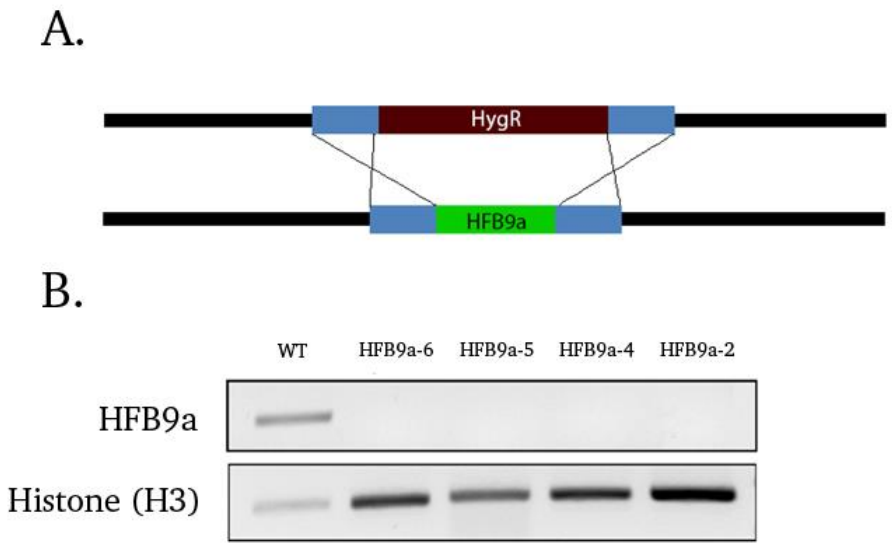

Figure 40. A. Homologous recombination strategy for deletion of HFB9a. B. PCR confirmation of deletion from putative mutants.

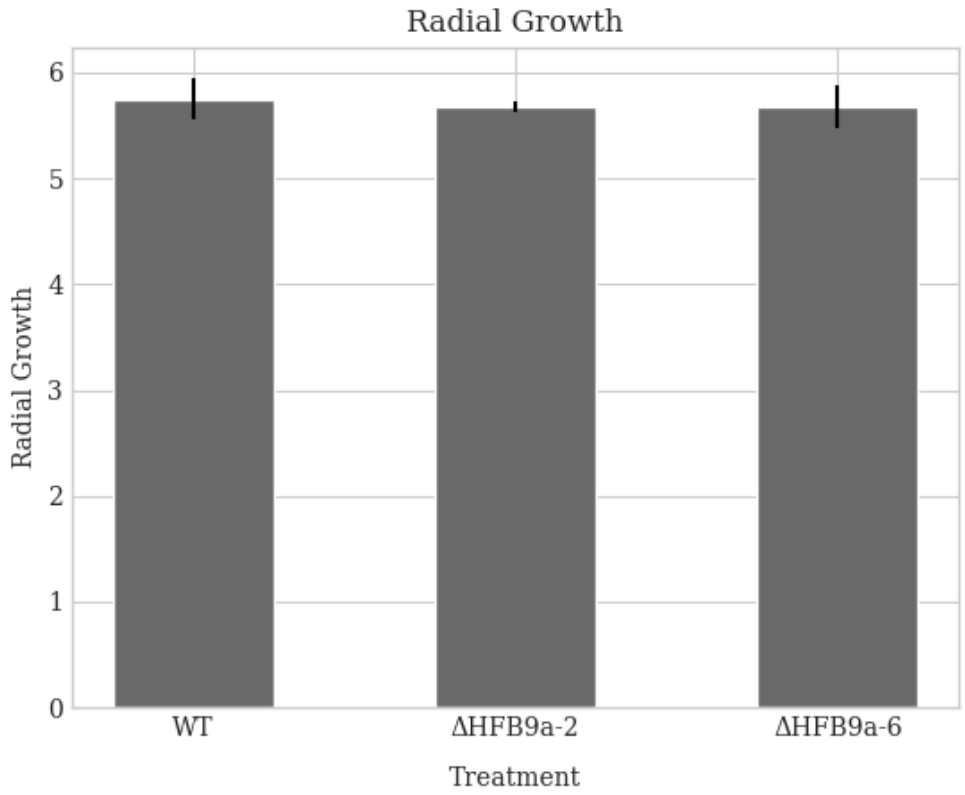

Figure 41. Radial growth comparison of mutants and wild-type strains on potato dextrose agar.

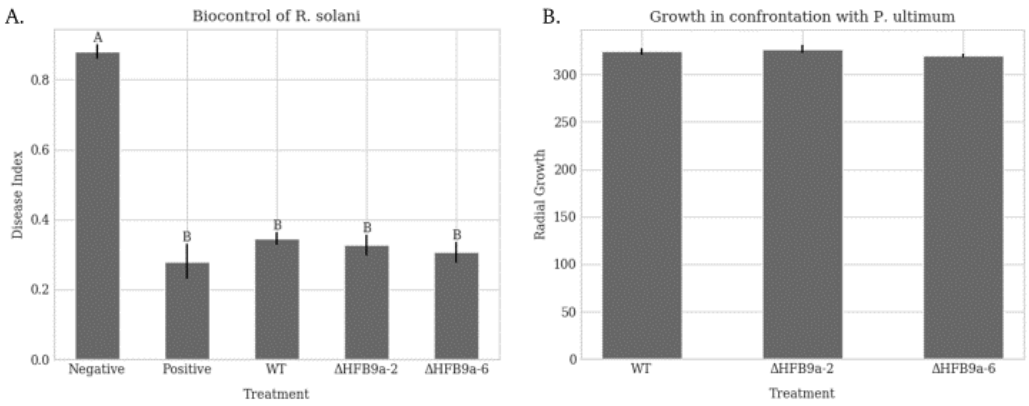

Figure 42. A. Biocontrol of *R. solani* by mutants and wild-type strains as measured by disease index. Negative control had no *Trichoderma* but was inoculated with *R. solani*. Positive control had no fungus or pathogen added. B. Growth of mutants and wild-type strains in confrontation with *P. ultimum.*